

HETEROCYCLE-BASED PUSH-PULL NLOPHORES: INVESTIGATION OF
LINEAR AND NON-LINEAR OPTICAL PROPERTIES

A THESIS SUBMITTED TO
THE GRADUATE SCHOOL OF NATURAL AND APPLIED SCIENCES
OF
MIDDLE EAST TECHNICAL UNIVERSITY

BY

BAŞAK KARAGÖLLÜ

IN PARTIAL FULFILLMENT OF THE REQUIREMENTS
FOR
THE DEGREE OF MASTER OF SCIENCE
IN
CHEMISTRY

DECEMBER 2022

Approval of the thesis:

**HETEROCYCLE-BASED PUSH-PULL NLOPHORES: INVESTIGATION
OF LINEAR AND NON-LINEAR OPTICAL PROPERTIES**

submitted by **BAŞAK KARAGÖLLÜ** in partial fulfillment of the requirements for
the degree of **Master of Science in Chemistry, Middle East Technical University**
by,

Prof. Dr. Halil Kalıpçılar
Dean, Graduate School of **Natural and Applied Sciences**

Prof. Dr. Özdemir Doğan
Head of the Department, **Chemistry**

Assoc. Prof. Dr. Çağatay Dengiz
Supervisor, **Chemistry, METU**

Examining Committee Members:

Prof. Dr. Cihangir Tanyeli
Chemistry, METU

Assoc. Prof. Dr. Çağatay Dengiz
Chemistry, METU

Prof. Dr. Özdemir Doğan
Chemistry, METU

Prof. Dr. Okan Esentürk
Chemistry, METU

Assoc. Prof. Dr. Serdal Kaya
Aircraft Eng., Necmettin Erbakan Uni.

Date: 19.12.2022

I hereby declare that all information in this document has been obtained and presented in accordance with academic rules and ethical conduct. I also declare that, as required by these rules and conduct, I have fully cited and referenced all material and results that are not original to this work.

Name Last name : Başak Karagöllü

Signature :

ABSTRACT

HETEROCYCLE-BASED PUSH-PULL NLOPHORES: INVESTIGATION OF LINEAR AND NON-LINEAR OPTICAL PROPERTIES

Karagöllü, Başak
Master of Science, Chemistry
Supervisor : Assoc. Prof. Dr. Çağatay Dengiz

December 2022, 118 pages

Organic nonlinear optical materials are substantial in the technology era we live in, due to their applications in telecommunications, data storage, real-time target recognition, optoelectronics, and optical signal processing. The distinct intramolecular charge transfer (ICT) properties of conjugated push-pull chromophores provide high polarization and thus a strong NLO response can be obtained. NLOphores are designed to obtain more efficient and rapid NLO responses and [2+2] cycloaddition-retroelectrocyclization reaction is one of the efficient strategies to synthesize them. In this thesis, target NLOphores were synthesized *via* the reactions of heterocycle-substituted alkynes with TCNE and TCNQ, their linear and nonlinear optical properties were investigated using both experimental and theoretical studies.

Keywords: [2+2] cycloaddition-retroelectrocyclization, push-pull NLOphores, heterocycles, optoelectronics

ÖZ

HETEROHALKA BAZLI İT-ÇEK TİPİ NLOFORLAR: LİNEER VE LİNEER OLMAYAN OPTİK ÖZELLİKLERİNİN ARAŞTIRILMASI

Karagöllü, Başak
Yüksek Lisans, Kimya
Tez Yöneticisi: Doç. Dr. Çağatay Dengiz

Aralık 2022, 118 sayfa

Organik, lineer olmayan optik (NLO) özelliklere sahip bileşikler telekomünikasyon, veri depolama, gerçek zamanlı hedef tanıma, optoelektronik ve optik sinyal işleme alanlarındaki uygulamaları sebebiyle yaşadığımız teknoloji çağında oldukça değerlidir. Konjüge it-çek tipi kromoforların belirgin molekül içi yük transfer özelliklerine sahip olmaları molekülün yüksek değerde polarize olmasını sağlamaktadır ve bu sayede bu moleküllerden güçlü NLO yanıtı alınabilmektedir. NLOforlar, daha verimli ve hızlı NLO yanıtları elde edebilmek için tasarlanırlar ve [2+2] siklokatalma-retroelektrosiklizasyon tepkimeleri bu yapıları sentezlemek için en etkili yöntemlerden biridir. Bu tezde, çeşitli heterosiklik moleküller ile türevlendirilmiş alkinlerin TCNE ve TCNQ ile reaksiyonları sonucu elde edilen NLOforların lineer ve lineer olmayan optik özellikleri teorik ve deneysel çalışmalarla incelenmiştir.

Anahtar Kelimeler: [2+2] siklokatalma-retroelektrosiklizasyon, it-çek tipi NLOforlar, heterosiklik, optoelektronik

to my little brother, Ege,

who is the only person I would do anything for his happiness

ACKNOWLEDGMENTS

First of all, I would like to thank my supervisor *Assoc. Prof. Dr. Çağatay Dengiz* for his guidance, patients, continuous support, and motivation since the first day I started working in the laboratory. In my first day, he said to me "You will learn everything from me, it will be very good for you, but you will learn everything from me, and it will also be very bad for you". He was right. I learned everything from him and I consider myself lucky. Thank you for everything.

I would like to thank to examining committee members *Prof. Dr. Cihangir Tanyeli*, *Prof. Dr. Özdemir Doğan*, *Prof. Dr. Okan Esentürk*, and *Dr. Serdal Kaya* for their time and contributions.

This thesis study is funded by Scientific and Technological Research Council of Turkey (TUBITAK) under grant number TUBITAK 120Z957.

I would like to thank DRG group members, *Efe Çelik*, *Fevzi İnyurt*, *İpek Savaş*, *Irmak Uzungel*, *İpek Öktem*, *Murat Can Kılıç*, and *Yağmur Ünal*. It was great pleasure to work with you. Thank you very much for your friendship, support and most importantly for making every moment I spend in the laboratory enjoyable.

I want to thank my three very special friends. Firstly, I would like to thank *Kübra Erden* for guiding me from the first day I started, for being my friend and, above all, being the best lab manager. Also, I would like to thank *Melih Günay* for being the subject of many happy memories that I can not count and for being with me during difficult times. I would like to thank my dear friend, *Flora Mammadova*, who is my source of happiness and motivation with her friendship, and who is with me in every trouble, and who always welcomes my little jokes with a smile.

I would like to say a special thank you to *Hazal Kayaş* not only for her contributions to my work, but also for being a kind-hearted friend who gives me endless support

in every aspect of my life. Every day I worked with her has been an unpredictable but fun adventure for me. Thank you for everything.

I am very thankful to my flatmates *Semin Özsinan* and *Selen Yalçın* for their understanding and moral support during hard times.

I would like to offer my special thanks to my friend, *Tamara Ecem Korkut*. Meeting with her was my biggest chance in my academic life. Without her motivation and friendship, I might not even be brave enough to complete my education.

I want to thank three special friends who have been in my life for years. *Serhat Elmas*, *Selimcan Özkan* and *Boğaçhan Alkan* thank you all for being with me at every moment for years. Even though we live in different cities now, your support was always with me.

Of course, nothing could be possible without my parents especially my mom who patiently re-motivated me every time I gave up. The greatest chance of every born child is to have a family that supports them and is there for them under all circumstances. I am so lucky to have you. Thank you for everything.

Finally, I would like to thank my little brother, *Ege*, who can make my life beautiful even with his presence since the day he was born. Every decision I make, every step I take is for you to have a happy life ahead. Thank you very much for your endless and innocent love for me and for all the support you have given me. I love you.

TABLE OF CONTENTS

ABSTRACT	v
ÖZ.....	vi
ACKNOWLEDGMENTS.....	viii
TABLE OF CONTENTS	x
LIST OF TABLES	xii
LIST OF FIGURES.....	xiii
LIST OF ABBREVIATIONS	xvi
LIST OF SCHEMES	xvii
CHAPTERS	
1 INTRODUCTION.....	1
1.1 Click Chemistry.....	4
1.1.1 Huisgen 1,3-dipolar Cycloaddition Reaction.....	4
1.1.2 Diels – Alder Reactions	6
1.2 Other Potential Pericyclic Reactions for the Synthesis of NLOphores.....	8
1.2.1 Photochemical [2+2] Cycloaddition Reactions	8
1.2.2 Thermal [2+2] Cycloaddition Reactions.....	12
1.2.3 [2+2] Cycloaddition – Retroelectrocyclization (CA-RE) Reactions	14
1.3 Aim of Study	21
2 RESULTS AND DISCUSSION.....	23
2.1 Design and Synthesis of Heterocycle-Based Push-Pull NLOphores using [2+2] Cycloaddition-Retroelectrocyclization Reactions	23

2.1.1	Synthetic Attempts Towards <i>N</i> -methylbenzimidazole-Substituted Push-Pull NLOphores	23
2.1.2	Synthesis of Heterocycle-Substituted Alkynes	25
2.1.3	Coupling Reactions Between Heterocyclic Aryl Halides and DEA-Substituted Alkyne.....	28
2.1.4	Synthesis of Heterocycle-Based CA-RE Products by Using TCNE and TCNQ	29
2.2	UV-Vis Spectroscopy	32
2.3	Theoretical Calculations	37
2.4	Nonlinear Optical Applications	43
3	CONCLUSION.....	47
4	EXPERIMENTAL	49
4.1	Materials and Methods.....	49
4.2	Synthetic Procedures.....	50
4.2.1	Synthetic Procedures for Benzimidazole Containing Disubstituted Alkyne	50
4.2.2	Synthetic Procedures for <i>N,N</i> -diethyl-4-ethynylaniline	52
4.2.3	Synthetic Procedures for Halogenated Heterocycles	53
4.2.4	General Synthetic Procedures for Coupling Products.....	55
4.2.5	General Synthetic Procedures for CA-RE Products 112-118	59
4.2.6	General Synthetic Procedures for CA-RE Products 119-125	63
	REFERENCES	69
	APPENDICES	83
A.	¹ H and ¹³ C NMR Spectra	83
B.	HR-MS.....	109

LIST OF TABLES

TABLES

Table 1. HOMO-LUMO representations and electrostatic potential map (ESP) of TCNE compounds 112-118	38
Table 2. HOMO-LUMO representations and electrostatic potential map (ESP) of TCNQ compounds 119-125	38
Table 3. The electric dipole moment μ (D), E_{HOMO} , E_{LUMO} , ΔE ($E_{\text{HOMO}}-E_{\text{LUMO}}$), electronegativity (χ), global chemical hardness (η), global softness (σ), average polarizability [$\alpha_{(\text{tot})}$], first hyperpolarizability [$\beta_{(\text{tot})}$] at the CAM-B3LYP/6-31G(d,p) level of theory in CH_2Cl_2 for compounds 112-118	42
Table 4. The electric dipole moment μ (D), E_{HOMO} , E_{LUMO} , ΔE ($E_{\text{HOMO}}-E_{\text{LUMO}}$), electronegativity (χ), global chemical hardness (η), global softness (σ), average polarizability [$\alpha_{(\text{tot})}$], first hyperpolarizability [$\beta_{(\text{tot})}$] at the CAM-B3LYP/6-31G(d,p) level of theory in CH_2Cl_2 for compounds 119-125	42
Table 5. Results of theoretical (red line) and experimental (black line) Z-scan curves, nonlinear absorbance (left) and nonlinear refractive index (right), with 632 nm laser of compounds 112 , 115 , and 116	44
Table 6. Results of theoretical (red line) and experimental (black line) Z-scan curves, nonlinear absorbance (left) and nonlinear refractive index (right), with 632 nm laser of compounds 122 , 124 , and 125	45

LIST OF FIGURES

FIGURES

Figure 1. Examples of push–pull NLOphores reported in the literature.....	2
Figure 2. Examples of e ⁻ -rich, π -bridge, and e ⁻ -deficient heterocycles.....	3
Figure 3. Thermally allowed (a) and forbidden (b) CA reactions.....	9
Figure 4. Investigated other transition metal (W, Fe and Ni) TCBD derivatives..	16
Figure 5. TCBD derivatives reported by Takashi et al. in 1990.	16
Figure 6. Examples of first purely organic NLOphores.....	17
Figure 7. Various alkyne structures used in [2+2] CA-RE reactions.....	19
Figure 8. Examples of carbazole derivatives that have different reactivities.	20
Figure 9. Commercially available acceptors used in [2+2] CA-RE transformations.	20
Figure 10. Cyanide-based electron deficient alkene examples.	21
Figure 11. Commercially available halogenated heterocyclic compounds.....	27
Figure 12. Possible regioisomers of indole containing scaffolds.....	31
Figure 13. X-ray analysis of compound 120	31
Figure 14. UV/Vis spectra of heterocycle-based push-pull NLOphores 112 (red line), 113 (purple line), 114 (yellow line), 115 (blue line), 116 (pink line), 117 (green line), and 118 (black line) in CH ₂ Cl ₂ at 298 K.	33
Figure 15. Solvatochromic study of compound 124 in the mixture of <i>n</i> - hexane/CH ₂ Cl ₂	34
Figure 16. Solvatochromic study of compound 117 in toluene (yellow line), ethanol (green line), acetonitrile (red line) and ethyl acetate (purple line).....	34
Figure 17. UV/Vis spectra of heterocycle-based push-pull NLOphores 119 (red line), 120 (purple line), 121 (yellow line), 122 (blue line), 123 (pink line), 124 (green line), and 125 (black line) in CH ₂ Cl ₂ at 298 K.	35
Figure 18. Solvatochromic study of compound 124 in the mixture of <i>n</i> -hexane/ CH ₂ Cl ₂	36

Figure 19. Solvatochromic study of compound 117 in toluene (yellow line), ethanol (green line), acetonitrile (red line) and ethyl acetate (purple line).	37
Figure 20. Energy level diagrams of compounds 112-125	39
Figure 21. a) Calculated (red-shifted by 0.50 eV, scaled by 3.1, blue line) TD-DFT:CAM-B3LYP/6-31G(d) level of theory in CH ₂ Cl ₂ and experimental UV/Vis spectrum of 114 in CH ₂ Cl ₂ (red line). b) Calculated (red-shifted by 0.27 eV, scaled by 3.2, blue line) TD-DFT:CAM-B3LYP/6-31G(d) level of theory in CH ₂ Cl ₂ and experimental UV/Vis spectrum of 121 in CH ₂ Cl ₂ (red line)	40
Figure 22. ¹ H NMR spectrum of 86 in CDCl ₃ solution (400 MHz).	83
Figure 23. ¹ H NMR spectrum of 87 in CDCl ₃ solution (400 MHz).	83
Figure 24. ¹ H NMR spectrum of 88 in CDCl ₃ solution (400 MHz).	84
Figure 25. ¹ H NMR spectrum of 92 in CDCl ₃ solution (400 MHz).	84
Figure 26. ¹ H NMR spectrum of 93 in CDCl ₃ solution (400 MHz).	85
Figure 27. ¹ H NMR spectrum of 94 in CDCl ₃ solution (400 MHz).	85
Figure 28. ¹ H NMR spectrum of 96 in CDCl ₃ solution (400 MHz).	86
Figure 29. ¹ H NMR spectrum of 99 in CDCl ₃ solution (400 MHz).	86
Figure 30. ¹ H NMR spectrum of 101 in CDCl ₃ solution (400 MHz).	87
Figure 31. ¹ H NMR spectrum of 105 in CDCl ₃ solution (400 MHz).	88
Figure 32. ¹³ C NMR spectrum of 105 in CDCl ₃ solution (100 MHz).	88
Figure 33. ¹ H NMR spectrum of 106 in CDCl ₃ solution (400 MHz).	89
Figure 34. ¹³ C NMR spectrum of 106 in CDCl ₃ solution (100 MHz).	89
Figure 35. ¹ H NMR spectrum of 107 in CDCl ₃ solution (400 MHz).	90
Figure 36. ¹³ C NMR spectrum of 107 in CDCl ₃ solution (100 MHz).	90
Figure 37. ¹ H NMR spectrum of 108 in CDCl ₃ solution (400 MHz).	91
Figure 38. ¹³ C NMR spectrum of 108 in CDCl ₃ solution (100 MHz).	91
Figure 39. ¹ H NMR spectrum of 109 in CDCl ₃ solution (400 MHz).	92
Figure 40. ¹³ C NMR spectrum of 109 in CDCl ₃ solution (100 MHz).	92
Figure 41. ¹ H NMR spectrum of 110 in CDCl ₃ solution (400 MHz).	93
Figure 42. ¹³ C NMR spectrum of 110 in CDCl ₃ solution (100 MHz).	93
Figure 43. ¹ H NMR spectrum of 111 in CDCl ₃ solution (400 MHz).	94

Figure 44. ^{13}C NMR spectrum of 111 in CDCl_3 solution (100 MHz).	94
Figure 45. ^1H NMR spectrum of 112 in CDCl_3 solution (400 MHz)	95
Figure 46. ^{13}C NMR spectrum of 112 in CDCl_3 solution (100 MHz).	95
Figure 47. ^1H NMR spectrum of 113 in CDCl_3 solution (400 MHz).	96
Figure 48. ^{13}C NMR spectrum of 113 in CDCl_3 solution (100 MHz).	96
Figure 49. ^1H NMR spectrum of 114 in CDCl_3 solution (400 MHz).	97
Figure 50. ^{13}C NMR spectrum of 114 in CDCl_3 solution (100 MHz).	97
Figure 51. ^1H NMR spectrum of 115 in CDCl_3 solution (400 MHz).	98
Figure 52. ^{13}C NMR spectrum of 115 in CDCl_3 solution (100 MHz).	98
Figure 53. ^1H NMR spectrum of 116 in CDCl_3 solution (400 MHz).	99
Figure 54. ^{13}C NMR spectrum of 116 in CDCl_3 solution (100 MHz).	99
Figure 55. ^1H NMR spectrum of 117 in CDCl_3 solution (400 MHz).	100
Figure 56. ^{13}C NMR spectrum of 117 in CDCl_3 solution (100 MHz).	100
Figure 57. ^1H NMR spectrum of 118 in CDCl_3 solution (400 MHz).	101
Figure 58. ^{13}C NMR spectrum of 118 in CDCl_3 solution (100 MHz).	101
Figure 59. ^1H NMR spectrum of 119 in CDCl_3 solution (400 MHz).	102
Figure 60. ^{13}C NMR spectrum of 119 in CDCl_3 solution (100 MHz).	102
Figure 61. ^1H NMR spectrum of 120 in CDCl_3 solution (400 MHz).	103
Figure 62. ^{13}C NMR spectrum of 120 in CDCl_3 solution (100 MHz).	103
Figure 63. ^1H NMR spectrum of 121 in CDCl_3 solution (400 MHz).	104
Figure 64. ^{13}C NMR spectrum of 121 in CDCl_3 solution (100 MHz).	104
Figure 65. ^1H NMR spectrum of 122 in CDCl_3 solution (400 MHz).	105
Figure 66. ^{13}C NMR spectrum of 122 in CDCl_3 solution (100 MHz).	105
Figure 67. ^1H NMR spectrum of 123 in CDCl_3 solution (400 MHz).	106
Figure 68. ^{13}C NMR spectrum of 123 in CDCl_3 solution (100 MHz).	106
Figure 69. ^1H NMR spectrum of 124 in CDCl_3 solution (400 MHz).	107
Figure 70. ^{13}C NMR spectrum of 124 in CDCl_3 solution (100 MHz).	107
Figure 71. ^1H NMR spectrum of 124 in CDCl_3 solution (400 MHz).	108
Figure 72. ^{13}C NMR spectrum of 124 in CDCl_3 solution (100 MHz).	108

LIST OF ABBREVIATIONS

NLO:	Nonlinear optics
EDG:	Electron donating group
ICT:	Intramolecular charge-transfer
CuAAC:	Copper-Catalyzed Azide–Alkyne Cycloaddition
CA:	Cycloaddition
CA-RE:	Cycloaddition–Retroelectrocyclization
HT:	Head to Tail
HH:	Head to Head
DDQ:	2,3-Dichloro-5,6-dicyano-1,4-benzoquinone
TCNE:	Tetracyanoethylene
TCNQ:	7,7,8,8-Tetracyanoquinodimethane
TCBD:	Tetracyanobutadiene
D-A:	Donor-Acceptor
DEA:	Diethylaniline
TD-DFT:	Time-dependent density functional theory
J:	Coupling constant
MHz:	Megahertz
M.p.:	Melting point
NMR:	Nuclear magnetic resonance

LIST OF SCHEMES

Scheme 1. Classical method of Huisgen 1,3-dipolar cycloaddition reactions.	5
Scheme 2. General representation of CuAAC reaction reported by Meldal et al. ...	5
Scheme 3. Pyrene based NLOphores reported by Liang et al.	6
Scheme 4. Discovery of the Diels-Alder Reaction.....	7
Scheme 5. Crosslinkable NLOphore dendrimers reported by Bae et al.....	7
Scheme 6. General representation of [2+2] photocycloadditions.	10
Scheme 7. Investigations to control streoselectivity by Cantrell et al.....	11
Scheme 8. Coumarin based NLO material reported by Essaïdi et al.	12
Scheme 9. Thermal [2+2] CA reaction scheme reported by Reinhoudt.....	13
Scheme 10. First examples of [2+2] cycloaddition reaction by using DDQ reported by a) Trofimov and b) Diederich.	14
Scheme 11. General representation of [2+2] CA-RE reaction.	15
Scheme 12. The first example of [2+2] CA-RE reaction reported by Bruce et al..	15
Scheme 13. Effect of the alkyne in [2+2] CA-RE reactions reported by Diederich.	18
Scheme 14. Proposed mechanism for [2+2] CA-RE reaction by Diederich et al. .	18
Scheme 15. Synthesis of 88	24
Scheme 16. Unsuccessful attempts towards to the synthesis of benzimidazole- containing push-pull NLOphores.	25
Scheme 17. Synthesis of <i>N,N</i> -diethyl-4-ethynylaniline (94).	26
Scheme 18. Synthesis of halogenated heterocycles.....	27
Scheme 19. Synthesis of heterocycle-substituted alkynes.....	28
Scheme 20. CA-RE transformations of heterocycle-based alkynes with TCNE. ..	29
Scheme 21. CA-RE reactions of heterocycle-based alkynes with TCNQ.....	30

CHAPTER 1

INTRODUCTION

The invention of the laser in the 1960s created a new research field, non-linear optics (NLO), that increased its significance and became more interesting over the years.¹ One of the sub-branches of modern physics, non-linear optics simply describes the light-matter interaction in nonlinear media. The applied light induces the polarization in matter, producing a nonlinear response depending on the power of the electric field of an optical wave.² Since nonlinearity can only be observed with intense light, the use of lasers is essential for nonlinear optics as they can have extremely high intensities.³

NLO plays a critical role in the development of modern technology as it has a wide range of applications such as telecommunications,⁴ data storage,⁵ real-time target recognition,⁶ optoelectronics,⁷ and optical signal processing⁸. NLO materials are classified into three groups according to the composition of these materials, namely inorganic, organic, and organometallic. In the early stages of the development, commercially produced NLO materials contained inorganic compounds. However, those materials had drawbacks such as higher dielectric constant and half-wave voltage and lower electro-optics coefficients.⁹ Due to the aforementioned disadvantages, the research direction was changed to developing organic nonlinear optical materials that can be used for the same objective.

Organic NLO materials have gained great importance in the area of nonlinear optics thanks to their advantages.¹⁰ For example, they possess smaller refractive indices, dielectric constants, and ultrafast response time due to the purely electronic origin of polarizability. Furthermore, the convenience of manufacturing and lower processing costs are some of the main advantages.¹¹ Many push-pull materials containing

electron donor and electron acceptor parts which are connected through a π -conjugated spacer are known for having nonlinear optical properties. Also, these types of materials are called push-pull NLOphores.¹² Several push-pull NLO materials have been synthesized, and their applications have been studied recently.

Examples of push-pull NLOphores, (*E*)-2-(3-(4-(4,5-diphenyl-1*H*-imidazol-2-yl)styryl)-5,5-dimethylcyclohex-2-en-1-ylidene)malononitrile (**1**)¹³, (*E*)-2-(3-(7-(diethylamino)-2-oxo-2*H*-chromen-3-yl)-1-phenylallylidene)malononitrile (**2**)¹⁴, (*E*)-4-(4-((2,6-diphenyl-4*H*-pyran-4-ylidene)methyl)styryl)pyrimidine (**3**)¹⁵, 2-((5-(1-methyl-1*H*-pyrrol-2-yl)-[2,2'-bithiophen]-5-yl)methylene)malononitrile (**4**)¹⁶, and 4-((7-((4,6-dimethylpyrimidin-2-yl)ethynyl)-9,9-dihexyl-9*H*-fluoren-2-yl)ethynyl)-*N,N*-dimethylaniline (**5**)¹⁷, were reported in the literature (Figure 1). Push-pull NLOphores can tolerate many functional groups such as alkenes, alkynes, ketones, amines, and heterocyclic groups (Figure 1).¹⁸

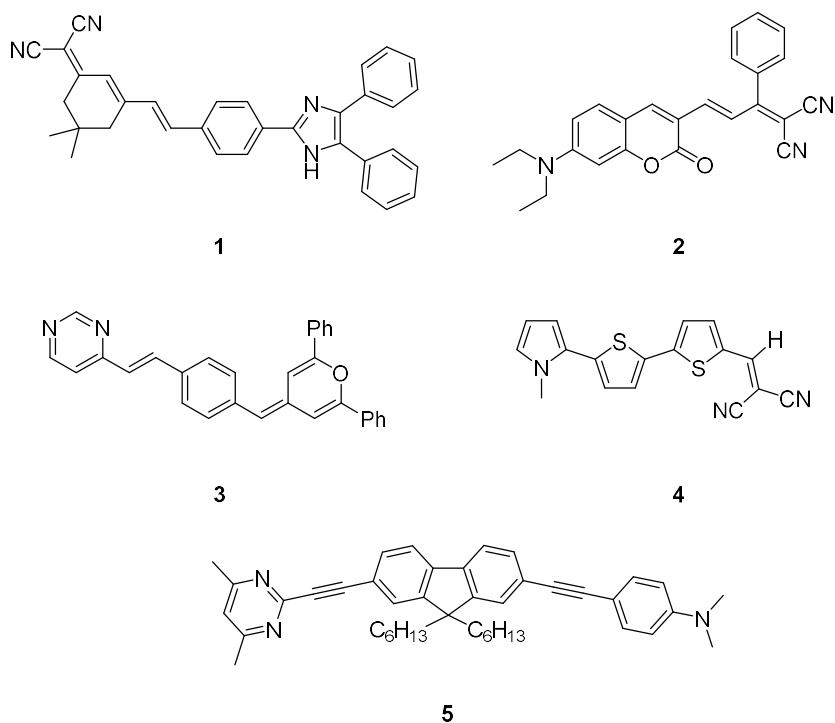


Figure 1. Examples of push-pull NLOphores reported in the literature.

Heterocycles are formed by combining atoms to form a ring structure, and the resulting cyclic molecules contain at least one non-carbon atom such as nitrogen (N), oxygen (O), and/or sulfur (S).¹⁹ The presence of heteroatom characteristically changes the physical and chemical properties of the molecule with respect to those of their all-carbon-ring analogs.²⁰ Due to distinctive properties, natural and synthetic heterocyclic compounds play an important role in chemistry. In addition to heterocyclic compounds found in natural products such as vitamins and natural antibiotics.^{20,21} There are heterocyclic molecules in biochemical materials necessary for life such as nucleic acids.²² Synthetic heterocycles have wide range of application areas that enable the development of modern society. For example, pharmaceuticals, agrochemicals and veterinary products²²⁻²⁴, sensitizers, antioxidants, copolymers, and dyes.^{16,22}

Heterocyclic compounds are of great importance in designing push-pull nonlinear optical materials. They have different electronic structures (electron rich or electron deficient) that can be used to tune optoelectronic properties of NLOphores.²⁵⁻²⁸ Figure 2 represents both electron-rich heterocycles, such as thiophene (**6**)²⁶, pyrrole (**7**)²⁶ and furan (**8**)²⁵ and electron-deficient heterocycles such as azole and azine derivatives^{25,27}, i.e., pyridine (**10**), thiazole (**11**) and triazole (**12**). In fact, heterocycles can be used as a π -bridge such as 2,5-dimethylthieno[3,2-*b*]thiophene (**9**).²⁸

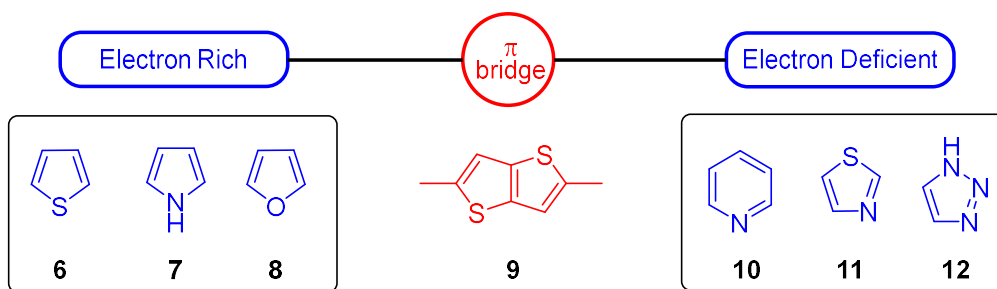


Figure 2. Examples of e⁻-rich, π -bridge, and e⁻-deficient heterocycles.

Many synthetic methods are available in the literature to design the desired heterocycle-based push-pull NLOphores. Synthetic methods involving cross-coupling reactions such as Stille²⁹, Suzuki³⁰, and Heck³¹ are generally used to synthesize these conjugated structures. However, these reactions require the usage of toxic metals and a large volume of solvent. The high cost makes these reactions disadvantageous, in addition to the long reaction time, instability of organometallic reagents, and low atom-economy.³² All these negative aspects have led researchers to develop green, environmentally-friendly methods. At this point, click chemistry is a good candidate for being an alternative approach to cross-coupling reactions because click-type reactions are known as eco-friendly, with relatively short reaction times.³³

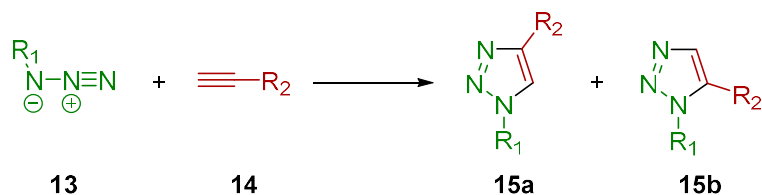
1.1 Click Chemistry

Click chemistry has significant impact on modern day organic chemistry. Kolb, Finn and Sharpless, who have mentioned the term “click chemistry” for the first time in 2001 called it “the reinvigoration of an old style of organic synthesis”, because this described new synthetic strategy is atom economic, regiospecific, and stereospecific with insensitivity to oxygen and water.^{33,34} Also, no by-product is formed or can be removed easily. Click-type reactions are performed under mild reaction conditions at room temperature, non-toxic solvent usage and using no catalyst. Reactions cover these criteria can be grouped under the term Click Chemistry.^{35,36} For example, Huisgen 1,3-dipolar cycloadditions and Diels-Alder cycloadditions are commonly known reactions, because these cycloadditions show most of the characteristics of click-type reactions.

1.1.1 Huisgen 1,3-dipolar Cycloaddition Reaction

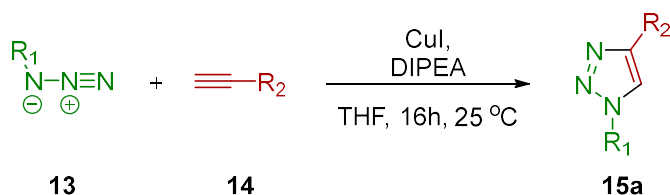
In 1960, Rolf Huisgen introduced the conceptual framework for 1,3-dipolar cycloadditions of azides **13** and alkynes **14** providing five-membered heterocycles

(**15a**, **15b**).³⁷ The classical Huisgen Azide–Alkyne Cycloaddition (AAC) reactions, with the final product 1,2,3-triazole ring take place at high temperatures and with long reaction times without copper catalyst. The absence of copper catalyst affected the selectivity and the products formed as a mixture of 1,4 (**15a**) and 1,5-triazole (**15b**) regioisomers when using asymmetric alkynes (Scheme 1).³⁸



Scheme 1. Classical method of Huisgen 1,3-dipolar cycloaddition reactions.

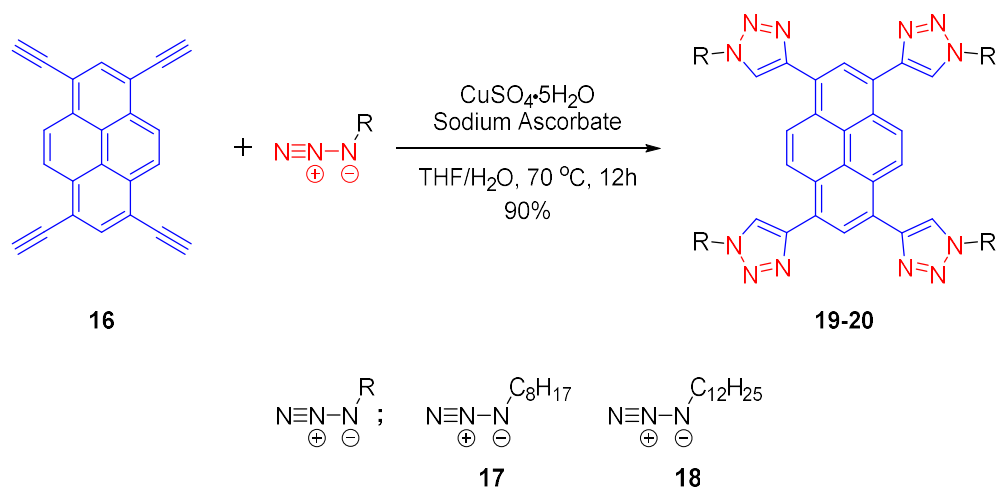
However, among the “click” criteria, selectivity of a reaction is one of the key elements. To improve regioselectivity, azide–alkyne cycloaddition (AAC) required modifications. In 2002, regioselective route for the synthesis of 1,2,3-triazoles was published by Meldal and his co-workers.³⁹ They reported that copper-catalyzed azide–alkyne cycloaddition (CuAAC) reactions proceed exclusively into the corresponding 1,4-disubstituted 1,2,3-triazoles under mild conditions (Scheme 2). Although catalyst-free reactions are desired in click chemistry, CuAAC reaction has taken its place among the most well-known click-type reactions because the copper catalyst is cheaper and less harmful compared to the other catalysts.³⁸



Scheme 2. General representation of CuAAC reaction reported by Meldal et al.

The selective and effective nature of CuAAC under mild reaction conditions has made it a practical method for the synthesis of heterocycle based NLO materials. For example, pyrene (**16**), 1,3-triazole ring-based small molecules **17** and **18** were synthesized by using CuAAC reaction and nonlinear optical properties of the

products were published by Liang et al. in 2015.⁴⁰ Two different pyrene derivatives were reported to be obtained in high yield by using $\text{CuSO}_4 \cdot 5\text{H}_2\text{O}$ as a catalyst (Scheme 3). On the top of that, these two electron-delocalized organic systems have third-order nonlinear optical response including the nonlinear absorption and nonlinear refraction which are investigated by Z-scan technique.



Scheme 3. Pyrene-based NLOphores reported by Liang et al.

1.1.2 Diels – Alder Reactions

In 1928, Professor Otto Diels and his student Kurt Alder made the discovery of [4+2] type cycloaddition reactions, known today as the Diels–Alder reaction. They obtained mono- **23** and diadduct **24** products as a result of the reaction between cyclopentadiene (**21**) and quinone (**22**) (Scheme 4).⁴¹ Over the years, the advantages of the Diels–Alder reaction such as being stereoselective, atom economic, and highly efficient has made it a powerful method in the synthesis of unsaturated 6-membered rings in organic chemistry.⁴² Therefore, the Diels–Alder reaction is one of the most widely used click-type reaction, especially in the total synthesis of natural products, as it fulfills the requirements of click chemistry.^{42,43}

1.2 Other Potential Pericyclic Reactions for the Synthesis of NLOphores

Although there are several applications of NLO materials synthesized by the above-mentioned click-type reactions, new synthetic methods have been sought due to some deficiencies of CuAAC and Diels–Alder reactions. For instance, the explosive nature of low molecular weight azides makes CuAAC reactions difficult to handle⁴⁵ and generation of the products that requires high temperature makes some cases of Diels–Alder cycloadditions undesirable.⁴⁶ [2+2] cycloaddition and [2+2] cycloaddition-retroelectrocyclization reactions can be good alternatives for the synthesis of NLOphores because of the attractive features of these transformations such as having high regio and stereoselectivity under mild conditions.⁴⁷

1.2.1 Photochemical [2+2] Cycloaddition Reactions

In the early 1960s, there was an obscurity for concerted reaction mechanisms among organic chemists. In fact, William von Eggers Doering, one of the well-known physical organic chemists at that time, gave the name “no-mechanism” to these reactions.⁴⁸ The term “no-mechanism” can be explained simply as a reaction that has no reactive intermediates.⁴⁹ In 1965, R.B. Woodward and R. Hoffmann published a series of papers, and their descriptions of the concept of orbital symmetry and the selection rules of concerted cycloadditions completely ended the "no-mechanism" understanding in the organic chemistry community in a very short time.^{48,50} Woodward and Hoffman explained the link between the mechanism of cycloaddition reactions and orbital symmetry in these papers. There was a selection rule for cycloaddition reactions. The occurrence of concerted cycloadditions depended on a "selection rule".⁴⁸⁻⁵¹ It was explained why some reactions can proceed in thermal conditions such as [4+2] cycloaddition (CA) and some in photochemical conditions such as [2+2] CA according to Woodward-Hoffmann rules. The overlapping of HOMO and LUMO was the key point for the result of the cycloaddition reactions (Figure 3).⁵¹

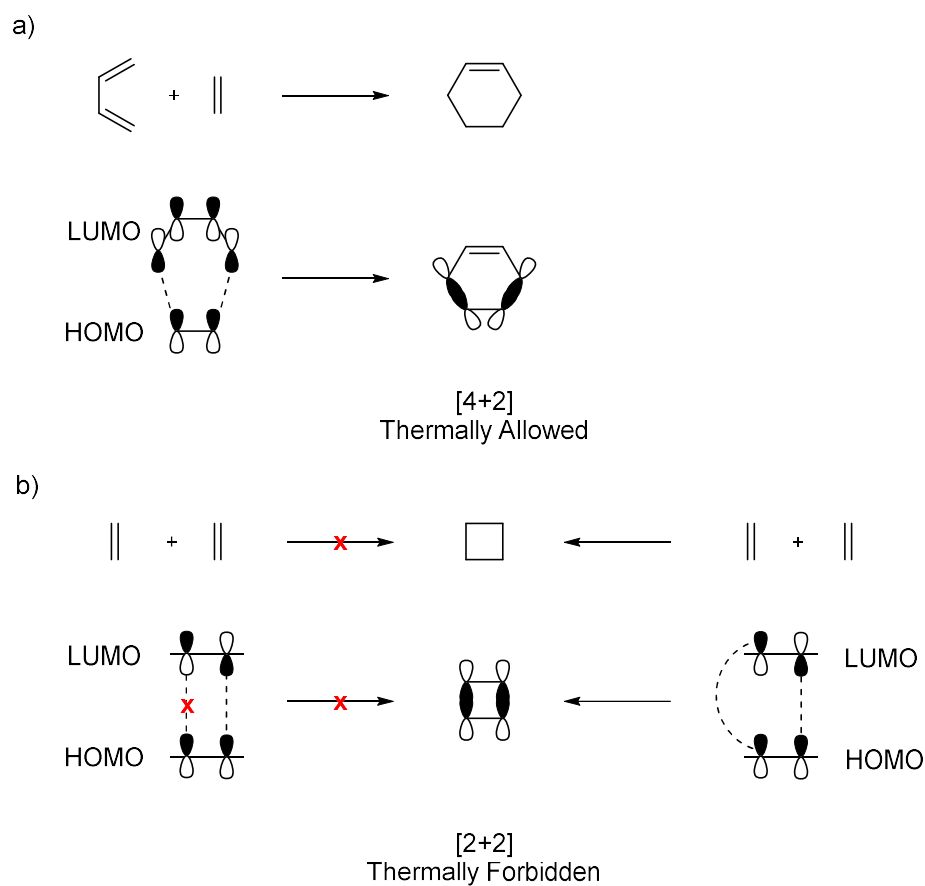
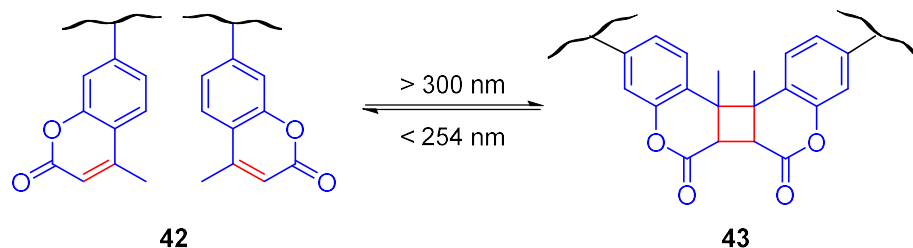


Figure 3. Thermally allowed (a) and forbidden (b) CA reactions.

In Figure 3a, it can be seen clearly HOMO of dienophile and LUMO of diene are overlapping with each other. Therefore, σ bond can be easily formed for [4+2] CA under thermal conditions. However, HOMO and LUMO do not overlap in the [2+2] cycloaddition (Figure 3b), and to achieve this overlapping, one electron in π orbital must be transferred to the σ^* . The reaction is considered thermally forbidden because the energy required for this transfer cannot be supplied under thermal conditions. The Woodward-Hoffmann rules say that [2+2] cycloaddition occurs only under photochemical conditions, thanks to the excitation of an electron and overlapping of HOMO and LUMO.^{50,51}

strategies.⁵⁸ Moreover, photoresponsive non-linear optical materials can be obtained by using [2+2] photocycloaddition reactions.

In 2012, Essaïdi and co-workers⁵⁹ published an article about NLO properties of photocross-linkable coumarin based polymers. In this paper, 4-methyl coumarin based copolymers **42** were synthesized and irradiated using two different wavelengths to obtain the reversible photocross-linked dimerization of coumarin adducts **43** (Scheme 8). They reported remarkable effect on the NLO response of the corresponding NLOphore based copolymer. Also, large second harmonic generation (SHG) response of this material is shown in the paper.

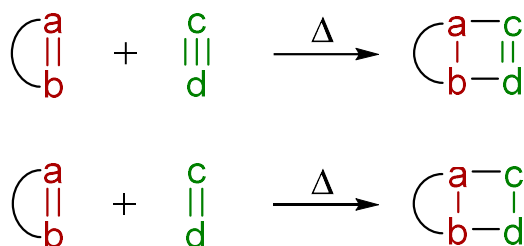


Scheme 8. Coumarin based NLO material reported by Essaïdi et al.

1.2.2 Thermal [2+2] Cycloaddition Reactions

Regardless of the Woodward Hoffmann rules, the statement of [2+2] cycloaddition reactions cannot proceed under thermal conditions was disproved by Reinholdt in 1974. According to his study, [2+2] cycloaddition reactions are thermally allowed depending on reactants that are strongly polarized and have difference in electron densities.⁶⁰ A related reaction, given in Scheme 9, is thermal cycloaddition between alkene-alkyne or alkene-alkene to give cyclobutene and cyclobutane substrates respectively. Many studies have been carried out to understand whether the σ bond formation in thermally allowed [2+2] cycloadditions take place *via* concerted or

stepwise mechanism.^{61,62} Epiotis's theory of mechanism satisfied most of the reported [2+2] thermal cycloaddition reactions. He claimed that the activation energy must be lowered for the reaction to take place in a concerted manner under mild conditions, and that this can only happen when one of the reactants has electron donor group and other has an electron acceptor group.

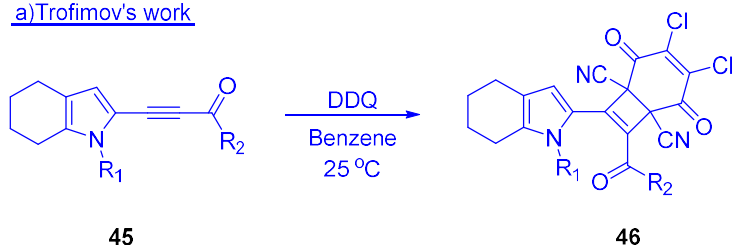


Scheme 9. Thermal [2+2] CA reaction scheme reported by Reinhoudt.

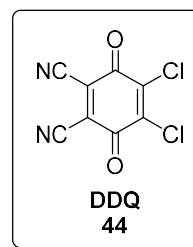
Over the years, thermally allowed [2+2] CA reactions have been reported in the literature using wide range of substrates. An interesting example is the discovery of the utilization of 2,3-dichloro-5,6-dicyano-1,4-benzoquinone (DDQ) **44** as a [2+2] CA reagent. It is an interesting example because until Trofimov's discovery in 2010, DDQ was known as a powerful oxidizing agent for dehydrogenation reactions and also was mainly used for aromatization reactions.⁶³ Trofimov reported that when tetrahydro-indole substituted alkyne derivative **45** treated with DDQ, homoconjugated [2+2] cycloadduct **46** was formed unexpectedly (Scheme 10a).⁶⁴ Almost at the same time, Diederich group's study reported that reaction between DDQ and electron-rich alkynes **47** provided cycloadduct **48** as well (Scheme 10b).⁶⁵ Diederich's work is important not only because he brought a new D- π -A systems to the literature by using DDQ, but also because the homoconjugated push-pull molecules have promising third-order nonlinear optical properties. Nevertheless, there are not enough studies focusing on substrate scopes or application areas in the literature for synthesizing NLOphores *via* [2+2] Cycloadditions. The main reason

behind this is that electron-rich alkyne substrates generally cannot be stored for long period of time due to stability problems.

a) Trofimov's work



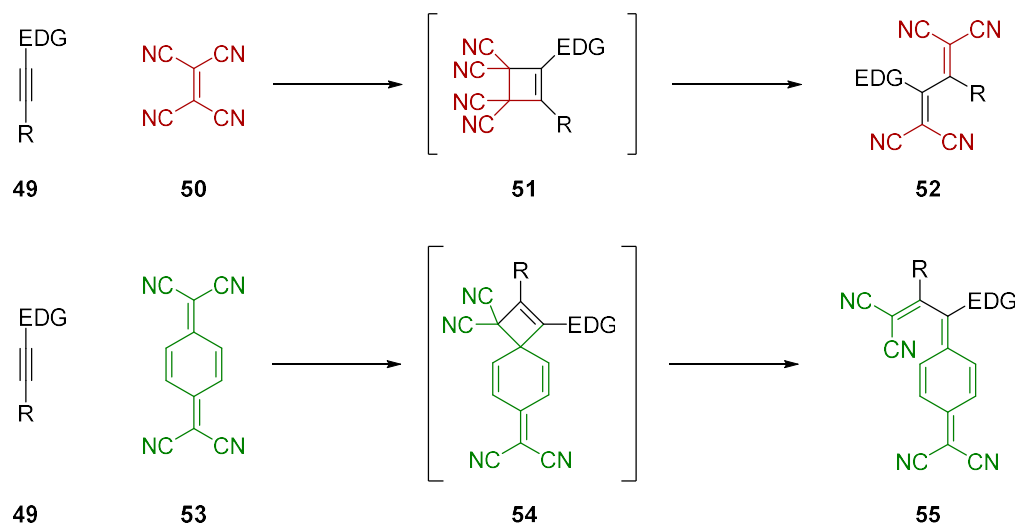
b) Diederich's work



Scheme 10. First examples of [2+2] cycloaddition reaction by using DDQ reported by a) Trofimov and b) Diederich.

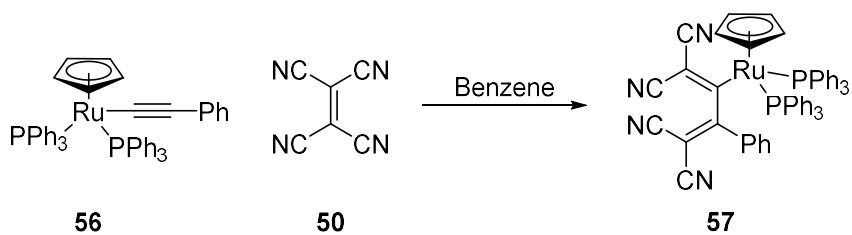
1.2.3 [2+2] Cycloaddition – Retroelectrocyclization (CA-RE) Reactions

[2+2] Cycloaddition-retroelectrocyclization (CA-RE) reaction is another click-type reaction used to obtain NLOphores. Synthesizing molecules with strong, low energy intramolecular charge transfer (ICT) bands is an important strategy because this type of reaction has many advantages as mentioned earlier. General representation of [2+2] CA-RE reaction is given in Scheme 11. Reaction starts with electron-rich alkyne and electron-deficient alkene such as tetracyanoethylene (TCNE) **50** and 7,7,8,8-tetracyanoquinodimethane (TCNQ) **53** forms an unstable cycloadduct **51** and **54**, then results in a 1,1,4,4-tetracyanobuta-1,3-diene (TCBD) derivative **52** and TCNQ adduct **55** by the retroelectrocyclization reaction (Scheme 11).



Scheme 11. General representation of [2+2] CA-RE reaction.

The existence of [2+2] CA-RE reactions in the literature has a history of more than 40 years. In 1981, the initial reports of this reaction were published by Bruce and co-workers.⁶⁶ Their study indicated that the reaction between Ru acetylide **56** and TCNE **50** was terminated with the formation of an orange colored TCBD derivative **57** (Scheme 12).



Scheme 12. The first example of [2+2] CA-RE reaction reported by Bruce et al.

Despite the fact that final TCBD product was confirmed by X-Ray crystal-structure analysis the reaction mechanism was not fully understood. Fortunately, in subsequent reports using tungsten, iron and nickel, the cyclobutene intermediate was isolated and characterized.^{67,68} Then, these intermediates transformed into the corresponding TCBD derivatives **58**, **59** and **60** under mild conditions (Figure 4).

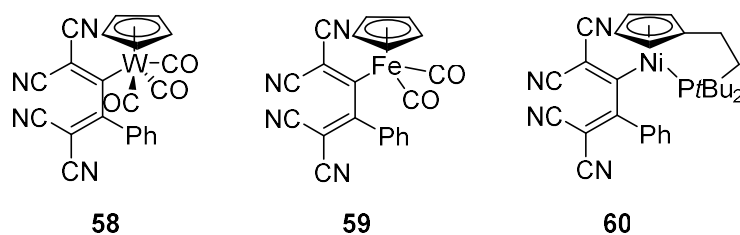


Figure 4. Investigated other transition metal (W, Fe and Ni) TCBD derivatives.

One of the important studies in this area was published by Takashi et al. in 1999.⁶⁹ Pt (II) acetylide derivatives were treated with TCNE and the resulting TCBD moieties were *s*-cis **61** or *s*-trans **62** conformers (Figure 5). Structures were confirmed using X-ray diffraction data and spectral analysis, but the mechanism remained unclear. However, it was explained by Takashi that the reason behind structural distinction is due to the bulkiness of the substituents attached to the Pt atom.⁶⁹

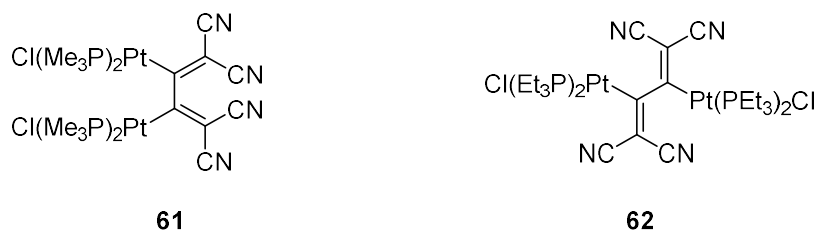


Figure 5. TCBD derivatives reported by Takashi et al. in 1990.

In the same year as Takashi's work, the first purely organic TCBD derivatives were reported independently by Jen and Sutter groups.^{70,71} Not only highly efficient, thermally, and chemically stable TCBD chromophores **63** and **64** were synthesized (Figure 6), but also nonlinear optical properties of these structures were investigated. Therefore, the work of Jen and Sutter has a significant place in the history of [2+2] CA-RE reactions. Until 2005, each of these early reports were of some interest, but none of them provided adequate explanations about how alkyne structure affects reactivity and overall yields.

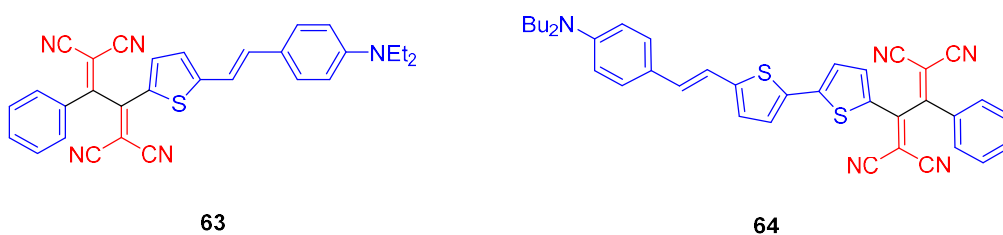
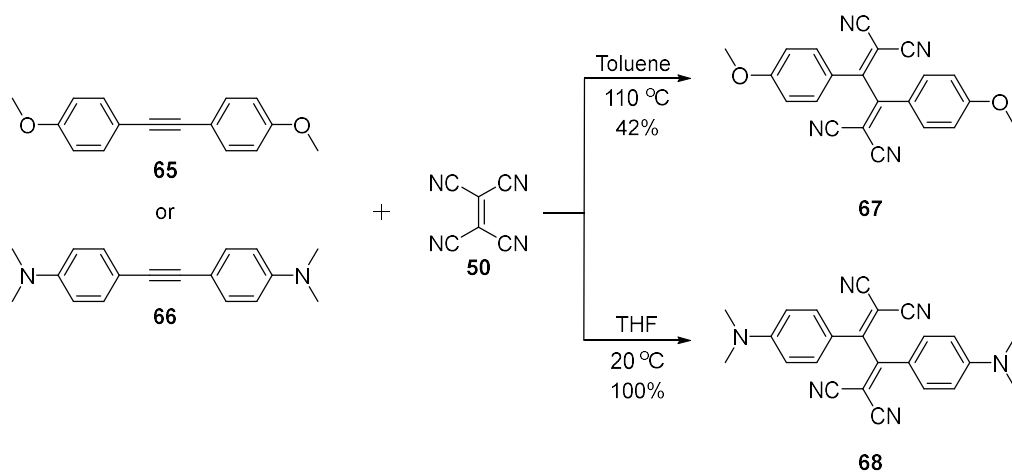


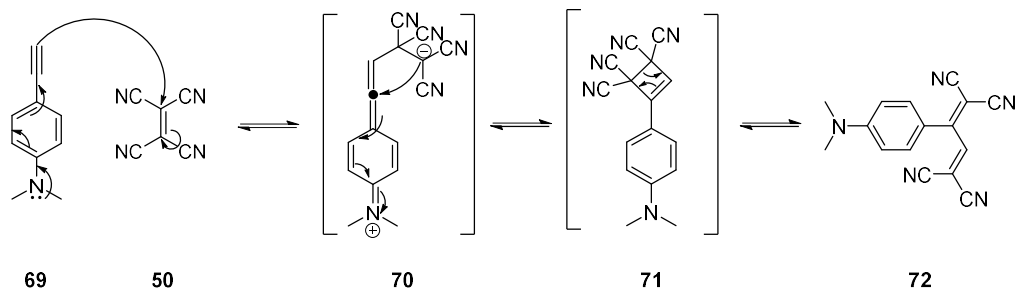
Figure 6. Examples of first purely organic NLOphores.

In 2005, Diederich's group published a paper that focused on the reactions of *p*-methoxyphenyl (**65**) and *p*-*N,N*-dimethylanilino (DMA) (**66**) substituted alkynes with TCNE in conjunction with the efficiencies of synthesized TCBD derivatives **67** and **68** to examine the effect of alkyne groups.^{72,73} Although this *p*-methoxyphenyl group is classified as a strong donor in organic chemistry, it failed to activate the alkyne group under mild conditions. For this reason, the reaction between *p*-methoxyphenyl attached alkyne and TCNE was carried out at high temperature, but the desired TCBD product was obtained in 42% yield (Scheme 16). In contrast, the reaction with DMA substituted alkyne and TCNE turned into the corresponding TCBD product quickly without by-product formation and was isolated in 100% yield (Scheme 13).



Scheme 13. Effect of the alkyne in [2+2] CA-RE reactions reported by Diederich.

In addition to investigating the effect of alkyne groups, Diederich et al. proposed the mechanism for [2+2] CA-RE transformations in 2007.⁷⁴ They stated that the reaction starts with nucleophilic addition of the terminal alkyne **69** to electrophile **50** to produce zwitterionic high-energy intermediate **70**, before cyclobutene formation **71** (Scheme 14).



Scheme 14. Proposed mechanism for [2+2] CA-RE reaction by Diederich et al.

Furthermore, starting from 2005, Diederich reported push pull systems synthesized by using [2+2] CA-RE with strong NLO properties.^{75,76} Associated with the presence of potential application areas, this “click-type” transformations are very advantageous because reactions are usually conducted at ambient temperature, no catalyst is required, using nontoxic solvents or without solvents and ended up with high yields without the formation of by-products. Over the years, due to aforementioned facts, the importance of this type of chromophores synthesized using [2+2] cycloaddition-retroelectrocyclization reactions have been realized in the chemistry community and has led to the improvement of substrate scope of push-pull chromophores. Thus, researchers are conducting studies to synthesize the most efficient chromophores and to expand their application areas by finding suitable substrates with donor groups and/or synthesizing new substrates with electron acceptor groups.

From the first papers until now, the substrate scope of appropriate donor structures has been expanded. For example, azulene derivatives **73**⁷⁷, indole derivatives **74**⁷⁸, ferrocene derivatives **75**⁷⁹, BODIPY derivatives **76**⁸⁰ and triazene derivatives **77**⁸¹ are some of the reported examples (Figure 7).

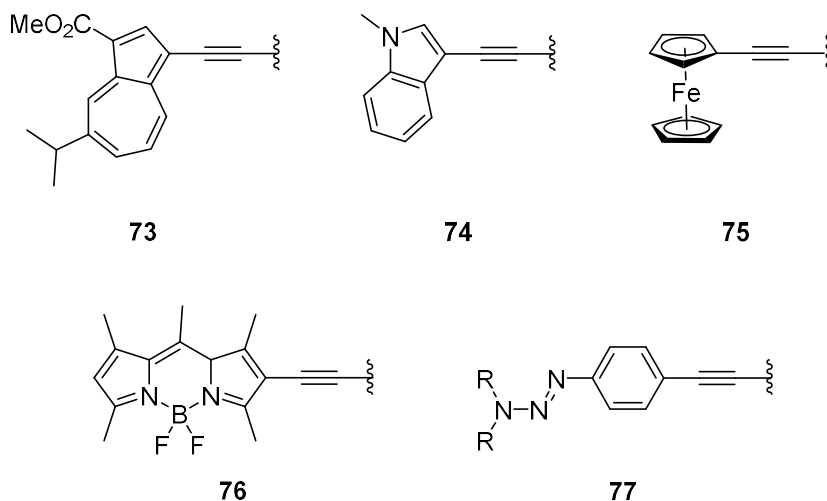


Figure 7. Various alkyne structures used in [2+2] CA-RE reactions.

Interestingly, even if a strong donor group is used, the substitution position of alkyne affects the reactivity. In case of carbazole derivative (Figure 8), when the alkyne is at the 1- and 3- position **78** and **79**, reaction proceeds under mild conditions. On the contrary, when it is attached at the 2- position **80**, high temperature is required to obtain TCBD derivatives. Thus, it shows that 1- and 3- substituted carbazole derivatives are more reactive.⁸²

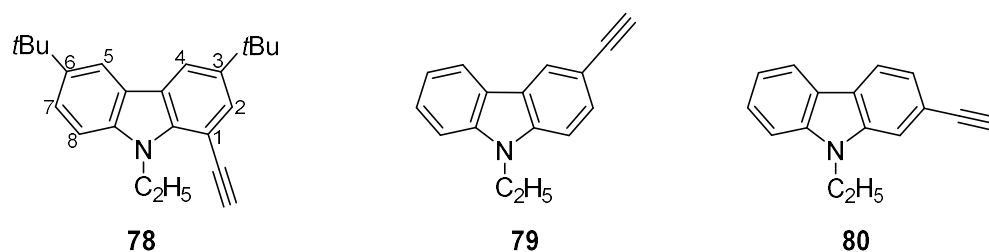


Figure 8. Examples of carbazole derivatives that have different reactivities.

The reported donor groups were treated with acceptor groups for the formation of new TCBD derivatives.⁸³ The most common and commercially available electron-deficient olefins are TCNE **50**, TCNQ **53**, and 2,3,5,6-tetrafluoro-TCNQ (F₄TCNQ) **81** (Figure 9).^{81,84}

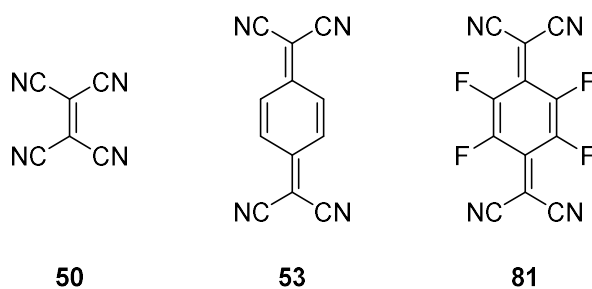


Figure 9. Commercially available acceptors used in [2+2] CA-RE transformations.

In addition to the commonly used acceptors, designing and synthesizing electron-poor structures has gained an interest for the development of [2+2] CA-RE reactions. Due to the strong electron-withdrawing properties of the cyanide, alkenes containing cyanide group come to the fore considering the reported structures.^{83,84} To illustrate, 2-(4-(dimethylamino)phenyl)ethene-1,1,2-tricarbonitrile (**82**)⁷⁴, ((3,6-bis(dicyanomethylene)cyclohexa-1,4-diene-1,4-diyl)bis(oxy))bis(ethane-2,1-diyl) dioctanoate (**83**)⁸⁵ and (*Z*)-2-(5-(4-(diethylamino)benzylidene)-4-phenylthiazol-2(*5H*)-ylidene)malononitrile (**84**)⁸⁶ are some of the examples of cyanide-based synthesized alkenes (Figure 10).

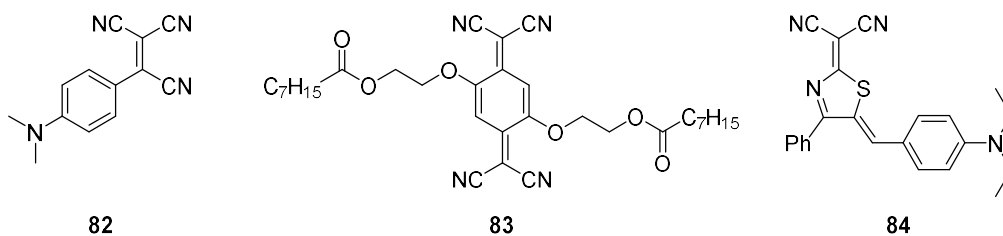


Figure 10. Cyanide-based electron deficient alkene examples.

1.3 Aim of Study

NLOphores with high intramolecular charge transfer (ICT) transitions are one of the most important building blocks for obtaining organic optoelectronic materials. To increase the NLO response rate and efficiency, the design of the molecules and the reaction conditions are very important. In order to produce these molecules in large scales for aforementioned application areas, the reaction should be carried out in high yields under mild conditions and, if possible, using of non-toxic solvents. At this point, “click chemistry” stands out as it meets all the requirements. Examples of click-type reactions that can be used are covered in this chapter. The second chapter of this thesis, concentrated on the synthesis of 14 different heterocycle-based push-

pull NLOphores using [2+2] cycloaddition-retroelectrocyclization reaction. ICT properties of synthesized TCBD derivatives were compared with UV/Vis data both experimentally and theoretically. In addition, the NLO responses of these heterocycle-based push-pull NLOphores were analyzed with a home-made Z-scan device.

CHAPTER 2

RESULTS AND DISCUSSION

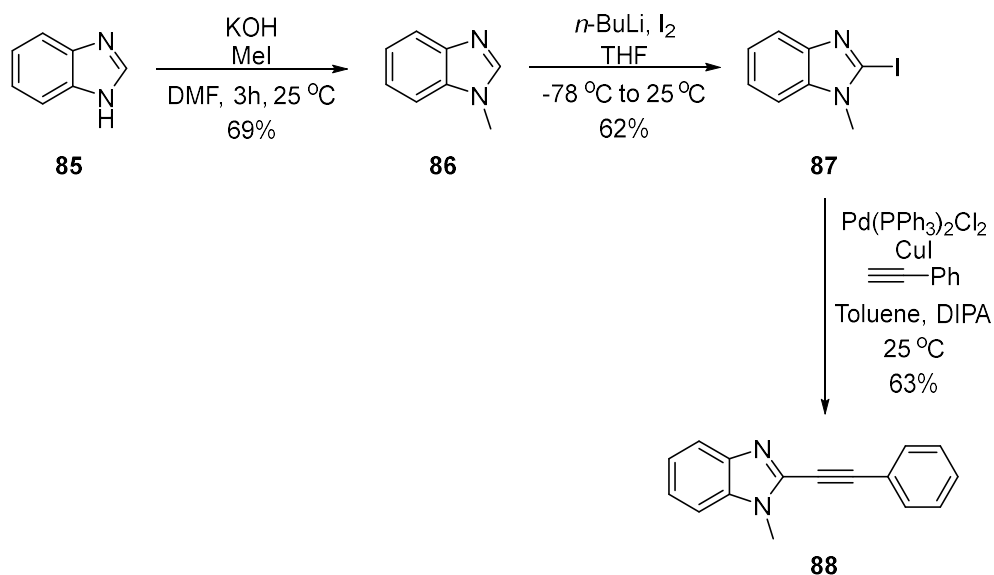
2.1 Design and Synthesis of Heterocycle-Based Push-Pull NLOphores using [2+2] Cycloaddition-Retroelectrocyclization Reactions

2.1.1 Synthetic Attempts Towards *N*-methylbenzimidazole-Substituted Push-Pull NLOphores

One of the key points in the design of push-pull type NLOphores is to find a group with high donor strength to be utilized in [2+2] CA-RE transformations. Although [2+2] CA-RE reactions have been studied for years, relevant donor groups are extremely limited. Recently, our group reported that indole, a heterocyclic compound, is a suitable donor group for above mentioned reactions.⁷⁸ The results were noteworthy because indole has never been tested in [2+2] CA-RE chemistry before. In the first phase of this thesis, our aim was to investigate whether the benzimidazole molecule could be used as an alternative donor group in CA-RE. The structural similarity between indole and benzimidazole was the sole motivation behind these investigations.

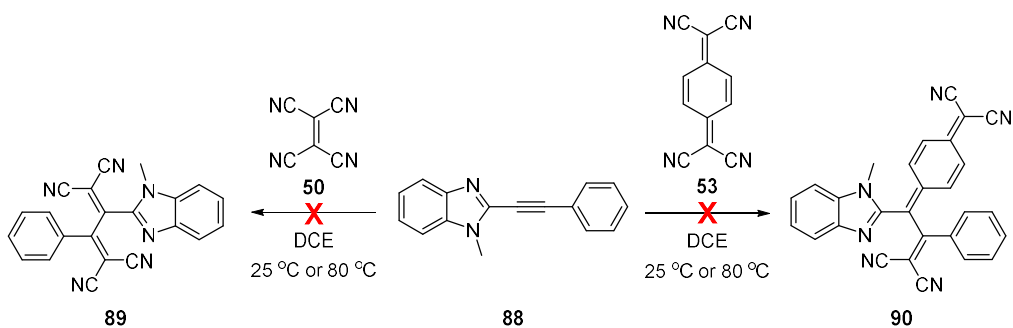
Synthesis of benzimidazole containing disubstituted alkyne proceeds in three steps (Scheme 15). Starting with commercially available benzimidazole **85**, *N*-methylbenzimidazole **86** was synthesized to protect the nitrogen by using KOH and MeI in 69% yield.⁸⁷ *N*-protection in benzimidazole was carried out considering the possibility of binding of acidic proton to the nitrogen lone pairs in the following steps.

In second stage, *N*-methylbenzimidazole was treated with *n*-BuLi and I₂ to obtain 2-iodo-*N*-methylbenzimidazole **87**.⁸⁸ The target iodine attached benzimidazole was isolated in moderate yield (62%). In the final step, to access benzimidazole containing disubstituted alkyne **88**, Sonogashira cross-coupling was performed successfully.



Scheme 15. Synthesis of **88**.

Compound **88** was obtained in 63% yield. NMR data was consistent with the data reported in the literature.^{89,90} Since the coupling product **88** has never been used as an electron-rich substrate for [2+2] CA-RE reactions before, we treated **88** with electron acceptor reagents TCNE **50** and TCNQ **53** to synthesize benzimidazole-containing push-pull NLOphores (Scheme 16). As shown in Scheme 16, reactions were carried out both at room temperature and elevated temperatures in dichloroethane (DCE). Nevertheless, the formation of target products **89** and **90** has not been observed.



Scheme 16. Unsuccessful attempts towards to the synthesis of benzimidazole-containing push-pull NLOphores.

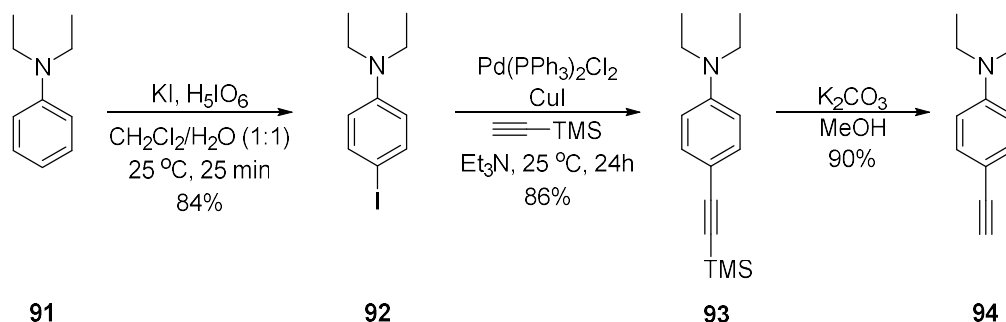
Failure of the target reaction with TCNE and TCNQ indicates that the benzimidazole scaffold does not have sufficient donor ability to activate the substrates for reaction. The fact that other benzimidazole-containing molecules reported in the literature do not have sufficient donor activity also confirms these results.^{91,92} Despite the high efficiency of the indole group⁷⁸ in similar reactions, the failure of benzimidazole made us think about the effect of heterocyclic groups on linear and nonlinear responses when designing push-pull NLOphores. To make this comparison, the alkyne group containing *N,N*-diethylaniline (**92**), a well-known strong electron donor, was chosen. In this way, the [2+2] CA-RE reaction will be activated smoothly and the effects of the heterocyclic groups used can also be discussed.

2.1.2 Synthesis of Heterocycle-Substituted Alkynes

2.1.2.1 Synthesis of *N,N*-diethyl-4-ethynylaniline

The diethylaniline (DEA) group, which is known as having high electron donor activity in the literature, was chosen for the reasons mentioned above.⁹³ Synthetic route for *N,N*-diethyl-4-ethynylaniline (**94**) is given in Scheme 17. First, 4-iodo-diethylaniline (**92**) was obtained starting from *N,N*-diethylaniline (**91**) by using KI and H₅IO₆.⁹⁴ Next, Sonogashira cross-coupling reaction was performed to attain

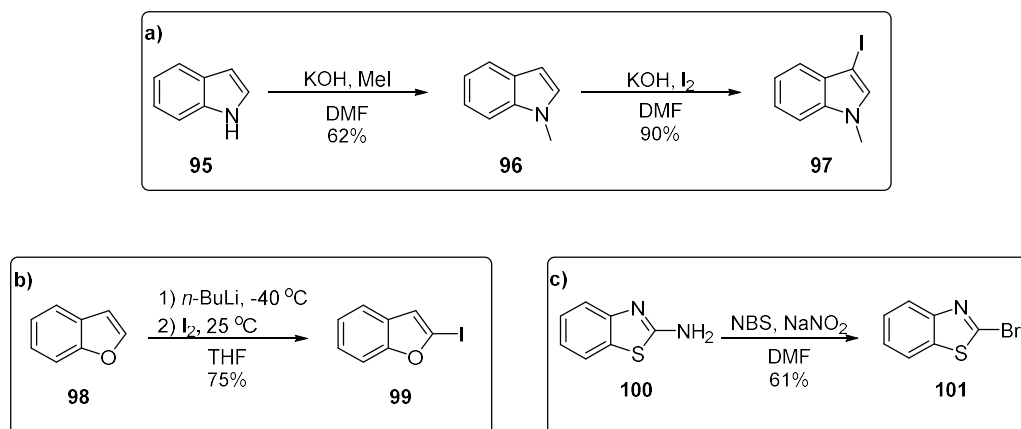
compound **93**. K_2CO_3 in MeOH was utilized at the last stage for TMS deprotection and compound **94** was isolated in 90% yield.⁹⁵



Scheme 17. Synthesis of *N,N*-diethyl-4-ethynylaniline (**94**).

2.1.2.2 Synthesis of Halogenated Heterocycle Groups

To carry out Sonogashira cross-coupling reaction between heterocyclic aryl halides and alkyne **94**, halogenation reactions were applied according to the literature procedures for the synthesis of four different substrates. In Scheme 15, iodination of *N*-methylbenzimidazole was demonstrated. 3-iodo-*N*-methylindole (**97**) was obtained in two steps (Scheme 18a). Starting with methylation reaction by using KOH and MeI in the first step, the target iodo-compound **97** was obtained with the help of KOH and I_2 in high yield.⁷⁸ Benzofuran (**98**) was treated with *n*-BuLi, I_2 , and 2-iodo-benzofuran (**99**) was obtained in 79% yield (Scheme 18b).⁹⁶ Lastly, the reaction between 2-amino-benzothiazole (**100**), NBS and $NaNO_2$ results in 2-bromo-benzothiazole (**101**) in 60% yield (Scheme 18c).⁹⁷



Scheme 18. Synthesis of halogenated heterocycles.

Besides halogenated benzimidazole, indole, benzofuran and benzothiazole derivatives, commercially available 2-iodothiophene (**102**), 2-bromoquinoline (**103**), and 2-iodopyridine (**104**) were used for Sonogashira cross-coupling step (Figure 11). To conclude, seven different types of halogenated heterocyclic molecules were used in Sonogashira cross-coupling reactions with DEA-substituted acetylene.

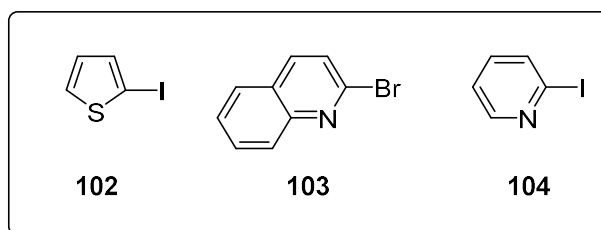
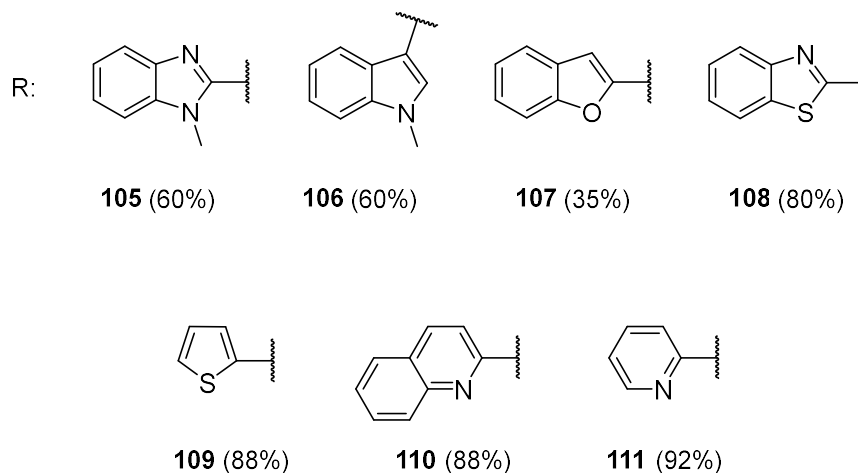
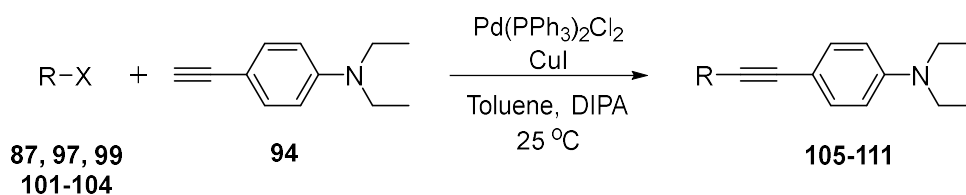


Figure 11. Commercially available halogenated heterocyclic compounds.

2.1.3 Coupling Reactions Between Heterocyclic Aryl Halides and DEA-Substituted Alkyne

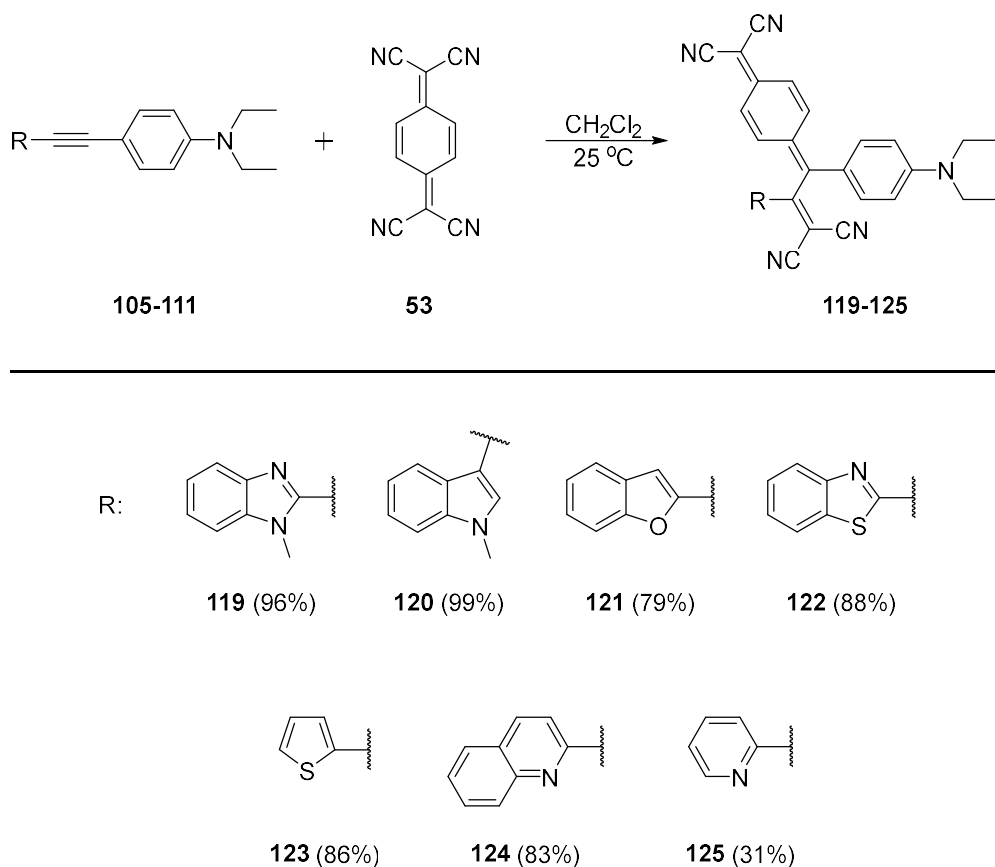
Sonogashira cross-coupling reactions were carried out between halogen attached heterocyclic groups **87**, **97**, **99**, **101-104** and alkyne **94** at room temperature in the presence of Pd and Cu catalysts. The coupling products **105-111** were isolated in 34-92% yields (Scheme 19). Stability of these compounds were quite high under ambient conditions. This observation was contrary to the common knowledge that electron-rich alkynes decompose easily.



X: I or Br

Scheme 19. Synthesis of heterocycle-substituted alkynes.

After target compounds **112-118** were effectively obtained using TCNE, we turned our attention to obtain seven additional NLOphores using another well-known electron acceptor TCNQ. Heterocycle containing electron-rich alkynes **105-111** reacted smoothly with TCNQ **53**, CA-RE products **119-125** were isolated high yields except for one example (Scheme 21). Although the reaction proceeded in high yield for compounds **119-124**, the pyridine containing NLOphore **125** was formed only in 30% yield. The reason is the isolation issues that we faced during the purification of compound **125**, therefore it is purified by precipitation method by using *n*-hexane. Due to the nature of the precipitation technique, the large amount of material may be lost, which explains why the isolated yield is low for compound **125**.



Scheme 21. CA-RE reactions of heterocycle-based alkynes with TCNQ.

When unsymmetrical alkynes treated with TCNQ, theoretically there two different regioisomers (**120** and **120'**) can be observed. Two possible regioisomers for indole derivative are shown in Figure 12. However, it was observed that only one isomer **120** was formed during the course of the reaction. This confirms that quinone ring stays closer to stronger donor group to increase the efficiency of intramolecular charge transfer.

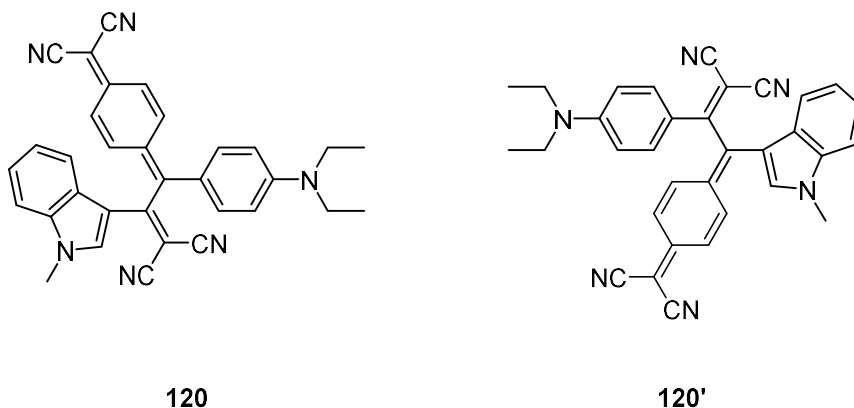


Figure 12. Possible regioisomers of indole containing scaffolds.

X-ray analysis was required to clarify precisely which isomer the resulting structure belongs to. According to the results obtained from X-ray studies, the formation of compound **120** was confirmed (Figure 13).

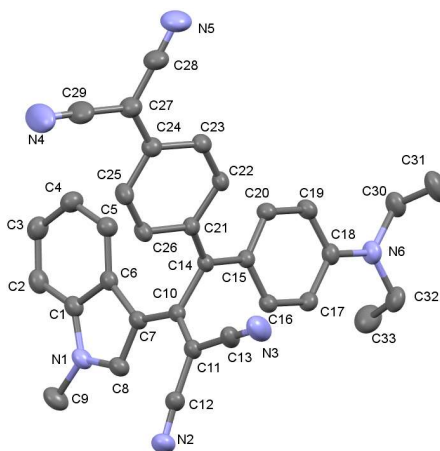


Figure 13. X-ray analysis of compound **120**.

2.2 UV-Vis Spectroscopy

As mentioned earlier in Chapter 1, intramolecular charge transfer (ICT) properties of push-pull NLOphores are distinct.^{11,12} To prove that the compounds **112-125** have intense ICT properties, UV-Vis spectroscopy is the most common and valid technique. UV-Vis spectra of TCNE products **112-118** are described in Figure 14. Each NLOphore have different color, and range of molar extinction values changed from 28054 M⁻¹cm⁻¹ to 41963 M⁻¹cm⁻¹. The strongest absorption wavelengths of TCNE compounds **112-118** are as follows; $\lambda_{\text{max}} = 424 \text{ nm}$ (32680 M⁻¹ cm⁻¹, for **112**), 475 nm (41963 M⁻¹ cm⁻¹ for **113**), 463 nm (30261 M⁻¹ cm⁻¹ for **114**), 466 nm (28677 M⁻¹ cm⁻¹ for **115**), 474 nm (33486 M⁻¹ cm⁻¹ for **116**), 460 nm (28200 M⁻¹ cm⁻¹ for **117**), and 470 nm (28054 M⁻¹ cm⁻¹ for **118**).

According to the spectral data, compounds **115**, **117** and **118** show weaker CT bands compare to other NLOphores ($\epsilon = 28677 \text{ M}^{-1} \text{ cm}^{-1}$, $28200 \text{ M}^{-1} \text{ cm}^{-1}$ and $28054 \text{ M}^{-1} \text{ cm}^{-1}$ respectively). Indole and thiophene groups are well-known as a donor group in the literature. Therefore, strong CT bands are actually expected from compound **113** ($41963 \text{ M}^{-1} \text{ cm}^{-1}$) and **116** ($33486 \text{ M}^{-1} \text{ cm}^{-1}$) due to enhanced D-A interactions. Moreover, molar extinction coefficient results of benzimidazole and benzofuran containing products **112** ($32680 \text{ M}^{-1} \text{ cm}^{-1}$) and **114** ($30261 \text{ M}^{-1} \text{ cm}^{-1}$) pointed the promising conjugation between donor and acceptor parts of the corresponding NLOphores. On the other hand, the hypsochromic shift was observed only for compound **112**. The reason behind this observation is the weak electron donating capability of benzimidazole unit which was explained in detail in section 2.1.1. Moreover, compounds **113** and **116**, which contain strong donor groups, shifted bathochromically as expected.

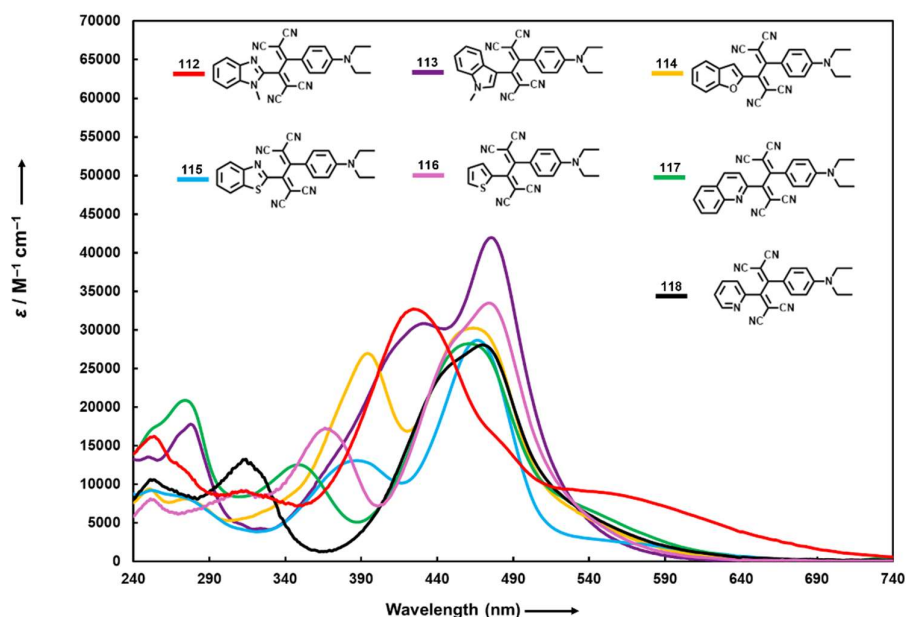


Figure 14. UV/Vis spectra of heterocycle-based push-pull NLOphores **112** (red line), **113** (purple line), **114** (yellow line), **115** (blue line), **116** (pink line), **117** (green line), and **118** (black line) in CH_2Cl_2 at 298 K.

Furthermore, quinoline containing TCNE product **117** was chosen for further solvatochromic study. Compound **117** significantly shifted (approx. 40 nm) from less polar solvent (*n*-Hexane) to more polar solvent (DCM) bathochromically (Figure 15). Corresponding bathochromic shift of compound **117** exhibits positive solvatochromism. This phenomena is another proof of ICT behavior of NLOphore **117**. The solvatochromic behavior of compound **117** was also studied in different solvents and positive solvatochromism was observed, similar to the previous case (Figure 16). In more polar solvents (EtOH and MeCN), bathochromic shift was observed compared to less polar solvents (Toluene and EtOAc).

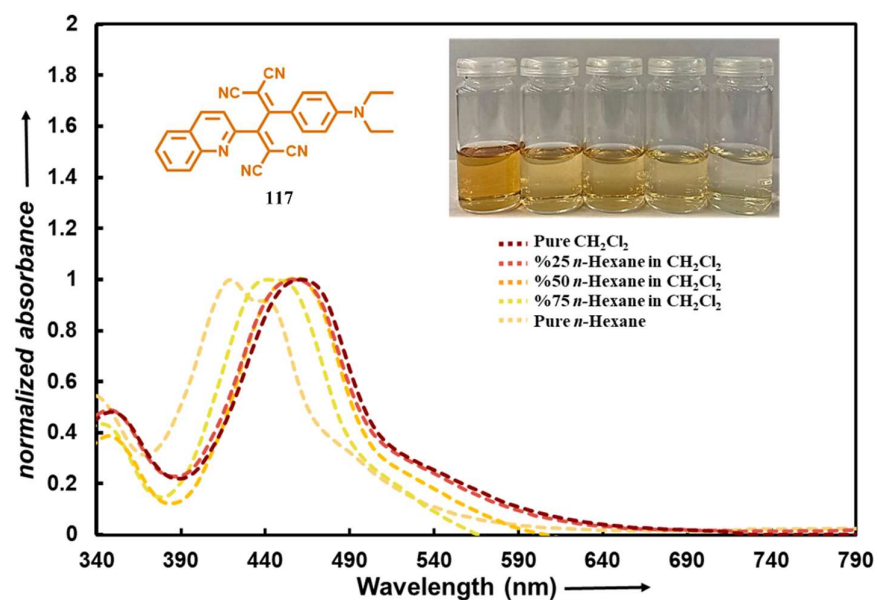


Figure 15. Solvatochromic study of compound **117** in the mixture of *n*-hexane/ CH_2Cl_2 .

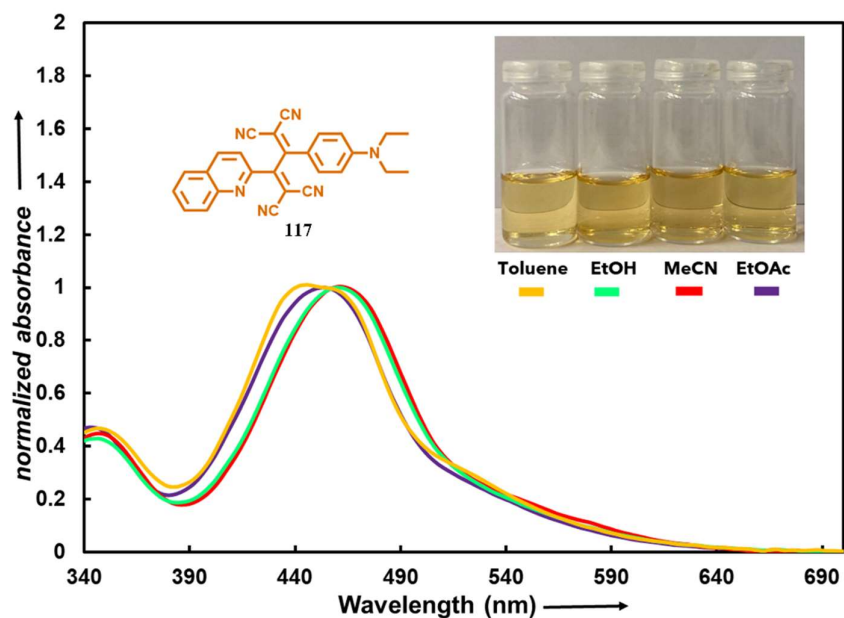


Figure 16. Solvatochromic study of compound **117** in toluene (yellow line), ethanol (green line), acetonitrile (red line) and ethyl acetate (purple line).

UV-Vis spectra of TCNQ products, push-pull NLOphores **119-125**, are shown in Figure 17. Each NLOphore have different color in the spectrum, and range of molar extinction values changed from 31907 M⁻¹cm⁻¹ to 51100 M⁻¹cm⁻¹. The strongest absorption wavelengths of TCNE compounds **119-125** are as follows; λ_{\max} = 758 nm (23833 M⁻¹ cm⁻¹ for **119**), 683 nm (51100 M⁻¹ cm⁻¹ for **120**), 694 nm (24308 M⁻¹ cm⁻¹ for **121**), 706 nm (27634 M⁻¹ cm⁻¹ for **122**), 683 nm (31907 M⁻¹ cm⁻¹ for **123**), 696 nm (26057 M⁻¹ cm⁻¹ for **124**), and 564 nm (9937 M⁻¹ cm⁻¹ for **125**).

The spectral data indicates that compound **125** show weakest CT bands among all TCNQ products ($\epsilon = 9398$ M⁻¹ cm⁻¹). Similar to TCNE products, indole and thiophene attached compounds **120** (51100 M⁻¹ cm⁻¹) and **123** (31907 M⁻¹ cm⁻¹) exhibit strong CT bands. The significant bathochromic shift was observed for compound **119** ($\lambda_{\max} = 758$ nm).

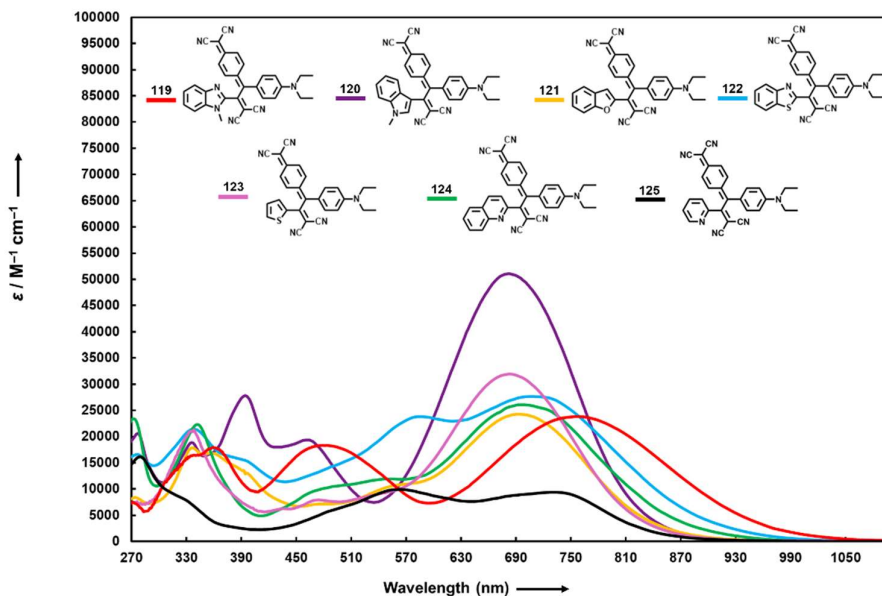


Figure 17. UV/Vis spectra of heterocycle-based push-pull NLOphores **119** (red line), **120** (purple line), **121** (yellow line), **122** (blue line), **123** (pink line), **124** (green line), and **125** (black line) in CH₂Cl₂ at 298 K.

Quinoline containing TCNQ product **124** was selected for solvatochromic study. Compound **124** significantly shifted (approx. 100 nm) from less polar solvent (*n*-Hexane) to more polar solvent (DCM) bathochromically (Figure 18). Compound **124** also exhibits positive solvatochromism similar to its TCNE counterparts. All these results additionally confirm ICT properties of obtained NLOphores. Positive solvatochromism was also observed when the absorption spectrum of **124** was measured in solvents with different polarities (Figure 19). In more polar solvents (EtOH and MeCN), bathochromic shift was observed compared to less polar solvents (Toluene and EtOAc).

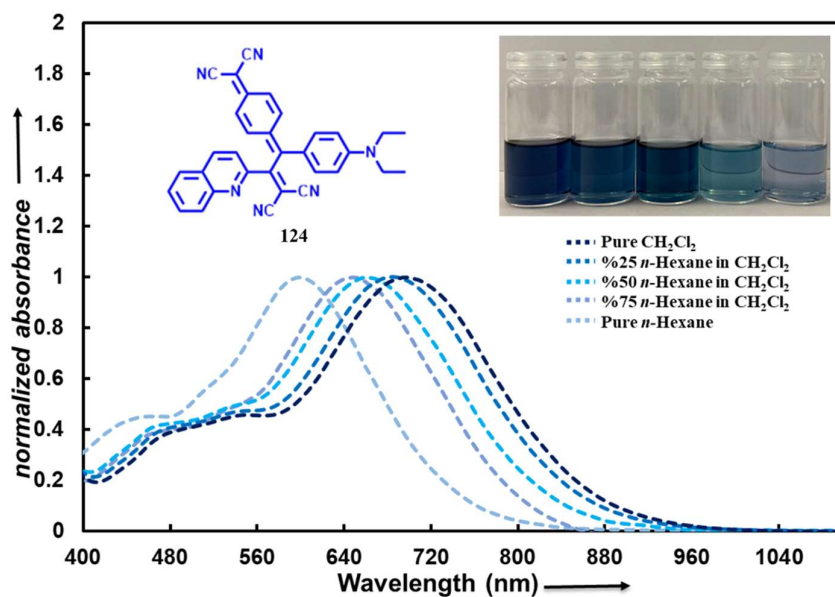


Figure 18. Solvatochromic study of compound **124** in the mixture of *n*-hexane/CH₂Cl₂.

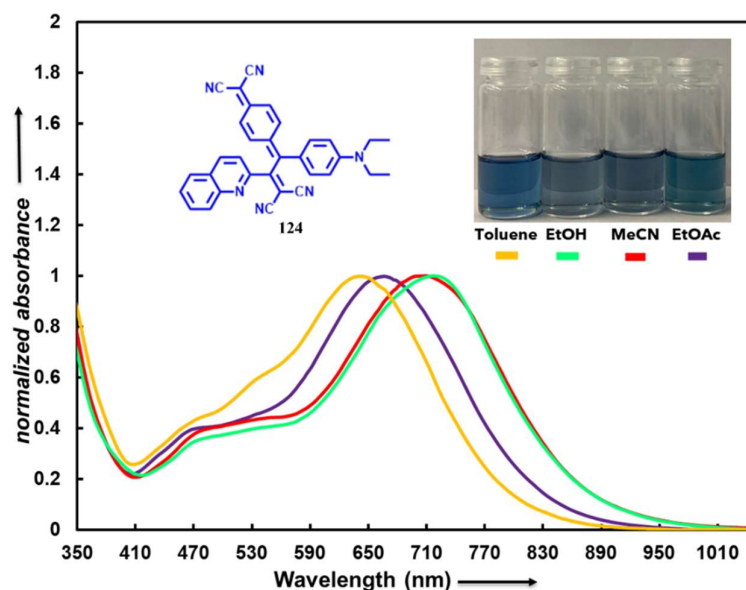


Figure 19. Solvatochromic study of compound **124** in toluene (yellow line), ethanol (green line), acetonitrile (red line) and ethyl acetate (purple line).

2.3 Theoretical Calculations

Computational study is another method to prove ICT properties of push-pull NLOphores. Since distribution of HOMO and LUMO orbitals can be calculated by theoretical approach, the charge transfer efficiency in a molecule can be explained. This efficiency can be interpreted by the overlap between the HOMO and LUMO depictions. Small overlap between these orbitals is another proof of highly efficient ICT behaviour. Geometry optimizations of all TCNE and TCNQ products were done by using B3LYP/6-31G(d) level of theory with the CPCM solvation model in CH_2Cl_2 at Gaussian09 software.⁹⁸ HOMO and LUMO depictions of TCNE and TCNQ NLOphores **112-125** are shown in Table 1 and Table 2. These depictions are proof of displaying the ICT properties of corresponding NLOphores. Moreover, electrostatic potential map (ESP) supports donor-acceptor characteristics of compounds **112-125**.⁹⁹ The regions with high electron density, shown in red color, are clustered around -cyano rich electron-acceptor groups. Similarly, the heterocycle

and diethylaniline units, which have low electron density since their electrons are withdrawn, are shown in blue color.

Table 1. HOMO-LUMO representations and electrostatic potential map (ESP) of TCNE compounds **112-118**.

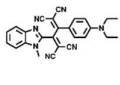
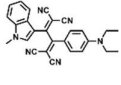
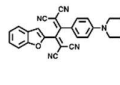
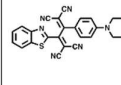
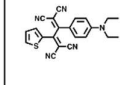
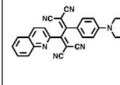
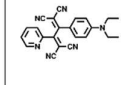
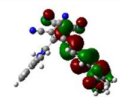
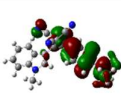
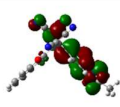
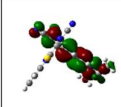
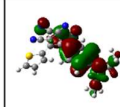
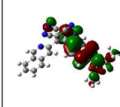
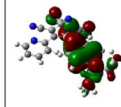
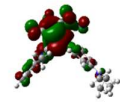
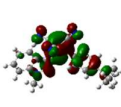
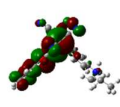
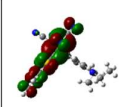
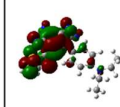
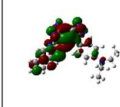
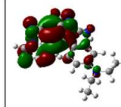
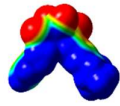
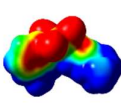

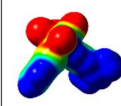
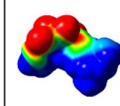
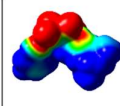
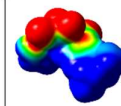
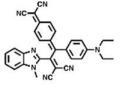
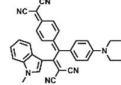
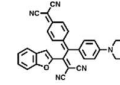
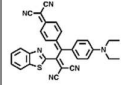
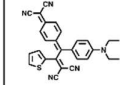
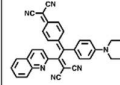
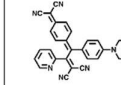
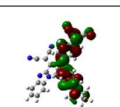
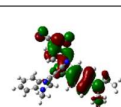
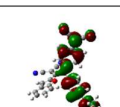
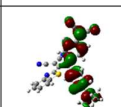
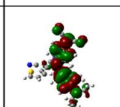
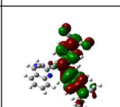
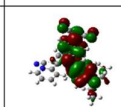
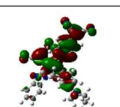
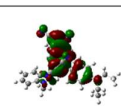
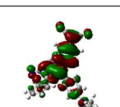
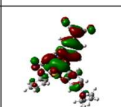
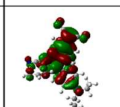
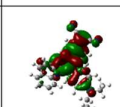
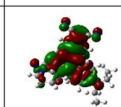
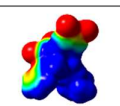
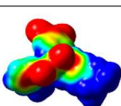
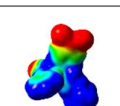
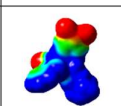
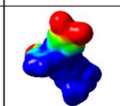
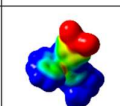
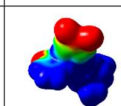
	112	113	114	115	116	117	118
<i>Molecular Structure</i>							
<i>HOMO</i>							
<i>LUMO</i>							
<i>ESP</i>							

Table 2. HOMO-LUMO representations and electrostatic potential map (ESP) of TCNQ compounds **119-125**.

	119	120	121	122	123	124	125
<i>Molecular Structure</i>							
<i>HOMO</i>							
<i>LUMO</i>							
<i>ESP</i>							

Furthermore, energy level diagrams of HOMO-LUMO bands of all compounds **112-125** are displayed in Figure 20. The range of ΔE ($E_{\text{HOMO}} - E_{\text{LUMO}}$) values of compounds changes from 3.79 eV to 5.05 eV. Accordingly, TCNQ products **119-125** have smaller band gap compared to TCNE products **112-118**. These results confirm the enhanced efficiency of CT in the case of TCNQ products.

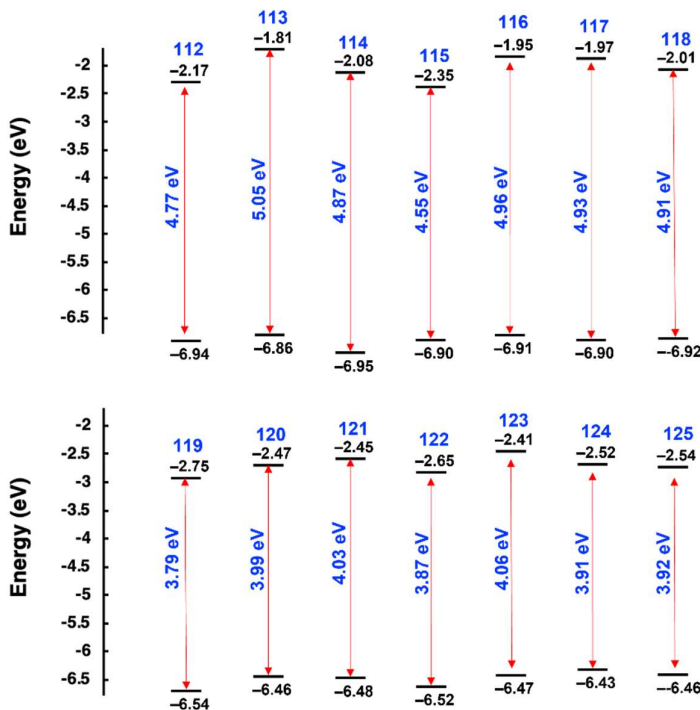


Figure 20. Energy level diagrams of compounds **112-125**.

Additionally, vertical optical transitions of synthesized push-pull NLOphores were calculated by using TD-DFT (Time-Dependent Density Functional Theory) at the CAM-B3LYP/6-31G(d) basis set with the CPCM solvation model in CH_2Cl_2 . Theoretical and experimental UV-Vis spectra of benzofuran attached CA-RE products **114** and **121** were compared in Figure 21. To match the theoretical and experimental spectra wavelengths were shifted to the red region of 0.50 eV and 0.27 eV for compounds **114** (Figure 21a) and **121** (Figure 21b), respectively. At the same

time, compound **114** was scaled to 3.1 and the compound **121** to 3.2 for the same reason.

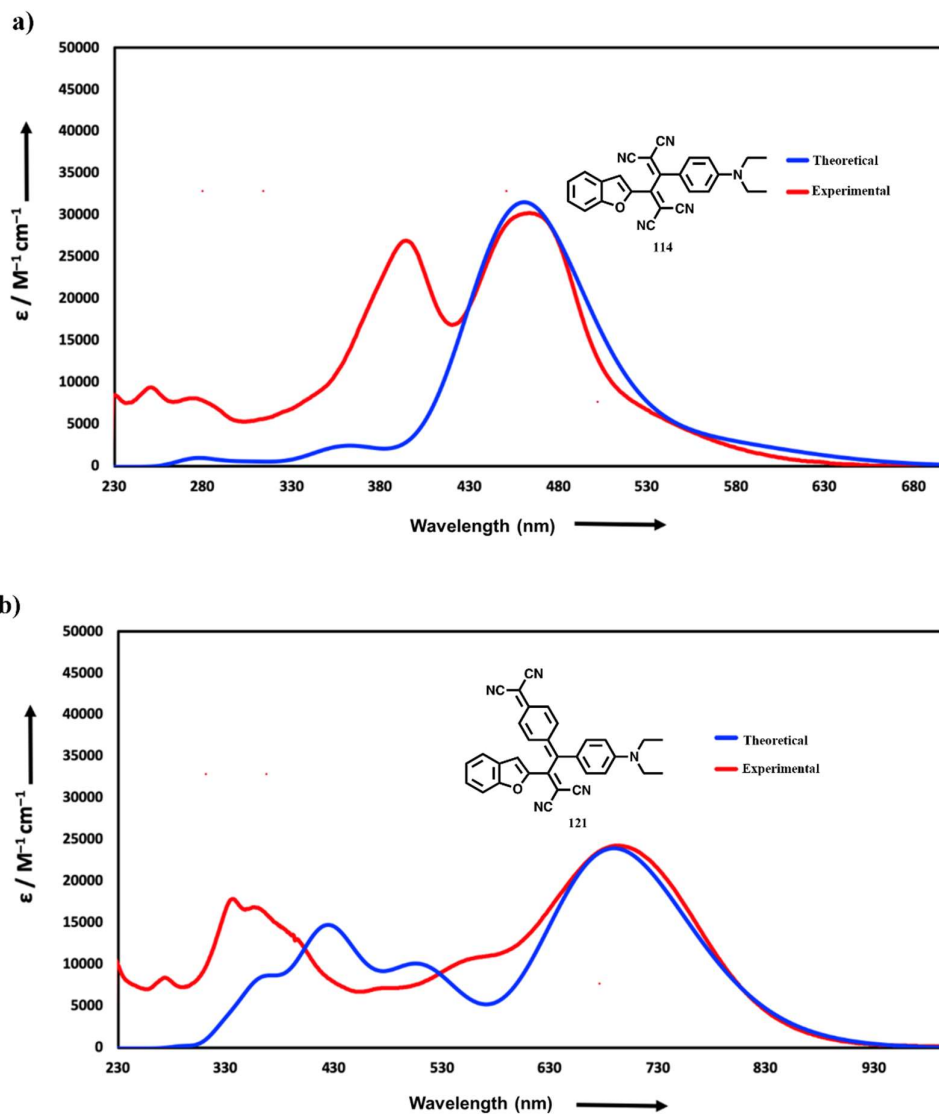


Figure 21. a) Calculated (red-shifted by 0.50 eV, scaled by 3.1, blue line) TD-DFT:CAM-B3LYP/6-31G(d) level of theory in CH_2Cl_2 and experimental UV/Vis spectrum of **114** in CH_2Cl_2 (red line). b) Calculated (red-shifted by 0.27 eV, scaled by 3.2, blue line) TD-DFT:CAM-B3LYP/6-31G(d) level of theory in CH_2Cl_2 and experimental UV/Vis spectrum of **121** in CH_2Cl_2 (red line)

Besides geometry optimization and vertical optical transitions measurements, theoretical studies were proceeded in detail by calculating some parameters. In these calculations, dipole moment (μ (D)), band gap $\Delta E(E_{\text{HOMO}} - E_{\text{LUMO}})$, electronegativity (χ), global chemical hardness (η) and softness (σ), average polarizability ($\alpha_{(\text{tot})}$), first hyperpolarizability ($\beta_{(\text{tot})}$) were investigated by using CAM-B3LYP/6-31G(d,p) level of theory in CH_2Cl_2 . Six different equations were used to calculate the parameters. Electric dipole moment calculations were utilized by using Equation 1. It can be clearly seen in the Tables 3&4, TCNE products **112-118** had lower value compared to TCNQ products **119-125**. To investigate the ionization potential and electron affinity, Koopmans' theorem was used (Equation 2) with the help of band gap energies. The global chemical hardness (η) was calculated by using Equation 3. Increase in the global chemical hardness means that difference in band gaps between HOMO and LUMO is large. Accordingly, global hardness values of TCNE products **112-118** are higher than TCNQ products **119-125** as expected. On the other hand, the softness of the NLOphores, which is calculated by Equation 4, increases when HOMO-LUMO gap decreases. Our results support this trend because softness values of the compounds **112-118** are higher compared to compounds **119-125** results. In general, the electronegativity, global chemical hardness and softness (Equation 2-4) was used to understand the chemical stability of the molecular structures.

$$\mu = [(\mu_x)^2 + (\mu_y)^2 + (\mu_z)^2]^{1/2} \text{ (Eq. 1)}$$

$$\chi = -1/2 (E_{\text{HOMO}} + E_{\text{LUMO}}) \text{ (Eq. 2)}$$

$$\eta = -1/2 (E_{\text{HOMO}} - E_{\text{LUMO}}) \text{ (Eq. 3)}$$

$$\sigma = 1/\eta \text{ (Eq. 4)}$$

$$\beta = [(\beta_{xxx} + \beta_{xyy} + \beta_{xzz})^2 + (\beta_{yyy} + \beta_{xxy} + \beta_{yzz})^2 + (\beta_{zzz} + \beta_{xxz} + \beta_{yyz})^2]^{1/2} \text{ (Eq. 5)}$$

$$\alpha = 1/3 (\alpha_{xx} + \alpha_{yy} + \alpha_{zz}) \text{ (Eq. 6)}$$

In addition to these parameters, equations 5 and 6 was utilized to interpret the average polarizability and first hyperpolarizability to study NLO properties. According to the results, there was a significant difference between TCNE **112-118** and TCNQ **119-125** products. TCNQ attached molecules show higher average

polarizabilities and first hyperpolarizabilities than TCNE attached molecules as expected because of enhanced charge transfer capabilities.

Table 3. The electric dipole moment μ (D), E_{HOMO} , E_{LUMO} , ΔE ($E_{\text{HOMO}}-E_{\text{LUMO}}$), electronegativity (χ), global chemical hardness (η), global softness (σ), average polarizability [$\alpha_{(\text{tot})}$], first hyperpolarizability [$\beta_{(\text{tot})}$] at the CAM-B3LYP/6-31G(d,p) level of theory in CH_2Cl_2 for compounds **112-118**.

	112	113	114	115	116	117	118
μ (D)	18.2590	16.2174	18.2476	16.6520	15.7565	17.1794	16.4419
E_{HOMO} (eV)	-6.94	-6.86	-6.95	-6.90	-6.91	-6.90	-6.92
E_{LUMO} (eV)	-2.17	-1.81	-2.08	-2.35	-1.95	-1.97	-2.01
ΔE (eV)	4.77	5.05	4.87	4.55	4.96	4.93	4.91
χ (eV)	4.56	4.34	4.52	4.63	4.43	4.44	4.47
η (eV)	2.39	2.53	2.44	2.28	2.48	2.47	2.46
σ (eV ⁻¹)	0.42	0.40	0.41	0.44	0.40	0.41	0.41
$\alpha_{(\text{tot})}$ ($\times 10^{-24}$ esu)	68.903	71.985	70.696	71.854	62.758	72.815	61.568
$\beta_{(\text{tot})}$ ($\times 10^{-30}$ esu)	158.622	135.202	157.484	156.349	143.077	144.028	145.648

Table 4. The electric dipole moment μ (D), E_{HOMO} , E_{LUMO} , ΔE ($E_{\text{HOMO}}-E_{\text{LUMO}}$), electronegativity (χ), global chemical hardness (η), global softness (σ), average polarizability [$\alpha_{(\text{tot})}$], first hyperpolarizability [$\beta_{(\text{tot})}$] at the CAM-B3LYP/6-31G(d,p) level of theory in CH_2Cl_2 for compounds **119-125**.

	119	120	121	122	123	124	125
μ (D)	22.8565	19.0793	23.2759	23.2712	20.3335	18.3283	20.0032
E_{HOMO} (eV)	-6.54	-6.46	-6.48	-6.52	-6.47	-6.43	-6.46
E_{LUMO} (eV)	-2.75	-2.47	-2.45	-2.65	-2.41	-2.52	-2.54
ΔE (eV)	3.79	3.99	4.03	3.87	4.06	3.91	3.92
χ (eV)	4.65	4.47	4.47	4.59	4.44	4.48	4.50
η (eV)	1.90	2.00	2.02	1.94	2.03	1.96	1.96
σ (eV ⁻¹)	0.53	0.50	0.50	0.52	0.49	0.51	0.51
$\alpha_{(\text{tot})}$ ($\times 10^{-24}$ esu)	114.176	112.766	109.933	112.885	103.081	112.422	104.300
$\beta_{(\text{tot})}$ ($\times 10^{-30}$ esu)	522.408	416.282	458.620	499.710	402.640	406.339	421.338

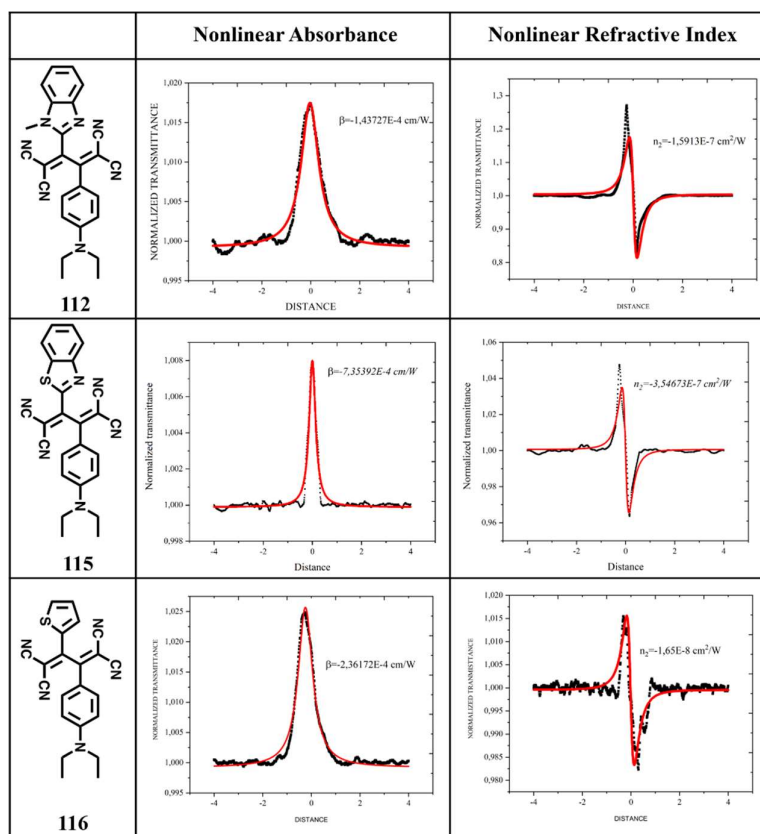
2.4 Nonlinear Optical Applications

There are various methods to explore NLO behavior of compounds. Z-scan is one of the reliable techniques applied to investigate the nonlinear optical properties of organic molecules.¹⁰⁰ Basically, it can be explained as the recording information of changes in intensity during the interaction between a moving sample in the z-position and the Gaussian laser beam. Thanks to these recorded interactions, nonlinear absorption coefficient (β) and nonlinear refractive index (n^2) values of corresponding molecule can be measured. In this thesis, NLO properties of push-pull compounds **112-125** were measured by using home-made Z-scan setup. This setup was constructed by MSc. Student Tolga Orçun Şengöz from Prof. Dr. Okan Esentürk Research Group. In order to validate this home-made device, firstly, studies were carried out on compounds (tungsten disulfide and methylene blue) with known NLO properties in the literature, and similar data were obtained. Then, the target products **112-125** were measured. Two different laser sources were used ($\lambda= 632$ nm and 800 nm) for the measurements. S120C - Standard Photodiode Power Sensor was used as a detector. PM100D digital handheld optical power and energy meter was utilized. PM100D was connected to a computer software which displayed changing interaction between laser source and matter. Thanks to this software, measurements were collected as called as raw data for open aperture (nonlinear absorption) and close aperture measurements (nonlinear refractive index). The difference between open and close aperture measurement was that removing the aperture in front of the detector to capture of all transmitting light. Finally, raw data was normalized and compared to fitting the theoretical data. Calculations were explained in detail in the thesis written by Tolga Orçun Şengöz.

Initially, the TCNE products **112-118** were tested. Indole **113**, benzofuran **114**, and quinoline **117** containing products did not show any nonlinearity in both absorption coefficient and refractive index results with 632 nm and 800 nm lasers. Moreover, only nonlinear refractive index output was collected for pyridine containing TCNE product **118**, but nonlinear absorption was not observed similar to other TCNE

products. The possible explanation behind these negative results is the wavelength or power of the lasers may be insufficient for these molecules. On the other hand, nonlinear absorption and refractive index was measured when 632nm laser was used for benzimidazole **112** ($\beta = 1.43727 \times 10^{-4} \text{ cm W}^{-1}$, $n^2 = 1.5913 \times 10^{-7} \text{ cm}^2 \text{ W}^{-1}$), benzothiazole **115** ($\beta = 7.35392 \times 10^{-4} \text{ cm W}^{-1}$, $n^2 = 3.54673 \times 10^{-7} \text{ cm}^2 \text{ W}^{-1}$), and thiophene **116** ($\beta = 2.36172 \times 10^{-4} \text{ cm W}^{-1}$, $n^2 = 1.65000 \times 10^{-8} \text{ cm}^2 \text{ W}^{-1}$) containing NLOphores (Table 5). In this table, well-fitting of theoretical curve (red line) and experimental curve (black line) can be seen clearly.

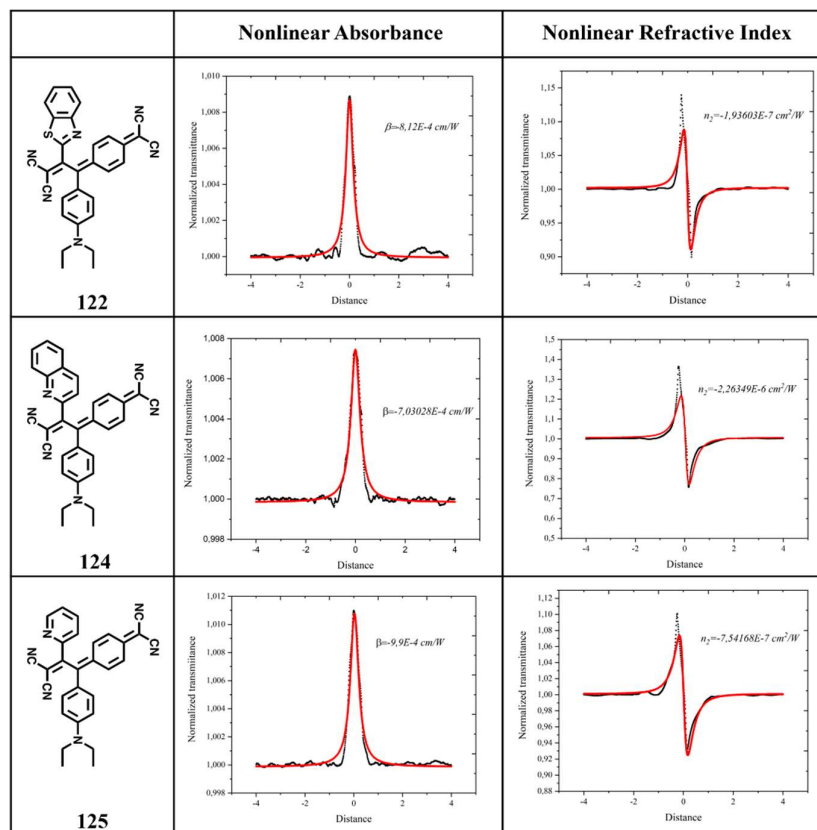
Table 5. Results of theoretical (red line) and experimental (black line) Z-scan curves, nonlinear absorbance (left) and nonlinear refractive index (right), with 632 nm laser of compounds **112**, **115**, and **116**.



Next, TCNQ products **119-125** were measured. Benzimidazole **119**, indole **120**, thiophene **123** containing products showed only nonlinear refractive index, but

nonlinear absorbance results could not be collected because of the probability of insufficient laser usage. Unfortunately, we can not see any nonlinear property for benzofuran containing TCNQ product **121**. On the other hand, nonlinear absorption and refractive index was measured successfully when 632nm laser was used for benzothiazole **122** ($\beta = 8.1200 \times 10^{-4} \text{ cm W}^{-1}$, $n^2 = 1.93693 \times 10^{-7} \text{ cm}^2 \text{ W}^{-1}$), quinoline **124** ($\beta = 7.03028 \times 10^{-4} \text{ cm W}^{-1}$, $n^2 = 2.26349 \times 10^{-6} \text{ cm}^2 \text{ W}^{-1}$), and pyridine **125** ($\beta = 9.9000 \times 10^{-4} \text{ cm W}^{-1}$, $n^2 = 7.54168 \times 10^{-7} \text{ cm}^2 \text{ W}^{-1}$) containing NLOphores (Table 6). As can be seen, theoretical curve (red line) fits experimental curve (black line) sufficiently.

Table 6. Results of theoretical (red line) and experimental (black line) Z-scan curves, nonlinear absorbance (left) and nonlinear refractive index (right), with 632 nm laser of compounds **122**, **124**, and **125**.



In conclusion, better NLO responses were collected with TCNQ products **119-125** compared to TCNE **112-118** products according to the experimental nonlinear absorption and nonlinear refractive index results. In addition, theoretical studies support our experimental measurements.

CHAPTER 3

CONCLUSION

In this thesis, benzimidazole, indole, benzofuran, benzothiazole, thiophene, quinoline and pyridine attached push-pull NLOphores were synthesized *via* click-type [2+2] CA-RE reactions. Heterocycle-based alkynes were treated with TCNE and TCNQ which are chosen as an electron acceptor groups. Hence, 14 different intense colored NLOphores were obtained in high efficiency. Moreover, ^1H and ^{13}C NMR analysis and HR-MS were used as a spectroscopic technique to characterize heterocycle-based dyes.

The linear and nonlinear optical properties of heterocycle-based push-pull NLOphores were studied both experimentally and theoretically. The ICT properties of push-pull molecules were investigated by using UV/Vis spectroscopy and solvatochromism study. In addition, Home-made Z-scan device was utilized to measure NLO response of each product. Furthermore, theoretical calculations were studied to supported the dyes' ICT behaviors which were obtained by experimentally.

CHAPTER 4

EXPERIMENTAL

4.1 Materials and Methods

Reagents were purchased as reagent grade and used without further purification. Commercially available chemicals were purchased by Merck, Fluka, Across, Abcr and Sigma Aldrich.

Solvents for extraction or Flash column chromatography were distilled.

Reactions on exclusion of air and moisture were performed in oven-dried glassware and under N₂ atmosphere.

Analytical thin layer chromatography (TLC) was performed on aluminum sheets coated with 0.2 mm silica gel 60 F254 (Merck) and visualized with a UV lamp (254 or 366 nm).

Evaporation in vacuo was performed at 25–60 °C and 900–10 mbar. Reported yields refer to spectroscopically and chromatographically pure compounds that were dried under high vacuum (0.1–0.05 mbar) before analytical characterization.

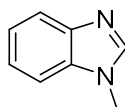
Nuclear magnetic resonance (NMR) spectra were recorded on Bruker Avance III Ultrashield 400 Hz NMR spectrometer in CDCl₃. Chemical shifts δ are reported in ppm downfield from tetramethylsilane (TMS) using the residual solvent signals as an internal reference (CDCl₃: $\delta_{\text{H}} = 7.26$ ppm, $\delta_{\text{C}} = 77.16$ ppm. For ¹H NMR, coupling constants *J* are reported in Hz and the resonance multiplicity is defined as s (singlet), d (doublet), t (triplet), q (quartet), quint (quintet), sext (sextet), sept (septet), m (multiplet), and br. (broad). All spectra were recorded at 298 K. NMR spectra were processed by using MestReNova program.

High-resolution mass spectrometry (HR-MS) was performed by the MS-service of METU Central Laboratory. Spectra were processed in electro spray ionization with positive mode using Time of Flight mass analyzer. Masses are reported in m/z units.

4.2 Synthetic Procedures

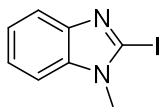
4.2.1 Synthetic Procedures for Benzimidazole Containing Disubstituted Alkyne

Compound 86



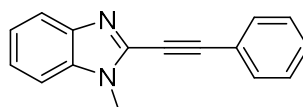
Target synthesis was carried out by following the literature procedure.⁸⁵ Benzimidazole (200 mg, 1.69 mmol, 1 equiv.) and KOH (190 mg, 3.39 mmol, 2 equiv.) was dissolved in 5 mL DMF. After the mixture was stirred for 15 min at 20 °C, iodomethane (240 mg, 1.69 mmol, 1 equiv.) was added dropwise while stirring. The reaction was terminated by diluting with 50 mL of water after 3 h. The mixture was extracted with DCM (3 x 25 mL). Combined organic phase washed with brine and dried over MgSO₄. The solvent was evaporated under vacuum. After column chromatography (SiO₂; EtOAc), the desired product **86** was obtained as a pale-brown liquid. [(155 mg, 1.17 mmol, 69%; R_f = 0.21 (SiO₂; EtOAc)] ¹H NMR (400 MHz, CDCl₃, 298 K) δ = 3.75 (s, 3H), 7.26–7.35 (m, 3H), 7.77–7.81 ppm (m, 2H). Spectral data was consistent with literature.⁸⁵

Compound 87



Target synthesis was carried out by following the literature.⁸⁶ Compound **86** (150 mg, 1.13 mmol, 1 equiv.) was dissolved in dry THF (5 mL) under N₂ and cooled to -78 °C. 1.6 M *n*-BuLi (1.42 mL 2.27 mmol, 2 equiv.) was added dropwise to this mixture during a period of 20 minutes. The solution was stirred for 1 h before iodine (375 mg, 1.48 mmol, 1.3 equiv.) was added in small portions. The mixture was stirred for an additional hour while warming up to room temperature. Reaction was quenched with saturated aqueous Na₂SO₃ (20 mL) and saturated aqueous NH₄Cl solutions (20 mL). The mixture was extracted with DCM (3 x 25 mL). Combined organic phase was dried over MgSO₄ and the solvent was evaporated under vacuum. After column chromatography (SiO₂; 2:1 *n*-Hexane:EtOAc), the desired product **87** was obtained as a white solid. [(182 mg, 0.71 mmol, 62%; R_f = 0.44 (SiO₂; 2:1 *n*-Hexane:EtOAc)]. ¹H NMR (400 MHz, CDCl₃, 298 K) δ = 3.78 (s, 3H), 7.20–7.27 (m, 2H), 7.34 (dd, *J* = 5.4, 1.7 Hz, 1H), 7.71 ppm (dd, *J* = 6.7, 1.7 Hz, 1H). Spectral data was consistent with the literature.⁸⁶

Compound 88

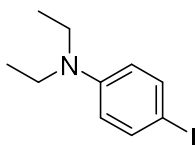


Compound **87** (150 mg, 0.58 mmol, 1 equiv.) was dissolved in 6 mL toluene in a 50 mL round-bottom flask. [Pd(PPh₃)₂Cl₂] (37 mg, 0.05 mmol, 0.09 equiv.) and CuI (10 mg, 0.05 mmol, 0.09 equiv.) was added to the solution and flushed with nitrogen for 15 minutes. Diisopropylamine (3 mL) was added, and the mixture was degassed with nitrogen for additional 15 minutes. After addition of phenylacetylene (59 mg, 0.58 mmol, 1 equiv.), reaction was stirred overnight at room temperature. The mixture was extracted with DCM (3 x 25 mL). Combined organic phase was dried over MgSO₄ and the solvent was evaporated under vacuum. After column chromatography (SiO₂; 2:1 *n*-Hexane:EtOAc), the desired product **88** was obtained as a yellow solid. [(85 mg, 0.37 mmol, 63%; R_f = 0.19 (SiO₂; 2:1 *n*-Hexane:EtOAc)].

^1H NMR (400 MHz, CDCl_3 , 298 K) δ = 3.94 (s, 3H), 7.29–7.42 (m, 6H), 7.59–7.65 (m, 2H), 7.73–7.79 ppm (m, 1H). Spectral data was consistent with the literature.^{87,88}

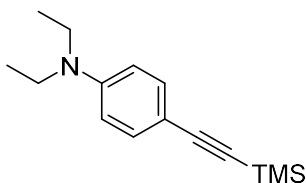
4.2.2 Synthetic Procedures for *N,N*-diethyl-4-ethynylaniline

Compound 92



N,N-diethylaniline (1g, 6.70 mmol, 1 equiv.) was dissolved in DCM. Then, KI (1.33 g, 8.04 mmol, 1.2 equiv.) and a solution of H_5IO_6 (1.83 g, 8.04 mmol, 1.2 equiv.) in 5 mL H_2O was added into the reaction mixture. After stirring vigorously for 25 min at room temperature, the mixture was quenched with 10% aq. Na_2SO_3 solution (25 mL). The mixture was extracted with DCM (3 x 25 mL). Combined organic phase was dried over MgSO_4 and the solvent was evaporated under vacuum. After column chromatography (SiO_2 ; *n*-Hexane), the desired product **92** was obtained as a yellow oil. [(1.55 g, 84%; R_f = 0.72 (SiO_2 ; hexanes)]. ^1H NMR (400 MHz, CDCl_3 , 298 K) δ = 1.14 (t, J = 7.1 Hz, 6H), 3.32 (q, J = 7.1 Hz, 4H), 6.45 (quasi d, J = 9.0 Hz, 2H), 7.43 ppm (quasi d, J = 9.0 Hz, 2H). Spectral data was consistent with literature.⁹⁹

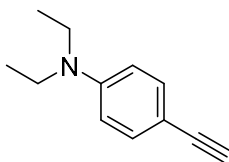
Compound 93



Compound **92** (1.5 g, 5.45 mmol, 1 equiv.) was dissolved in 8 mL triethylamine in a 50 mL round bottom flask. $[\text{Pd}(\text{PPh}_3)_2\text{Cl}_2]$ (114 mg, 0.16 mmol, 0.03 equiv.) and CuI (30 mg, 0.16 mmol, 0.03 equiv) was added to a solution and the solution was flushed with nitrogen for 30 minutes. After addition of trimethylsilylacetylene (590 mg, 6.00

mmol, 1.2 equiv.), reaction was stirred overnight at room temperature. The mixture was extracted with DCM (3 x 25 mL). Combined organic phase was dried over MgSO₄ and the solvent was evaporated under vacuum. After column chromatography (SiO₂; 9:1 *n*-Hexane:EtOAc), the desired product **93** was obtained as a yellow solid. [(1.19 g, 86%; R_f = 0.4 (SiO₂; 9:1 *n*-Hexane:EtOAc)]. ¹H NMR (400 MHz, CDCl₃, 298 K): δ = 0.23 (s, 9H), 1.16 (t, *J* = 7.1 Hz, 6H), 3.35 (q, *J* = 7.1 Hz, 4H), 6.55 (quasi d, *J* = 9.0 Hz, 2H), 7.31 ppm (quasi d, *J* = 9.0 Hz, 2H). Spectral data was consistent with the literature.⁹⁹

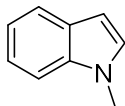
Compound 94



To a solution Compound **93** (1g, 4.7 mmol, 1 equiv.) in methanol (15 mL), K₂CO₃ (1.86 g, 13.45 mmol, 3.30 equiv.) was added. Reaction was stirred for 3 hours under inert atmosphere. After filtration, the solvent was evaporated under vacuum. Column chromatography (SiO₂; 9:1 *n*-Hexane:EtOAc) was performed, and the desired product **94** was obtained as a yellowish oil (Yield; 640 mg, 90%). ¹H NMR (400 MHz, CDCl₃, 298 K): δ = 1.17 (t, *J* = 7.1 Hz, 6H), 2.97 (s, 1H), 3.35 (q, *J* = 7.1 Hz, 4H), 6.58 (quasi d, *J* = 9.0 Hz, 2H), 7.34 ppm (quasi d, *J* = 9.0 Hz, 2H). Spectral data was consistent with literature.⁹⁹

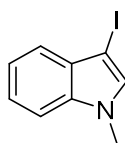
4.2.3 Synthetic Procedures for Halogenated Heterocycles

Compound 96



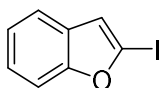
Indole (1.0 g, 8.54 mmol, 1 equiv.) and KOH (2.39 g, 42.68 mmol, 5 equiv.) was dissolved in 10 mL DMF. Then, iodomethane (2.42 g, 17 mmol, 2 equiv.) was added into reaction mixture, and the reaction mixture was stirred for 20 min at room temperature. After filtration by using SiO₂ column, H₂O was added to the mixture. Aqueous phase was extracted with DCM (2 x 50 mL). Combined organic phase was dried over MgSO₄ and the solvent was evaporated under vacuum. Compound **96** was obtained as a yellow liquid. [(692 mg, 62%; R_f = 0.73 (SiO₂; 1:1 *n*-Hexane:DCM)]. ¹H NMR (400 MHz, CDCl₃, 298 K) δ = 3.63 (s, 3H), 6.44–6.46 (m, 1H), 6.93–6.96 (m, 1H), 7.07–7.12 (m, 1H) 7.17–7.22 (m, 1H), 7.24–7.27 (m, 1H), 7.60–7.63 ppm (m, 1H). Spectral data was consistent with literature.⁷⁶

Compound 97



To a solution of compound **96** (200 mg, 1.52 mmol, 1 equiv.) in DMF, KOH (171 mg, 3.05 mmol, 2 equiv.) was added. After excess iodine was added into solution, the reaction mixture was stirred for 10 min at room temperature. The reaction mixture is then poured into ice and water containing 10% Na₂S₂O₃. The white precipitate was collected, washed with cold water, and dried. The desired product **97** was obtained in 90% yield (355 mg) without further purification.⁷⁶ This compound could not be characterized because of the stability issues and used for the next step without any further purification.

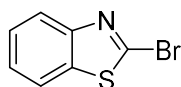
Compound 99



Under inert atmosphere, benzofuran (200 mg, 1.69 mmol, 1 equiv.) was dissolved in dry THF (10 mL). After the mixture was cooled to -40 °C, *n*-BuLi (163 mg, 2.54 mmol, 1.5 equiv.) was added into the reaction mixture. Reaction was stirred for 1

hour, and iodine (645 mg, 2.54 mmol, 1.5 equiv.) solution in 10 mL THF was added into the mixture. The solution was warmed up to room temperature and stirred for additional 2.5 h. Then, the reaction was quenched with saturated Na₂S₂O₃ solution (50 mL). The mixture was extracted with EtOAc (3 x 25 mL). Combined organic phase was dried over MgSO₄ and the solvent was evaporated under vacuum. The desired product **99** was obtained as a dark-red liquid. [(308 mg, 75%; R_f = 0.80 (SiO₂; 9:1 *n*-Hexane:DCM)]. ¹H NMR (400 MHz, CDCl₃, 298 K): δ = 6.95 (s, 1 H), 7.19–7.24 (m, 2H), 7.44–7.53 ppm (m, 2H). Spectral data was consistent with literature.⁹⁴

Compound 101



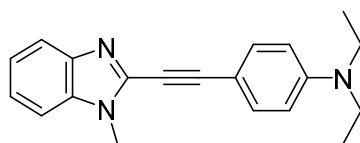
2-aminobenzothiazole (200 mg, 1.33 mmol, 1 equiv.) was dissolved in 6 mL DMF. After NaNO₂ (138 mg, 2.00 mmol, 1.5 equiv.) and NBS (237 mg, 1.33 mmol, 1 equiv.) were added to the mixture, the solution was stirred for 4 h at room temperature. Then, the reaction was quenched with %10 Na₂SO₃ solution (10 mL). The mixture was extracted with EtOAc (3 x 25 mL). Combined organic phase was dried over MgSO₄ and the solvent was evaporated under vacuum. After column chromatography (SiO₂; 4:1 *n*-Hexane:EtOAc), the desired product **101** was obtained as a orange oil. [(173 mg, 61%; R_f = 0.82 (SiO₂; 9:1 *n*-Hexane:EtOAc)]. ¹H NMR (400 MHz, CDCl₃, 298 K): δ = 7.39–7.43 (td, *J* = 7.7, 1.2 Hz, 1H), 7.45–7.49 (td, *J* = 8.0, 1.3 Hz, 1H), 7.80 (dd, *J* = 8.0, 0.7 Hz, 1H), 7.98 ppm (d, *J* = 7.7 Hz, 1H). Spectral data was consistent with literature.⁹⁵

4.2.4 General Synthetic Procedures for Coupling Products

Halogenated heterocycles **87**, **97**, **99** or **101-104** (150 mg, 1 equiv.) was dissolved in 6 mL toluene in a 50 mL round bottom flask. Pd(PPh₃)₂Cl₂ (0.09 equiv.) and CuI (0.09 equiv.) was added to this solution and the reaction mixture was degassed with nitrogen for 15 minutes. Then, diisopropylamine (3 mL) was added and the mixture

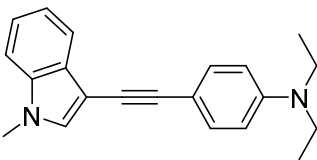
was degassed again with nitrogen for an additional 15 minutes. After addition of alkyne **94** (3 equiv.), reaction was stirred overnight at room temperature. The mixture was extracted with DCM (3 x 25 mL). Combined organic phase was dried over MgSO₄ and the solvent was evaporated under vacuum. Then, column chromatography was performed to obtain desired products **105-111**.

Compound 105



Yield: 106 mg; an orange solid; 60%; CC: (SiO₂; 2:1 *n*-Hexane : EtOAc); R_f = 0.41 (SiO₂; 2:1 *n*-Hexane : EtOAc); m.p. 104–106 °C; ¹H NMR (400 MHz, CDCl₃, 298 K): δ = 1.18 (t, *J* = 7.0 Hz, 6H), 3.39 (q, *J* = 7.0 Hz, 4H), 3.90 (s, 3H), 6.62 (quasi d, AA'part of AA'XX'-system, *J* = 9.0 Hz, 2H), 7.27–7.31 (m, 3H), 7.47 (quasi d, XX'part of AA'XX'-system, *J* = 9.0 Hz, 2H) 7.73–7.54 ppm (m, 1H); ¹³C NMR (100 MHz, CDCl₃, 298 K): δ = 148.5, 143.3, 138.9, 134.9, 133.9, 133.7, 123.3, 122.6, 119.9, 111.2, 109.3, 106.4, 97.5, 44.5, 30.7, 12.6 ppm; HRMS (ESI): *m/z* calcd for C₂₀H₂₂N₃⁺: 304.1814; found: 304.1815 [M + H]⁺.

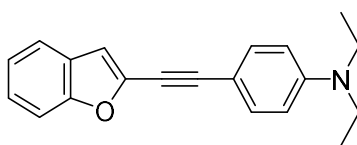
Compound 106



Yield: 106 mg; a yellow solid; 60%. CC: (SiO₂; 9:1 *n*-Hexane:EtOAc); R_f = 0.7 (SiO₂; 9:1 *n*-Hexane:EtOAc); m.p. = 79–83 °C decompose; ¹H NMR (400 MHz, CDCl₃, 298K): δ = 1.18 (t, *J* = 7.1 Hz, 6H), 3.38 (q, *J* = 7.1 Hz, 4H), 3.79 (s, 3H), 6.64 (quasi d, AA'part of AA'XX'-system, *J* = 8.8 Hz, 2H), 7.20 (t, *J* = 7.3 Hz, 1H),

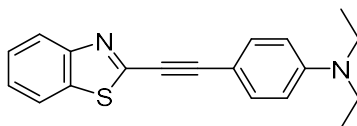
7.25–7.35 (m, 3H), 7.42 (quasi d, XX'part of AA'XX'-system, $J = 8.8$ Hz, 2H), 7.82 ppm (d, $J = 7.8$ Hz, 1H); ^{13}C NMR (100 MHz, CDCl_3 , 298K); $\delta = 146.9, 136.1, 132.5, 131.3, 129.1, 122.3, 120.1, 119.8, 111.1, 109.9, 109.2, 97.7, 91.6, 79.8, 44.2, 32.8, 12.4$ ppm. HRMS (ESI): m/z calcd for $\text{C}_{21}\text{H}_{23}\text{N}_2^+$: 303.1861; found: 303.1861 $[\text{M} + \text{H}]^+$.

Compound 107



Yield: 62 mg; an orange solid; 35%; CC: (SiO_2 ; 9:1 *n*-Hexane : EtOAc) $R_f = 0.50$ (SiO_2 ; 9:1 *n*-Hexane : EtOAc); m.p. 114–116 °C; ^1H NMR (400 MHz, CDCl_3 , 298 K): $\delta = 1.18$ (t, $J = 7.1$ Hz, 6H), 3.39 (q, $J = 7.1$ Hz, 4H), 6.62 (quasi d, AA'part of AA'XX'-system, $J = 9.0$ Hz, 2H), 6.90 (d, $J = 0.8$ Hz, 1H), 7.20–7.25 (m, 1H), 7.28–7.32 (m, 1H), 7.42 (quasi d, XX'part of AA'XX'-system, $J = 9.0$ Hz, 2H), 7.45 (dd, $J = 7.5, 0.6$ Hz, 1H), 7.54 ppm (d, $J = 7.2$ Hz, 1H); ^{13}C NMR (100 MHz, CDCl_3 , 298 K): $\delta = 154.8, 148.3, 140.0, 133.4, 128.3, 125.1, 123.2, 121.0, 111.3, 111.2, 110.1, 107.2, 97.0, 76.7, 44.5, 12.7$ ppm; HRMS (ESI): m/z calcd for $\text{C}_{20}\text{H}_{20}\text{NO}^+$: 290.1545; found: 290.1536 $[\text{M} + \text{H}]^+$.

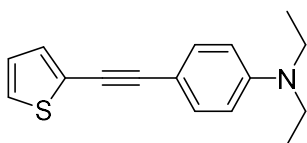
Compound 108



Yield: 172 mg; a yellow solid; 80%; CC: (SiO_2 ; 9:1 *n*-Hexane:EtOAc) $R_f = 0.45$ (SiO_2 ; 9:1 *n*-Hexane:EtOAc); m.p. 118–120 °C; ^1H NMR (400 MHz, CDCl_3 , 298 K): $\delta = 1.19$ (t, $J = 7.1$ Hz, 6H), 3.40 (q, $J = 7.1$ Hz, 4H), 6.62 (quasi d, AA'part

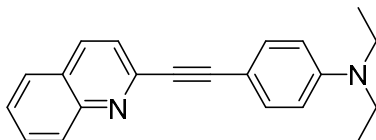
of AA'XX'-system, $J = 8.9$ Hz, 2H), 7.34–7.42 (m, 2H), 7.48 (quasi d, XX'part of AA'XX'-system, $J = 8.9$ Hz, 2H) 7.84 (d, $J = 7.9$, 1H), 8.02 ppm (d, $J = 7.9$, 1H); ^{13}C NMR (100 MHz, CDCl_3 , 298 K): $\delta = 153.2$, 149.9, 148.8, 135.4, 134.1, 126.6, 125.7, 123.3, 121.3, 111.2, 106.2, 99.2, 81.9, 44.6, 12.7 ppm; HRMS (ESI): m/z calcd for $\text{C}_{19}\text{H}_{19}\text{N}_2\text{S}^+$: 307.1269; found: 307.1269 $[\text{M} + \text{H}]^+$.

Compound 109



Yield: 161 mg; a pale yellow solid; 88%; CC: (SiO_2 ; 7:3 *n*-Hexane:DCM) $R_f = 0.28$ (SiO_2 ; 7:3 *n*-Hexane:DCM); m.p. 103–105 °C; ^1H NMR (400 MHz, CDCl_3 , 298 K): $\delta = 1.17$ (t, $J = 7.0$ Hz, 6H), 3.37 (q, $J = 7.0$ Hz, 4H), 6.60 (quasi d, AA'part of AA'XX'-system, $J = 8.8$ Hz, 2H), 6.98 (dd, $J = 5.1$, 3.7 Hz, 1H), 7.20–7.22 (m, 2H), 7.36 ppm (quasi d, XX'part of AA'XX'-system, $J = 8.8$ Hz, 2H); ^{13}C NMR (100 MHz, CDCl_3 , 298 K): $\delta = 147.8$, 133.0, 130.8, 127.1, 126.2, 124.7, 111.3, 108.6, 94.6, 80.3, 44.5, 12.7 ppm; HRMS (ESI): m/z calcd for $\text{C}_{16}\text{H}_{18}\text{NS}^+$: 256.1160; found: 256.1160 $[\text{M} + \text{H}]^+$.

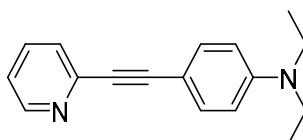
Compound 110



Yield: 191 mg; a yellow oil; 88%; CC: (SiO_2 ; DCM) $R_f = 0.33$ (SiO_2 ; DCM); ^1H NMR (400 MHz, CDCl_3 , 298 K): $\delta = 1.19$ (t, $J = 7.1$ Hz, 6H), 3.39 (q, $J = 7.1$ Hz, 4H), 6.62 (quasi d, $J = 9.0$ Hz, 2H), 7.48–7.53 (m, 3H), 7.56 (d, $J = 8.5$ Hz, 1H), 7.68–7.72 (m, 1H), 7.77 (d, $J = 8.1$ Hz, 1H), 8.09 ppm (m, 2H); ^{13}C NMR (100 MHz,

CDCl₃, 298 K): δ = 148.4, 136.0, 134.0, 130.0, 129.3, 127.6, 126.9, 126.6, 124.5, 111.2, 107.6, 95.7, 88.2, 44.5, 12.7 ppm (15 out of 17 signals expected); HRMS (ESI): m/z calcd for C₂₁H₂₁N₂⁺: 301.1705; found: 301.1717 [M + H]⁺.

Compound 111

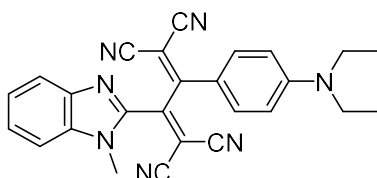


Yield: 170 mg; a bright brown solid; 92%; CC: (SiO₂; 2:1 *n*-Hexane:EtOAc) R_f = 0.43 (SiO₂; 2:1 *n*-Hexane:EtOAc); m.p. 127–129 °C; ¹H NMR (400 MHz, CDCl₃, 298 K): δ = 1.17 (t, J = 7.0 Hz, 6 H), 3.37 (q, J = 7.0 Hz, 4H), 6.60 (quasi d, J = 8.9 Hz, 2H), 7.14–7.17 (m, 1H), 7.43–7.46 (m, 3H), 7.60–7.64 (m, 1H), 8.56 ppm (s, 1H); ¹³C NMR (100 MHz, CDCl₃, 298 K): δ = 150.0, 148.2, 144.5, 136.1, 133.7, 126.7, 121.9, 111.2, 107.8, 91.6, 87.1, 44.5, 12.7 ppm; HRMS (ESI): m/z calcd for C₁₇H₁₉N₂⁺: 251.1548; found: 251.1548 [M + H]⁺.

4.2.5 General Synthetic Procedures for CA-RE Products 112-118

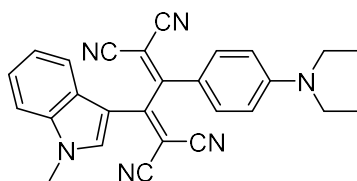
To a solution of coupling products **119-125** (50 mg, 1 equiv.) in DCM (5 mL), TCNE **50** (1 equiv.) was added and stirred for 24 hours at room temperature. The solvent was removed under reduced pressure. Then, column chromatography was performed to obtain target compounds.

Compound 112



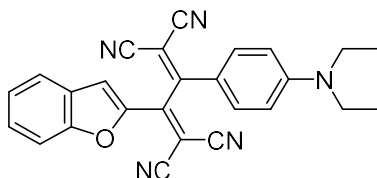
Yield: 36 mg; dark-red solid; 51%; CC: (SiO₂; DCM); R_f = 0.27 (SiO₂; DCM); m.p. 165–167 °C; ¹H NMR (400 MHz, CDCl₃, 298 K): δ = 1.25 (t, *J* = 7.0 Hz, 6 H), 3.49 (q, *J* = 7.0 Hz, 4H), 3.97 (s, 3H), 6.68 (quasi d, AA'part of AA'XX'-system, *J* = 9.4 Hz, 2H), 7.39–7.43 (m, 1H), 7.45–7.52 (m, 2H), 7.85 (quasi d, XX'part of AA'XX'-system, *J* = 9.4 Hz, 2H), 7.88 ppm (d, *J* = 8.2 Hz, 1H); ¹³C NMR (100 MHz, CDCl₃, 298 K): δ = 161.5, 158.0, 153.1, 145.0, 143.8, 137.4, 133.6, 127.1, 124.9, 122.1, 118.7, 114.5, 114.3, 112.2, 111.9, 111.1, 110.8, 92.2, 74.1, 45.3, 33.6, 12.7 ppm; λ_{max} (ε) = 253 (16174), 424 nm (32680 M⁻¹ cm⁻¹); HRMS (ESI): *m/z* calcd for C₂₆H₂₂N₇⁺: 432.1937; found: 432.1937 [M + H]⁺.

Compound 113



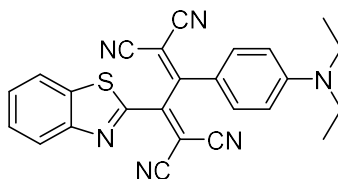
Yield: 67 mg; dark orange-red solid; 94%; CC: (SiO₂; DCM); R_f = 0.41 (SiO₂; DCM); m.p. = 247–251 °C (decompose); ¹H NMR (400 MHz, CDCl₃, 298K); δ = 1.24 (t, *J* = 7.1 Hz, 6H), 3.46 (q, *J* = 7.1 Hz, 4H), 3.97 (s, 3H), 6.67 (quasi d, AA'part of AA'XX'-system, *J* = 9.4 Hz, 2H), 7.21–7.24 (m, 1H), 7.34–7.39 (m, 2H), 7.43 (d, *J* = 8.7 Hz, 1H), 7.86 (quasi d, XX'part of AA'XX'-system, *J* = 9.1 Hz, 2H), 8.66 ppm (s, 1H); ¹³C NMR (100 MHz, CDCl₃, 298K); δ = 164.2, 162.1, 152.8, 137.9, 137.1, 133.2, 125.5, 124.8, 124.4, 121.0, 117.8, 115.6, 115.1, 113.7, 113.2, 112.0, 111.3, 110.1, 73.8, 73.2, 45.2, 34.7, 12.7 ppm. λ_{max} (ε) = 277 (17761), 475 (41963 M⁻¹ cm⁻¹); HRMS (ESI): *m/z* calcd for C₂₇H₂₄N₆⁺: 431.1984; found: 431.1984 [M + H]⁺. Spectral data was consistent with literature.¹⁰⁰

Compound 114



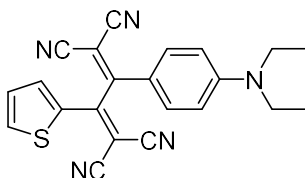
Yield: 57 mg; dark green solid; 79%; CC: (SiO₂; DCM); R_f = 0.6 (SiO₂; DCM); m.p. 147–149 °C; ¹H NMR (400 MHz, CDCl₃, 298 K): δ = 1.24 (t, *J* = 7.1 Hz, 6H), 3.48 (q, *J* = 7.1 Hz, 4H), 6.68 (quasi d, AA'part of AA'XX'-system, *J* = 9.4 Hz, 2H), 7.37 (t, *J* = 7.1 Hz, 1H), 7.51 (s, 1H), 7.56–7.70 (m, 3H), 7.79 ppm (quasi d, XX'part of AA'XX'-system, *J* = 9.4 Hz, 2H); ¹³C NMR (100 MHz, CDCl₃, 298 K): δ = 159.4, 157.3, 153.4, 152.9, 148.1, 132.9, 131.0, 127.5, 125.3, 123.7, 120.2, 117.7, 114.7, 113.7, 112.9, 112.2, 112.1, 111.8, 82.0, 74.1, 45.3, 12.7 ppm; λ_{max} (ε) = 394 (26965), 463 nm (30261 M⁻¹ cm⁻¹); HRMS (ESI): *m/z* calcd for C₂₆H₂₀N₅O⁺: 418.1666; found: 418.1668 [M + H]⁺.

Compound 115



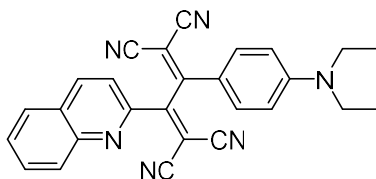
Yield: 61 mg; brown–orange solid; 86%; CC: (SiO₂; DCM); R_f = 0.38 (SiO₂; DCM); m.p. 195–197 °C; ¹H NMR (400 MHz, CDCl₃, 298 K): δ = 1.23 (t, *J* = 7.1 Hz, 6H), 3.47 (q, *J* = 7.1 Hz, 4H), 6.68 (quasi d, AA'part of AA'XX'-system, *J* = 9.4 Hz, 2H), 7.54–7.72 (m, 2H), 7.77 (quasi d, XX'part of AA'XX'-system, *J* = 9.4 Hz, 2H), 7.96 (d, *J* = 8.6 Hz, 1H), 8.27 ppm (d, *J* = 7.8 Hz, 1H); ¹³C NMR (100 MHz, CDCl₃, 298 K): δ = 165.9, 161.4, 152.8, 150.6, 149.2, 137.8, 133.0, 127.7, 125.4, 117.7, 114.7, 114.6, 113.8, 112.1, 111.9, 111.7, 100.1, 89.8, 73.6, 45.3, 12.7 ppm; λ_{max} (ε) = 386 (13074), 466 nm (28677 M⁻¹ cm⁻¹); HRMS (ESI): *m/z* calcd for C₂₅H₁₉N₆S⁺: 435.1386; found: 435.1392 [M + H]⁺.

Compound 116



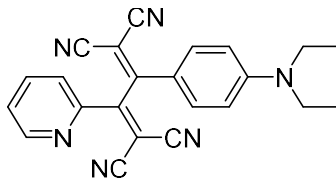
Yield: 66 mg; reddish-orange solid; 88%; CC: (SiO₂; DCM); R_f = 0.45 (SiO₂; DCM); m.p. 211–213 °C; ¹H NMR (400 MHz, CDCl₃, 298 K): δ = 1.24 (t, *J* = 7.1 Hz, 6H), 3.48 (q, *J* = 7.1 Hz, 4H), 6.68 (quasi d, AA'part of AA'XX'-system, *J* = 8.8 Hz, 2H), 7.26–7.28 (m, 1H), 7.78 (quasi d, XX'part of AA'XX'-system, *J* = 8.8 Hz, 2H) 7.89 (d, *J* = 3.9 Hz, 1H), 7.92 ppm (d, *J* = 4.9 Hz, 1H); ¹³C NMR (100 MHz, CDCl₃, 298 K): δ = 162.0, 160.1, 152.9, 138.0, 137.3, 135.6, 133.0, 129.9, 117.2, 114.6, 113.6, 113.0, 112.1, 111.8, 80.3, 73.4, 45.3, 12.7 ppm; λ_{max} (ε) = 366 (17278), 474 nm (33486 M⁻¹ cm⁻¹); HRMS (ESI): *m/z* calcd for C₂₂H₁₈N₅S⁺: 384.1283; found: 384.1282 [M + H]⁺.

Compound 117



Yield: 58 mg; dark-orange solid; 81%; CC: (SiO₂; DCM); R_f = 0.30 (SiO₂; DCM); m.p. 93–95 °C; ¹H NMR (400 MHz, CDCl₃, 298 K): δ = 1.22 (t, *J* = 7.1 Hz, 6H), 3.46 (q, *J* = 7.1 Hz, 4H), 6.66 (quasi d, AA'part of AA'XX'-system, *J* = 9.4 Hz, 2H), 7.57 (d, *J* = 8.5 Hz, 1H), 7.69–7.73 (m, 1H), 7.81 (quasi d, XX'part of AA'XX'-system, *J* = 9.4 Hz, 2H) 7.85–7.88 (m, 2H), 8.20–8.35 ppm (m, 2H); ¹³C NMR (100 MHz, CDCl₃, 298 K): δ = 165.8, 161.5, 152.8, 148.3, 148.0, 138.3, 133.1, 131.5, 130.6, 130.2, 129.3, 127.7, 120.5, 117.8, 114.7, 113.9, 112.1, 90.2, 73.9, 45.3, 12.7 ppm (21 out of 23 signals expected); λ_{max} (ε) = 274 (20868), 348 (12521), 460 nm (28200 M⁻¹ cm⁻¹); HRMS (ESI): *m/z* calcd for C₂₇H₂₁N₆⁺: 429.1842; found: 429.1842 [M + H]⁺.

Compound 118

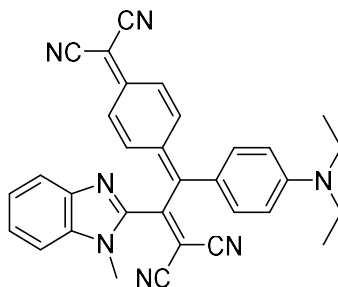


Yield: 69 mg; A dark-red solid; 91%; CC: (SiO₂; DCM); R_f=0.64 (SiO₂; DCM); m.p. 183–185 °C; ¹H NMR (400 MHz, CDCl₃, 298 K): δ = 1.26 (t, *J* = 7.1 Hz, 6 H), 3.49 (q, *J* = 7.1 Hz, 4H), 6.69 (quasi d, AA'part of AA'XX'-system, *J* = 9.3 Hz, 2H), 7.53–7.62 (m, 2H), 7.78 (quasi d, XX'part of AA'XX'-system, *J* = 9.3 Hz, 2H), 7.86–7.90 (m, 1H) 8.86 ppm (d, *J* = 5.1 Hz, 1H); ¹³C NMR (100 MHz, CDCl₃, 298 K): δ = 165.9, 161.4, 152.8, 150.6, 149.2, 137.9, 133.0, 127.7, 125.4, 117.7, 114.7, 113.8, 112.1, 111.9, 111.7, 89.8, 73.6, 45.3, 12.7 ppm; λ_{max} (ε) = 317 (12801), 470 nm (28054 M⁻¹ cm⁻¹); HRMS (ESI): m/z calcd for C₂₃H₁₉N₆⁺: 379.1671; found: 379.1668 [M + H]⁺.

4.2.6 General Synthetic Procedures for CA-RE Products 119-125

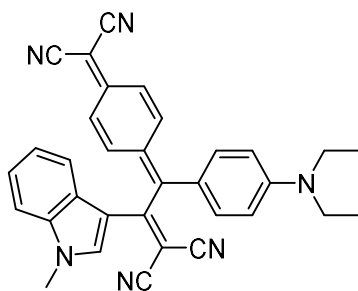
To a solution of coupling products **119-125** (50 mg, 1 equiv.) in DCM (5 mL), TCNQ **53** (1 equiv.) was added and stirred for 24 hours at room temperature. The solvent was removed under reduced pressure. Then, column chromatography was performed to obtain target products.

Compound 119



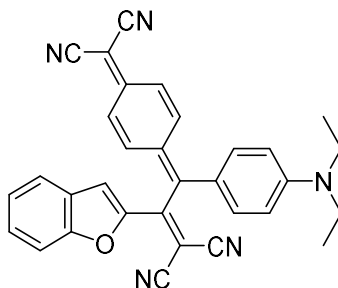
Yield: 80 mg; dark blue solid; 96%; CC: (SiO₂; DCM) R_f = 0.11 (SiO₂; DCM); m.p. 157–159 °C; ¹H NMR (400 MHz, CDCl₃, 298 K): δ = 1.23 (t, J = 7.0 Hz, 6H), 3.46 (q, J = 7.0 Hz, 4H), 3.60 (s, 3H), 6.72 (quasi d, J = 9.0 Hz, 2H), 7.07 (dd, J = 8.2, 1.1 Hz, 1H), 7.16 (dd, J = 8.2, 1.1 Hz, 1H) 7.29–7.32 (m, 4H), 7.38–7.47 (m, 3H), 7.91 ppm (d, J = 7.3 Hz, 1H); ¹³C NMR (100 MHz, CDCl₃, 298 K): δ = 158.7, 153.6, 151.7, 147.8, 146.6, 143.0, 137.3, 136.1, 135.5, 133.8, 126.6, 126.0, 125.8, 124.7, 123.3, 122.1, 114.9, 113.1, 112.7, 112.3, 110.4, 100.1, 93.0, 72.7, 45.2, 31.7, 12.8 ppm; λ_{\max} (ϵ) = 359 (17956), 479 (18321), 758 (23833 M⁻¹ cm⁻¹); HRMS (ESI): m/z calcd for C₃₂H₂₆N₇⁺: 508.2250; found: 508.2250 [M + H]⁺.

Compound 120



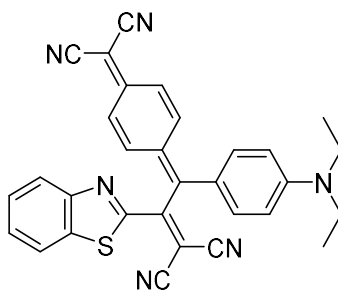
Yield: 83 mg; dark-green solid; 99%; CC: (SiO₂; DCM); R_f = 0.15 (SiO₂;DCM). m.p =252–254 °C decompose; ¹H NMR (400 MHz, CDCl₃, 298K); δ = 1.24 (t, J = 7.1 Hz, 6H), 3.46 (q, J = 7.1 Hz, 4H), 3.96 (s, 3H), 6.69 (d, J = 9.1 Hz, 2H), 6.98–7.09 (m, 2H), 7.12 (t, J = 7.5 Hz, 1H), 7.26–7.34 (m, 3H), 7.40 (t, J = 8.2 Hz, 3H), 7.65 (dd, J = 9.5, 1.6 Hz, 1H), 8.55 ppm (s, 1H); ¹³C NMR (100 MHz, CDCl₃, 298K); δ = 165.8, 154.6, 153.5, 151.4, 137.8, 135.9, 135.5, 134.7, 129.8, 125.9, 125.0, 124.6, 124.2, 123.9, 122.9, 121.2, 116.0, 115.5, 115.4, 113.9, 112.5, 112.4, 111.1, 75.8, 69.3, 45.1, 34.6, 12.8 ppm (28 out of 29 signals expected); λ_{\max} (ϵ) = 277 (20640), 335 (18887), 394 (27855), 463 (19388), 683 nm (51100 M⁻¹ cm⁻¹); HRMS: m/z calcd for C₃₃H₂₇N₆⁺: 507.2297; found: 507.2297 [M + H]⁺. Spectral data was consistent with literature.¹⁰⁰

Compound 121



Yield: 67 mg; dark blue solid; 79%; CC: (SiO₂; DCM); $R_f = 0.2$ (SiO₂; DCM); m.p. 250–252 °C; ¹H NMR (400 MHz, CDCl₃, 298 K): $\delta = 1.26$ (t, $J = 7.1$ Hz, 6H), 3.49 (q, $J = 7.1$ Hz, 4H), 6.73 (quasi d, $J = 9.2$ Hz, 2H), 6.99 (dd, $J = 9.5, 1.9$ Hz, 1H), 7.13 (dd, $J = 9.5, 1.9$ Hz, 1H), 7.18 (s, 1H), 7.27–7.32 (m, 1H), 7.33–7.40 (m, 3H), 7.51–7.71 ppm (m, 4H); ¹³C NMR (100 MHz, CDCl₃, 298 K): $\delta = 156.9, 156.5, 154.4, 151.4, 150.1, 148.3, 135.6, 134.8, 134.3, 130.73, 130.68, 127.5, 125.2, 125.1, 124.6, 123.5, 123.2, 120.6, 115.1, 115.0, 112.72, 112.70, 112.63, 112.55, 82.9, 70.7, 45.1, 12.8$ ppm; $\lambda_{\max} (\epsilon) = 336$ (17891), 694 nm (24302 M⁻¹ cm⁻¹); HRMS (ESI): m/z calcd for C₃₂H₂₄N₅O⁺: 494.1981; found: 494.1976 [M + H]⁺.

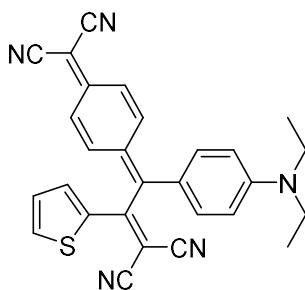
Compound 122



Yield: 73 mg; dark blue solid; 88%; CC: (SiO₂; DCM); $R_f = 0.28$ (SiO₂; DCM); m.p. 146–148 °C decompose; ¹H NMR (400 MHz, CDCl₃, 298 K): $\delta = 1.25$ (t, $J = 7.0$ Hz, 6H), 3.48 (q, $J = 7.0$ Hz, 4H), 6.73 (quasi d, AA' part of AA'XX' system, $J = 9.1$ Hz, 2H), 7.00 (dd, $J = 7.5, 1.8$ Hz, 1H), 7.15 (dd, $J = 7.5, 1.8$ Hz,

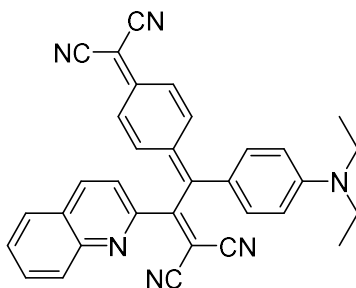
1H), 7.34 (quasi d, XX'part of AA'XX'-system, $J = 9.1$ Hz, 2H), 7.51–7.65 (m, 4H), 7.86 (d, $J = 8.1$ Hz, 1H), 8.28 ppm (d, $J = 8.2$ Hz, 1H); ^{13}C NMR (100 MHz, CDCl_3 , 298 K): $\delta = 160.8, 160.0, 154.2, 153.6, 151.5, 148.4, 138.4, 136.2, 135.5, 135.0, 134.1, 131.5, 128.6, 128.3, 125.9, 125.7, 125.1, 122.8, 122.0, 115.0, 114.8, 112.7, 112.3, 112.23, 112.20, 111.6, 88.8, 72.0, 45.2, 12.8$ ppm; $\lambda_{\text{max}} (\epsilon) = 338 (21433), 586 (23800), 706 \text{ nm} (27634 \text{ M}^{-1} \text{ cm}^{-1})$; HRMS (ESI): m/z calcd for $\text{C}_{31}\text{H}_{23}\text{N}_6\text{S}^+$: 511.1705; found: 511.1717 $[\text{M} + \text{H}]^+$.

Compound 123



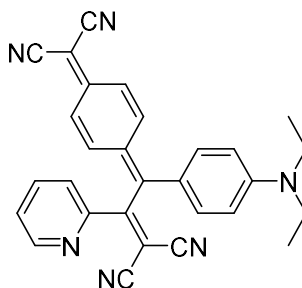
Yield: 86%; dark blue solid; 86%; CC: (SiO_2 ; DCM); $R_f = 0.43$ (SiO_2 ; DCM); m.p. 238–240 °C; ^1H NMR (400 MHz, CDCl_3 , 298 K): $\delta = 1.25$ (t, $J = 7.1$ Hz, 6H), 3.48 (q, $J = 7.1$ Hz, 4H), 6.72 (quasi d, AA'part of AA'XX'-system, $J = 9.0$ Hz, 2H), 6.94 (dd, $J = 7.7, 1.8$ Hz, 1H), 7.13 (dd, $J = 7.7, 1.8$ Hz, 1H), 7.23 (t, $J = 4.1$ Hz, 1H), 7.28 (m, 1H), 7.32 (quasi d, XX'part of AA'XX'-system, $J = 9.0$ Hz, 2H), 7.56 (dd, $J = 7.8, 1.7$ Hz, 1H), 7.85 (d, $J = 5.0$ Hz, 1H), 7.95 ppm (d, $J = 4.0$ Hz, 1H); ^{13}C NMR (100 MHz, CDCl_3 , 298 K): $\delta = 163.3, 154.4, 151.2, 138.3, 137.7, 136.5, 135.6, 134.8, 134.3, 130.0, 129.9, 125.2, 124.6, 122.8, 115.2, 115.1, 113.6, 112.60, 112.55, 81.0, 70.6, 45.2, 12.8$ ppm; $\lambda_{\text{max}} (\epsilon) = 338 (21272), 683 \text{ nm} (31907 \text{ M}^{-1} \text{ cm}^{-1})$; HRMS (ESI): m/z calcd for $\text{C}_{28}\text{H}_{22}\text{N}_5\text{S}^+$: 460.1596; found: 460.1596 $[\text{M} + \text{H}]^+$.

Compound 124



Yield: 70 mg; a purple-blue solid; 83%; CC: (SiO₂; DCM); R_f = 0.13 (SiO₂; DCM); m.p. 130–132 °C; ¹H NMR (400 MHz, CDCl₃, 298 K): δ = 1.23 (t, *J* = 7.1 Hz, 6H), 3.46 (q, *J* = 7.1 Hz, 4H), 6.70 (quasi d, AA'part of AA'XX'-system, *J* = 9.2 Hz, 2H), 7.05 (dd, *J* = 7.5, 1.9 Hz, 1H), 7.11 (dd, *J* = 7.5, 2.0 Hz, 1H), 7.26–7.31 (m, 2H), 7.36 (quasi d, XX'part of AA'XX'-system, *J* = 9.2 Hz, 2H), 7.60 (dd, *J* = 7.5, 2.0 Hz, 1H), 7.67–7.71 (m, 1H), 7.82–7.87 (m, 2H), 8.16 (d, *J* = 8.5 Hz, 1H), 8.29 ppm (d, *J* = 8.4 Hz, 1H); ¹³C NMR (100 MHz, CDCl₃, 298 K): δ = 169.0, 154.3, 151.4, 150.8, 150.1, 147.7, 138.0, 135.7, 134.4, 134.0, 131.6, 131.5, 130.3, 129.9, 129.0, 127.7, 125.4, 124.9, 123.1, 121.3, 115.2, 115.0, 112.9, 112.8, 112.6, 90.8, 71.0, 45.2, 12.8 ppm; λ_{max} (ε) = 342 (22308), 696 nm (26057 M⁻¹ cm⁻¹); HRMS (ESI): *m/z* calcd for C₃₃H₂₄N₆⁺: 505.2141; found: 505.2137 [M + H]⁺.

Compound 125



Yield: 28 mg; a dark blue solid; 31%; Precipitation: (*n*-Hexane/DCM); $R_f = 0.08$ (SiO₂; 1:1 *n*-Hexane:EtOAc); m.p. 171-173 °C decompose; ¹H NMR (400 MHz, CDCl₃, 298 K): $\delta = 1.24$ (t, $J = 7.1$ Hz, 6H), 3.47 (q, $J = 7.1$ Hz, 4H), 6.70 (quasi d, $J = 9.1$ Hz, 2H), 6.92 (dd, $J = 7.7, 1.7$ Hz, 1H), 7.12 (dd, $J = 7.7, 1.7$ Hz, 1H), 7.30 (m, 4H), 7.44 (dd, $J = 7.6, 4.8$ Hz, 1H), 7.56 (dd, $J = 7.8, 1.6$ Hz, 1H), 7.74 (td, $J = 6.2, 1.5$ Hz, 1H), 7.83 ppm (d, $J = 4.3$ Hz, 1H); ¹³C NMR (100 MHz, CDCl₃, 298 K): $\delta = 169.1, 154.3, 151.6, 151.4, 150.3, 150.1, 137.7, 135.7, 135.0, 134.4, 131.3, 127.3, 126.0, 125.3, 124.9, 123.0, 115.1, 115.0, 112.7, 112.6, 112.5, 90.3, 71.0, 45.2, 12.8$ ppm; $\lambda_{\max} (\epsilon) = 564 (9937), 732 \text{ nm} (9398 \text{ M}^{-1} \text{ cm}^{-1})$.

REFERENCES

1. Franken, P. A.; Hill, A. E.; Peters, C. W.; Weinreich, G. Generation of Optical Harmonics. *Phys. Rev. Lett.* **1961**, *7*(4), 118–119. DOI: 10.1103/physrevlett.7.118
2. Wen, X.; Gong, Z.; Li, D. Nonlinear Optics of Two-Dimensional Transition Metal Dichalcogenides. *InfoMat* **2019**, *1*(3), 317–337. DOI: 10.1002/inf2.12024
3. Suresh, S.; Ramanand, A.; Jayaraman, D.; Mani, P. Review on Theoretical Aspect of Nonlinear Optics. *Rev. Adv. Mater. Sci.* **2012**, *30*(2), 175–183.
4. Dorn, R.; Baums, D.; Kersten, P.; Regener, R. Nonlinear Optical Materials for Integrated Optics: Telecommunications and Sensors. *Adv. Mater.* **1992**, *4*(7-8), 464–473. DOI: 10.1002/adma.19920040703
5. Strickler, J. H.; Webb, W. W. Three-Dimensional Optical Data Storage in Refractive Media by Two-Photon Point Excitation. *Opt. Lett.* **1991**, *16*(22), 1780. DOI: 10.1364/ol.16.001780
6. Weaver, S.; Wagner, K. Nonlinear Techniques in Optical Synthetic Aperture Radar Image Generation and Target Recognition. *Appl. Opt.* **1995**, *34*(20), 3981. DOI: 10.1364/ao.34.003981
7. Luo, Z.; Wu, D.; Xu, B.; Xu, H.; Cai, Z.; Peng, J.; Weng, J.; Xu, S.; Zhu, C.; Wang, F.; Sun, Z.; Zhang, H. Two-Dimensional Material-Based Saturable Absorbers: Towards Compact Visible-Wavelength All-Fiber Pulsed Lasers. *Nanoscale* **2016**, *8*(2), 1066–1072. DOI: 10.1039/c5nr06981e
8. Eaton, D. F. Nonlinear Optical Materials. *Science* **1991**, *253*(5017), 281–287. DOI: 10.1126/science.253.5017.281
9. Prasad, P. N.; Reinhardt, B. A. Is There a Role for Organic Materials Chemistry in Nonlinear Optics and Photonics? *Chem. Mater.* **1990**, *2*(6), 660–669. DOI: 10.1021/cm00012a014

10. Kanis, D. R.; Ratner, M. A.; Marks, T. J. Design and Construction of Molecular Assemblies with Large Second-Order Optical Nonlinearities. Quantum Chemical Aspects. *Chem. Rev.* **1994**, *94*(1), 195–242. DOI: 10.1021/cr00025a007
11. Bredas, J. L.; Adant, C.; Tackx, P.; Persoons, A.; Pierce, B. M. Third-order Nonlinear Optical Response in Organic Materials: Theoretical and Experimental Aspects. *Chem. Rev.* **1994**, *94*(1), 243–278. DOI: 10.1021/cr00025a008
12. Marder, S. R.; Perry, J. W. Molecular Materials for Second-Order Nonlinear Optical Applications. *Adv. Mater.* **1993**, *5*(11), 804–815. DOI:rg/10.1002/adma.19930051104
13. Erande, Y.; Sreenath, M. C.; Chitrabalam, S.; Joe, I. H.; Sekar, N. Spectroscopic, DFT and Z-scan Supported Investigation of Dicyanoisophorone Based Push-Pull NLOphoric Styryl Dyes. *Opt. Mater.* **2017**, *66*, 494–511. DOI: 10.1016/j.optmat.2017.03.005
14. Lanke, S. K.; Sekar, N. Coumarin Push-Pull NLOphores with Red Emission: Solvatochromic and Theoretical approach. *J. Fluoresc.* **2016**, *26*(3), 949–962. DOI: 10.1007/s10895-016-1783-6
15. Achelle, S.; Malval, J. P.; Aloïse, S.; Barsella, A.; Spangenberg, A.; Mager, L.; Akdas-Kilig, H.; Fillaut, J. L.; Caro, B.; Robin-le Guen, F. Synthesis, Photophysics and Nonlinear Optical Properties of Stilbenoid Pyrimidine-Based Dyes Bearing Methylene-pyran Donor Groups. *ChemPhysChem* **2013**, *14*(12), 2725–2736. DOI: 10.1002/cphc.201300419
16. Castro, M. C.; Belsley, M.; Raposo, M. M. Synthesis and Characterization of Push–Pull Bithienylpyrrole NLOphores with Enhanced Hyperpolarizabilities. *Dyes Pigm.* **2016**, *131*, 333–339. DOI: 10.1016/j.dyepig.2016.04.027
17. Denneval, C.; Moldovan, O.; Baudequin, C.; Achelle, S.; Baldeck, P.; Plé, N.; Darabantu, M.; Ramondenc, Y. Synthesis and Photophysical Properties of Push-Pull Structures Incorporating Diazines as Attracting Part with a

- Fluorene Core. *Eur. J. Org. Chem.* **2013**, 2013(25), 5591–5602. DOI: 10.1002/ejoc.201300458
18. Rajeshirke, M.; Sekar, N. Multi-Stimuli Responsive Emissive NLOphoric Colorants – a Recent Trend in Research. *Dyes Pigm.* **2019**, 163, 675–683. DOI: 10.1016/j.dyepig.2018.12.063
19. Gupta, R. R.; Kumar, M.; Gupta, V. *Heterocyclic Chemistry Volume II: Five-Membered Heterocycles.* **1999**, Springer Berlin Heidelberg, DOI: 10.1007/978-3-662-07757-3
20. Arora P.; Arora V.; Lamba H. S.; Wadhwa D. Importance of Heterocyclic Chemistry: A Review. *Int. J Pharm. Res. Sci.* **2009**, 3(9); 2947- 2955.
21. Shipman, M. Aromatic Heterocycles as Intermediates in Natural Product Synthesis. *Contemp. Org. Synth.* **1995**, 2(1), 1. DOI: 10.1039/co9950200001
22. Eliel, E. L. Conformational analysis in saturated heterocyclic compounds. *Acc. Chem. Res.* **1970**, 3(1), 1–8. DOI: 10.1021/ar50025a001
23. Theodoridis, G. Chapter 4 Fluorine-Containing Agrochemicals: An Overview of Recent Developments. *Adv. Fluorine Sci.* **2006**, 2, 121–175. DOI: 10.1016/s1872-0358(06)02004-5
24. Selvam, T. P.; James, C. R.; Dniandev, P. V.; Valzita, S. K. A mini review of pyrimidine and fused pyrimidine marketed drugs. *Research in Pharmacy*, **2015**, 2(4), 1–9.
25. Fernandes, S. S.; Castro, M. C.; Ivanou, D.; Mendes, A.; Raposo, M. M. Push-Pull Heterocyclic Dyes Based on Pyrrole and Thiophene: Synthesis and Evaluation of Their Optical, Redox and Photovoltaic Properties. *Coatings*, **2021**, 12(1), 34. DOI: 10.3390/coatings12010034
26. Pina, J.; Seixas de Melo, J. S.; Batista, R. M.; Costa, S. P.; Raposo, M. M. The Influence of The Relative Position of The Thiophene and Pyrrole Rings in Donor–Acceptor Thienylpyrrolyl-benzothiazole Derivatives. A Photophysical and Theoretical Investigation. *Phys. Chem. Chem. Phys.* **2010**, 12(33), 9719. DOI: 10.1039/c002434a

27. Bureš, F. Fundamental Aspects of Property Tuning in Push–Pull Molecules. *RSC Adv.* **2014**, *4*(102), 58826–58851. DOI: 10.1039/c4ra11264d
28. Fernandes, S. S.; Castro, M. C.; Pereira, A. I.; Mendes, A.; Serpa, C.; Pina, J.; Justino, L. L.; Burrows, H. D.; Raposo, M. M. Optical and Photovoltaic Properties of Thieno[3,2-*b*]thiophene-Based Push–Pull Organic Dyes with Different Anchoring Groups for Dye-Sensitized Solar Cells. *ACS Omega*, **2017**, *2*(12), 9268–9279. DOI: 10.1021/acsomega.7b01195
29. Ramirez, M. A.; Custodio, R.; Cuadro, A. M.; Alvarez-Builla, J.; Clays, K.; Asselberghs, I.; Mendicuti, F.; Castaño, O.; Andrés, J. L.; Vaquero, J. J. Synthesis of Charged Bis-Heteroaryl Donor–Acceptor (D–A⁺) NLO-phores Coupling (π -deficient– π -excessive) Heteroaromatic Rings. *Org. Biomol. Chem.*, **2013**, *11*(41), 7145. DOI: 10.1039/c3ob41159a
30. Schomaker, J. M.; Delia, T. J. Arylation of Halogenated Pyrimidines *via* a Suzuki Coupling Reaction. *J. Org. Chem.* **2001**, *66*(21), 7125–7128. DOI: 10.1021/jo010573+
31. Teimuri-Mofrad, R.; Rahimpour, K.; Ghadari, R. Design, Synthesis and Characterization of Ferrocene Based V-shaped Chromophores with Modified Nonlinear Effect. *J. Organomet. Chem.* **2017**, *846*, 397–406. DOI: 10.1016/j.jorganchem.2017.07.023
32. Fihri, A.; Luart, D.; Len, C.; Solhy, A.; Chevrin, C.; Polshettiwar, V. Suzuki–Miyaura Cross-Coupling Coupling Reactions with Low Catalyst Loading: A Green and Sustainable Protocol in Pure Water. *Dalton Trans.* **2011**, *40*(13), 3116. DOI: 10.1039/c0dt01637c
33. Moses, J. E.; Moorhouse, A. D. The Growing Applications of Click Chemistry. *Chem. Soc. Rev.* **2007**, *36*(8), 1249–1262. DOI: 10.1039/b613014n
34. Kolb, H. C.; Finn, M. G.; Sharpless, K. B. Click Chemistry: Diverse Chemical Function from a Few Good Reactions. *Angew. Chem. Int. Ed.* **2001**, *40*, 2004–2021. DOI: 10.1002/1521-3773(20010601)40

35. Hoyle, C. E.; Bowman, C. N. Thiol-Ene Click Chemistry. *Angew. Chem. Int. Ed.* **2010**, *49*(9), 1540–1573. DOI: 10.1002/anie.200903924
36. Kaur, J.; Saxena, M.; Rishi, N. (2021). An Overview of Recent Advances in Biomedical Applications of Click Chemistry. *Bioconjug. Chem.* **2021**, *32*(8), 1455–1471. DOI: 10.1021/acs.bioconjchem.1c00247
37. Breugst, M.; Reissig, H. U. The Huisgen reaction: Milestones of The 1,3-Dipolar Cycloaddition *Angew. Chem. Int. Ed.* **2020** *59*(30), 12293–12307. DOI: 10.1002/anie.202003115
38. Chassaing, S.; Bénétiau, V.; Pale, P. When CUAAC 'Click Chemistry' Goes Heterogeneous. *Catal. Sci. Technol.* **2016**, *6*(4), 923–957. DOI: 10.1039/c5cy01847a
39. Tornøe, C. W.; Christensen, C.; Meldal, M. Peptidotriazoles on Solid Phase: [1,2,3]-Triazoles by Regiospecific Copper(I)-Catalyzed 1,3-Dipolar Cycloadditions of Terminal Alkynes to Azides. *J. Org. Chem.* **2002**, *67*(9), 3057–3064. DOI: 10.1021/jo011148j
40. Liang, P.; Li, Z.; Mi, Y.; Yang, Z.; Wang, D.; Cao, H.; He, W.; Yang, H. Pyrene-Based Small Molecular Nonlinear Optical Materials Modified by “Click-Reaction”. *J. Electron. Mater.* **2015**, *44*(8), 2883–2889. DOI: 10.1007/s11664-015-3736-2
41. Diels, O.; Alder, K. (1928). Synthesen in Der Hydroaromatischen Reihe. *Liebigs Ann.* **1928**, *460*(1), 98–122. DOI: 10.1002/jlac.19284600106
42. Nicolaou, K. C.; Snyder, S. A.; Montagnon, T.; Vassilikogiannakis, G. The Diels-Alder Reaction in Total Synthesis. *Angew. Chem. Int. Ed.* **2002**, *41*(10), 1668–1698. DOI: 10.1002/1521-3773(20020517)41:10<1668::aid-anie1668>3.0.co;2-z
43. Gregoritza, M.; Brandl, F. P. The Diels–Alder Reaction: A Powerful Tool for The Design of Drug Delivery Systems and Biomaterials. *Eur. J. Pharm. Biopharm.* **2015**, *97*, 438–453. DOI: 10.1016/j.ejpb.2015.06.007
44. Bae, S. H.; Kim, H. M.; Min, H. S.; Kim, D.; Kim, T. D. (2012). Crosslinkable Nonlinear Optical Dendrimers Synthesized by Diels-Alder

- Reaction. *J. Nanosci. Nanotechnol.* **2012**, *12*(1), 730–736. DOI: 10.1166/jnn.2012.5357
45. Shamim, T.; Paul, S. Silica Functionalized Cu(I) as a Green and Recyclable Heterogeneous Catalyst for The Huisgen 1,3-Dipolar Cycloaddition in Water at Room Temperature. *Catal. Lett.* **2010**, *136*(3-4), 260–265. DOI: 10.1007/s10562-010-0330-3
46. Uygun, M.; Tasdelen, M. A.; Yagci, Y. Influence of Type of Initiation on Thiol-Ene “Click” Chemistry. *Macromol. Chem. Phys.* **2009**, *211*(1), 103–110. DOI: 10.1002/macp.200900442
47. Sarkar, D.; Bera, N.; Ghosh, S. [2+2] Photochemical Cycloaddition in Organic Synthesis. *Eur. J. Org. Chem.* **2019**, *2020*(10), 1310–1326. DOI: 10.1002/ejoc.201901143
48. Seeman, J. I. (2022). History of The Woodward-Hoffmann Rules. The No-Mechanism Puzzle**. *Chem. Rec.* **2022**, *22*(2). DOI: 10.1002/tcr.202100212
49. Anslyn, E. V.; Dougherty, D. A. Thermal Pericyclic Reactions. In *Modern Physical Organic Chemistry*, Univ. Science Books **2005**.
50. Palazzo, T. A.; Mose, R.; Jørgensen, K. A. Cycloaddition Reactions: Why Is It So Challenging to Move From Six To Ten Electrons? *Angew. Chem. Int. Ed.* **2017**, *56*(34), 10033–10038. DOI: 10.1002/anie.201701085
51. Hoffmann, R.; Woodward, R. B. Orbital Symmetries and Endo-Exo Relationships in Concerted Cycloaddition Reactions. *J. Am. Chem. Soc.* **1965**, *87*(19), 4388–4389. DOI: 10.1021/ja00947a033
52. Ha, S.; Lee, Y.; Kwak, Y.; Mishra, A.; Yu, E.; Ryou, B.; Park, C. M. Alkyne–Alkene [2 + 2] Cycloaddition Based On Visible Light Photocatalysis. *Nat. Commun.* **2020**, *11*(1). DOI: 10.1038/s41467-020-16283-9
53. Kokubo, K.; Yamaguchi, H.; Kawamoto, T.; Oshima, T. Substituent Effects on The Stereochemistry in The [2 + 2] Photocycloaddition Reaction of Homobenzoquinone Derivative with Variously Substituted Alkenes and Alkynes. *J. Am. Chem. Soc.* **2002**, *124*(30), 8912–8921. DOI: 10.1021/ja025593n

54. Eaton, P. E. The Tricyclo[5.3.0.0^{2,6}]decane System. The Photodimers of Cyclopentenone. *J. Am. Chem. Soc.* **1962**, *84*(12), 2344–2348. DOI: 10.1021/ja00871a015
55. Cantrell, T. S. Photochemical Transformations of Some β -substituted Enones. *Tetrahedron*, **1971**, *27*(6), 1227–1237. DOI: 10.1016/s0040-4020(01)90871-3
56. Cantrell, T. S.; Haller, W. S.; Williams, J. C. Photocycloaddition Reactions of Some 3-substituted Cyclohexenones. *J. Org. Chem.* **1969**, *34*(3), 509–519. DOI: 10.1021/jo01255a007
57. Poplata, S.; Tröster, A.; Zou, Y. Q.; Bach, T. Recent Advances in The Synthesis of Cyclobutanes by Olefin [2 + 2] Photocycloaddition Reactions. *Chem. Rev.* **2006**, *116*(17), 9748–9815. DOI: 10.1021/acs.chemrev.5b00723
58. Iriando-Alberdi, J.; Greaney, M. F. (2007). Photocycloaddition in Natural Product Synthesis. *Eur. J. Org. Chem.* **2007**, *2007*(29), 4801–4815. DOI: 10.1002/ejoc.200700239
59. Essaïdi, Z.; Krupka, O.; Iliopoulos, K.; Champigny, E.; Sahraoui, B.; Sallé, M.; Gindre, D. Synthesis and Functionalization of Coumarin-Containing Copolymers for Second Order Optical Nonlinearities. *Opt. Mater.* **2013**, *35*(3), 576–581. DOI: 10.1016/j.optmat.2012.10.011
60. Reinhoudt, D. N. (2 + 2)-Cycloaddition and (2 + 2)-Cycloreversion Reactions of Teterocyclic Compounds. *Adv Heterocycl. Chem.* **1977**, *21*, 253–321. DOI: 10.1016/s0065-2725(08)60734-5
61. Reinhoudt, D. N.; Kouwenhoven, C. G. The First Synthesis of Monocyclic Thiepins. *Tetrahedron*, **1974**, *30*(14), 2093–2098. DOI: 10.1016/s0040-4020(01)97344-2
62. Reinhoudt, D. N.; Kouwenhoven, C. G. A Novel Route for The Synthesis of benzo[b]thiepins. *Tetrahedron*, **1974**, *30*(15), 2431–2436. DOI: 10.1016/s0040-4020(01)97113-3
63. Walker, D.; Hiebert, J. D. 2,3-Dichloro-5,6-Dicyanobenzoquinone and Its Reactions. *Chem. Rev.* **1967**, *67*(2), 153–195. DOI: 10.1021/cr60246a002

64. Trofimov, B.; Sobenina, L.; Stepanova, Z.; Ushakov, I.; Sinegovskaya, L.; Vakul'skaya, T.; Mikhaleva, A. Facile [2+2] Cycloaddition of DDQ to An Alkyne: Synthesis of Pyrrolyl- and Indolylbicyclo[4.2.0]octadienes from C-ethynylpyrroles or C-ethynylindoles. *Synthesis*, **2009**, 2010(03), 470–476. DOI: 10.1055/s-0029-1217133
65. Kato, S.; Beels, M. T. R.; La Porta, P.; Schweizer, W. B.; Boudon, C.; Gisselbrecht, J. P.; Biaggio, I.; Diederich, F. Homoconjugated Push-Pull and Spiro Systems: Intramolecular Charge-Transfer Interactions and Third-Order Optical Nonlinearities. *Angew. Chem. Int. Ed.* **2010**, 49(35), 6207–6211. DOI: 10.1002/anie.201002236
66. Michinobu, T.; May, J. C.; Lim, J. H.; Boudon, C.; Gisselbrecht, J. P.; Seiler, P.; Gross, M.; Biaggio, I.; Diederich, F. A New Class of Organic Donor–Acceptor Molecules with Large Third-Order Optical Nonlinearities. *Chem. Commun.* **2005**, 737–739. DOI: 10.1039/b417393g
67. Bruce, M. I.; Rodgers, J. R.; Snow, M. R.; Swincer, A. G. Cyclopentadienyl-Ruthenium and -Osmium Chemistry. Cleavage of Tetracyanoethylene Under Mild Conditions: X-Ray Crystal Structures of $[\text{Ru}\{\eta^3\text{-C}(\text{CN})_2\text{CPHC}=\text{C}(\text{CN})_2\}(\text{PPh}_3)(\eta\text{-C}_5\text{H}_5)]$ and $[\text{Ru}\{\text{C}[\text{=c}(\text{cn})_2]\text{CPH}=\text{C}(\text{CN})_2\}-(\text{CNBut})(\text{PPh}_3)(\eta\text{-C}_5\text{H}_5)]$. *J. Chem. Soc., Chem. Commun.* **1981**, 271–272. DOI: 10.1039/c39810000271
68. Bruce, M. I.; Neil Duffy, D.; Liddell, M. J.; Snow, M. R.; Tiekink, E. R. T. Reactions of Transition Metal σ -Acetylide Complexes X. Cycloaddition of Tetracyanoethene to Manganese, Iron and Nickel Complexes, and Hydration of a Related Tungsten Complex. X-ray Structures of $\text{Fe}\{\text{C}[\text{=C}(\text{CN})_2]\text{CPH}=\text{C}(\text{CN})_2\}(\text{CO})_2(\eta\text{-C}_5\text{H}_5)$ and $\text{Ni}\{\text{C}[\text{=C}(\text{CN})_2]\text{CPH}=\text{C}(\text{CN})_2\}(\text{PPh}_3)(\eta\text{-C}_5\text{H}_5)$. *J. Organomet. Chem.* **1987**, 335(3), 365–378. DOI: 10.1016/s0022-328x(00)99412-9

69. Hussain, M.; Albert, D.; Wartchow, R.; Butenschön, H. The First Cclopentadienylalkylphosphane Nickel Chelates: Synthesis, Structures, and Reactions. *Chem.: Asian J.* **2007**, *2*(6), 782–793. DOI: 10.1002/asia.200700032
70. Onitsuka, K.; Ose, N.; Ozawa, F.; Takahashi, S. Reactions of Acetylene-Bridged Diplatinum Complexes with Tetracyanoethylene. *J. Organomet. Chem.* **1999**, *578*(1-2), 169–177. DOI: 10.1016/s0022-328x(98)01119-x
71. Wu, X.; Wu, J.; Liu, Y.; Jen, A. K. Y. Highly Efficient, Thermally and Chemically Stable Second Order Nonlinear Optical Chromophores Containing a 2-Phenyl-Tetracyanobutadienyl Acceptor. *J. Am. Chem. Soc.* **1998**, *121*(2), 472–473. DOI: 10.1021/ja983537+
72. Cai, C.; Liakatas, I.; Wong, M. S.; Bösch, M.; Bosshard, C.; Günter, P.; Concilio, S.; Tirelli, N.; Suter, U. W. Donor–Acceptor-Substituted Phenylethenyl Bithiophenes: Highly Efficient and Stable Nonlinear Optical Chromophores. *Org. Lett.* **1999**, *1*(11), 1847–1849. DOI: 10.1021/ol991118r
73. Michinobu, T.; Boudon, C.; Gisselbrecht, J. P.; Seiler, P.; Frank, B.; Moonen, N. N.; Gross, M.; Diederich, F. Donor-Substituted 1,1,4,4-Tetracyanobutadienes (TCBDs): New Chromophores with Efficient Intramolecular Charge-Transfer Interactions by Atom-Economic Synthesis. *Chem. Eur. J.*, **2006**, *12*(7), 1889–1905. DOI: 10.1002/chem.200501113
74. Jarowski, P. D.; Wu, Y. L.; Boudon, C.; Gisselbrecht, J. P.; Gross, M.; Schweizer, W. B.; Diederich, F. New Donor–Acceptor Chromophores by Formal [2+2] Cycloaddition of Donor-Substituted Alkynes to Dicyanovinyl Derivatives. *Org. Biomol. Chem.* **2009**, *7*(7), 1312. DOI: 10.1039/b821230a
75. Kivala, M.; Diederich, F. Conjugation and Optoelectronic Properties of Acetylenic Scaffolds and Charge-Transfer Chromophores. *Pure Appl. Chem.* **2008**, *80*(3), 411–427. DOI: 10.1351/pac200880030411
76. Kato, S. I.; Diederich, F. Non-Planar Push–Pull Chromophores. *Chem. Commun.* **2010**, *46*(12), 1994. DOI: 10.1039/b926601a

77. Shoji, T.; Maruyama, M.; Ito, S.; Morita, N. Synthesis and Properties of Mono-, Bis-, Tris-, and Tetrakis[1,1,4,4-Tetracyano-2-(1-Azulenyl)-1,3-Butadien-3-yl] Chromophores Connected to a Benzene Ring by Phenylethynyl- and 2-Thienylethynyl Spacers. *Bull. Chem. Soc. Jpn.* **2012**, *85*(7), 761–773. DOI: 10.1246/bcsj.20120037
78. Erden, K.; Dengiz, C. 3-Alkynylindoles as Building Blocks for The Synthesis of Electronically Tunable Indole-Based Push–Pull Chromophores. *J. Org. Chem.* **2022**, *87*(6), 4385–4399. DOI: 10.1021/acs.joc.2c00067
79. Kato, S. I.; Kivala, M.; Schweizer, W. B.; Boudon, C.; Gisselbrecht, J. P.; Diederich, F. Origin of Intense Intramolecular Charge-Transfer Interactions in Nonplanar Push-Pull Chromophores. *Chem. Eur. J.* **2009**, *15*(35), 8687–8691. DOI: 10.1002/chem. 200901630
80. Niu, S.; Ulrich, G.; Retailleau, P.; Ziessel, R. Regioselective Synthesis of 5-Monostyryl and 2-Tetracyanobutadiene BODIPY Dyes. *Org. Lett.* **2011**, *13*(19), 4996–4999. DOI: 10.1021/ol201600s
81. Mammadova, F.; Ozsinan, S.; Okutan, M.; Dengiz, C. Synthesis, Characterization, and Theoretical Investigation of Optical and Nonlinear Optical (NLO) Properties of Triazene-Based Push–Pull Chromophores. *J. Mol. Struct.* **2020**, *1220*, 128726. DOI: 10.1016/j.molstruc.2020.128726
82. Kato, S.I.; Noguchi, H.; Jin, S.; Nakamura, Y. Synthesis and Electronic, Optical, and Electrochemical Properties of a Series of Tetracyanobutadiene-Substituted Carbazoles. *Asian J. Org. Chem.* **2015**, *5*(2), 246–256. DOI: 10.1002/ajoc.201500431
83. Kivala, M.; Diederich, F. Acetylene-Derived Strong Organic Acceptors for Planar and Nonplanar Push–Pull Chromophores. *Acc. Chem. Res.* **2008**, *42*(2), 235–248. DOI: 10.1021/ar8001238
84. Kivala, M.; Boudon, C.; Gisselbrecht, J. P.; Enko, B.; Seiler, P.; Müller, I. B.; Langer, N.; Jarowski, P. D.; Gescheidt, G.; Diederich, F. Organic Super-Acceptors with Efficient Intramolecular Charge-Transfer Interactions by [2+2] Cycloadditions of TCNE, TCNQ, and F₄TCNQ to Donor-Substituted

- Cyanoalkynes. *Chem. Eur. J.* **2009**, *15*(16), 4111–4123. DOI: 10.1002/chem.200802563
85. Washino, Y.; Murata, K.; Ashizawa, M.; Kawauchi, S.; Michinobu, T. Creation of Persistent Charge-Transfer Interactions in TCNQ Polyester. *Polym. J.* **2011**, *43*(4), 364–369. DOI: 10.1038/pj.2011.2
86. Galán, E.; Andreu, R.; Garín, J.; Orduna, J.; Villacampa, B.; Diosdado, B. E. Cycloaddition Reactions of Polyenic Donor– π -Acceptor Systems with an Electron-Rich Alkyne: Access to New Chromophores with Second-Order Optical Nonlinearities. *Org. Biomol. Chem.* **2012**, *10*(43), 8684. DOI: 10.1039/c2ob26515j
87. Banerjee, K.; Bhattacharjee, D.; Mahato, S. K.; Sufian, A.; Bhabak, K. P. Benzimidazole- and Imidazole-Fused Selenazolium and Selenazinium Selenocyanates: Ionic Organoselenium Compounds with Efficient Peroxide Scavenging Activities. *Inorg. Chem.* **2021**, *60*(17), 12984–12999. DOI: 10.1021/acs.inorgchem.1c01410
88. Breugst, M.; von der Heiden, D.; Detmar, E.; Kuchta, R. Activation of Michael Acceptors by Halogen-Bond Donors. *Synlett.* **2017**, *29*(10), 1307–1313. DOI: 10.1055/s-0036-1591841
89. Moulton, B. E.; Whitwood, A. C.; Duhme-Klair, A. K.; Lynam, J. M.; Fairlamb, I. J. Regiochemistry in Cobalt-Mediated Intermolecular Pauson–Khand Reactions of Unsymmetrical Internal Heteroaromatic Alkynes with Norbornene. *J. Org. Chem.* **2011**, *76*(13), 5320–5334. DOI: 10.1021/jo200664m
90. Bellina, F.; Biagetti, M.; Guariento, S.; Lessi, M.; Fausti, M.; Ronchi, P.; Rosadoni, E. Ligand-free PD/AG-Mediated Dehydrogenative Alkynylation of Imidazole Derivatives. *RSC Adv.* **2021**, *11*(41), 25504–25509. DOI: 10.1039/d1ra05303e

91. Ergun, C.; Gul, E. Chemical Insight into Benzimidazole Containing Donor-Acceptor-Donor Type II-Conjugated Polymers: Benzimidazole as an Acceptor. *Polym. Rev.* **2017**, *58*(1), 42–62. DOI: 10.1080/15583724.2017.1329210
92. Jana, P.; Yadav, M.; Kumar, T.; Kanvah, S. (2021). Benzimidazole-Acrylonitriles as Chemosensors for Picric Acid Detection. *J. Photochem. Photobiol. A: Chem.* **2021**, *404*, 112874. DOI: 10.1016/j.jphotochem.2020.112874
93. Moonen, N. N.; Gist, R.; Boudon, C.; Gisselbrecht, J.-P.; Seiler, P.; Kawai, T.; Kishioka, A.; Gross, M.; Irie, M.; Diederich, F. Donor-Substituted Cyanoethynylethenes: Powerful Chromophores for Opto-Electronic Applications. *Org. Biomol. Chem.* **2003**, *1*, 2032. DOI: 10.1039/b303879c
94. Zolfigol, M. A.; Khazaei, A.; Kolvari, E.; Koukabi, N.; Soltani, H.; Behjunia, M. H₅IO₆/KI: A New Combination Reagent for Iodination of Aromatic Amines, and Trimethylsilylation of Alcohols and Phenols Through *in situ* Generation of Iodine Under Mild Conditions. *Helv. Chim. Acta.* **2010**, *93*(3), 587–594. DOI: 10.1002/hlca.200900259
95. Wardrop, D. J.; Komenda, J. P. Dehydrative Fragmentation of 5-Hydroxyalkyl-1h-Tetrazoles: A Mild Route to Alkylidenecarbenes. *Org. Lett.* **2012**, *14*, 1548–1551. DOI: 10.1021/ol300276p
96. Gorski, K.; Mech-Piskorz, J.; Noworyta, K.; Lesniewska, B.; Pietraszkiewicz, M. Efficient Synthesis of 5-Oxatruxene and the Unusual Influence of Oxygen Heteroatom on Its Physico-Chemical Properties. *New J. Chem.* **2018**, *42*, 5844–5852. DOI: 10.1039/C7NJ04729K
97. Mukhopadhyay, S.; Batra, S. Direct Transformation of Arylamines to Aryl Halides *via* Sodium Nitrite and *N*-Halosuccinimide. *Chem. Eur. J.* **2018** *24*(55), 14622–14626. DOI: 10.1002/chem.201803347

98. Frisch, M.J., Trucks, G. W. , Schlegel, H. B., Scuseria, G. E., Robb, M. A., Cheeseman, J. R., Scalmani, G., Barone, V., Mennucci, B., Petersson, G. A., Nakatsuji, H., Caricato, M., Li, X., Hratchian, H. P., Izmaylov, A. F., Bloino, J., Zheng, G., Sonnenberg, J. L., Hada, M., Ehara, M., Toyota, K., Fukuda, R., Hasegawa, J., Ishida, M., Nakajima, T., Honda, Y., Kitao, O., Nakai, H., Vreven, T., Montgomery, J. A., Peralta, Jr., J. E., Ogliaro, F., Bearpark, M., Heyd, J. J., Brothers, E., Kudin, K. N., Staroverov, V. N., Kobayashi, R., Normand, J., Raghavachari, K., Rendell, A., Burant, J. C., Iyengar, S., S., Tomasi, J., Cossi, M., Rega, N., Millam, J. M., Klene, M., Knox, J. E., Cross, J. B., Bakken, V., Adamo, C., Jaramillo, J., Gomperts, R., Stratmann, R.E, Yazyev, O., Austin, A., J., Cammi, R., Pomelli, C., Ochterski, J. W., Martin, R. L., Morokuma, K., Zakrzewski, V. G. Voth, G. A., Salvador, P., Dannenberg, J. J., Dapprich, S., Daniels, A. D., Farkas, Ö., Foresman, J. B., Ortiz, J. V., Cioslowski, J., Fox, D. J.; Gaussian 09, Revision D.01.
99. Lokhande, P. K.; Patil, D. S.; Kadam, M. M.; Sekar, N. Theoretical Investigation of Optical and Nonlinear Optical (NLO) Properties of 3-Azabenzanthrone Analogues : DFT and TD-DFT Approach. *ChemistrySelect* **2019**, *4*, 10033–10045. DOI: 10.1002/slct.201901681
100. Sreenath, M. C.; Hubert Joe, I.; Rastogi, V. K. (2018). Experimental and Theoretical Investigation of Third-Order Nonlinear Optical Properties of Azo Dye 1-(2, 5-Dimethoxy-phenylazo)-Naphthalen-2-ol by Z-scan Technique and Quantum Chemical Computations. *Dyes Pigm.* **2018**, *157*, 163–178. DOI: 10.1016/j.dyepig.2018.04.044
101. Tancini, F.; Wu, Y. L.; Schweizer, W. B.; Gisselbrecht, J. P.; Boudon, C.; Jarowski, P. D.; Beels, M. T.; Biaggio, I.; Diederich, F. 1,1-Dicyano-4-[4-(diethylamino)phenyl]buta-1,3-dienes: Structure-Property Relationships. *Eur. J. Org. Chem.* **2012**, *2012*, 2756–2765. DOI: 10.1002/ejoc.201200111

102. ERDEN, K. *Design And Synthesis Of Triazene And Indole-Substituted Push–Pull Chromophores Via Click-Type Transformations: Effects Of Donor Groups On The Optoelectronic Properties* [M.S. - Master of Science]. **2021**. Middle East Technical University.



Figure 26. ¹H NMR spectrum of **93** in CDCl₃ solution (400 MHz).

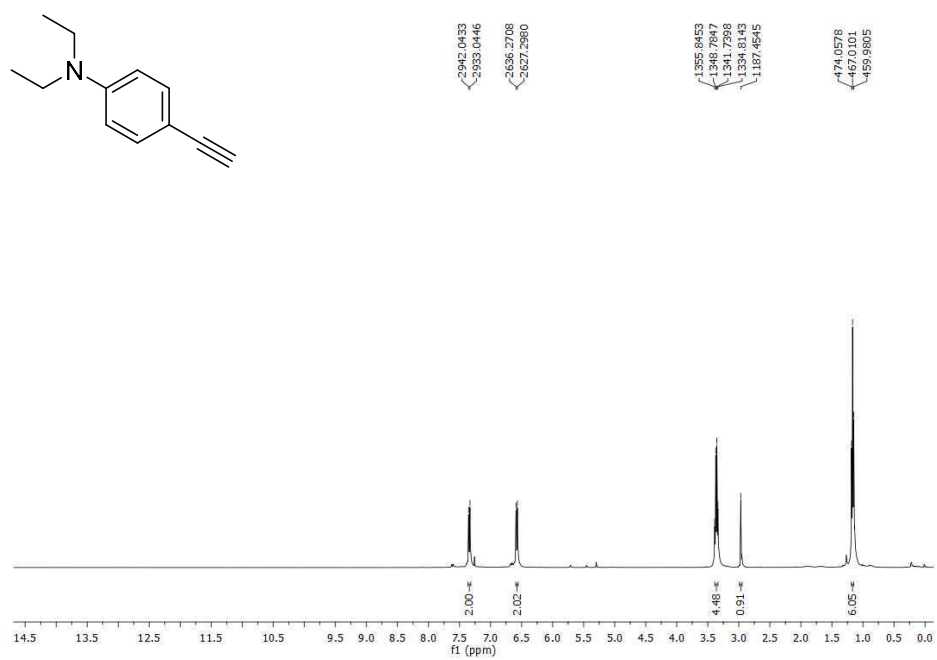


Figure 27. ¹H NMR spectrum of **94** in CDCl₃ solution (400 MHz).

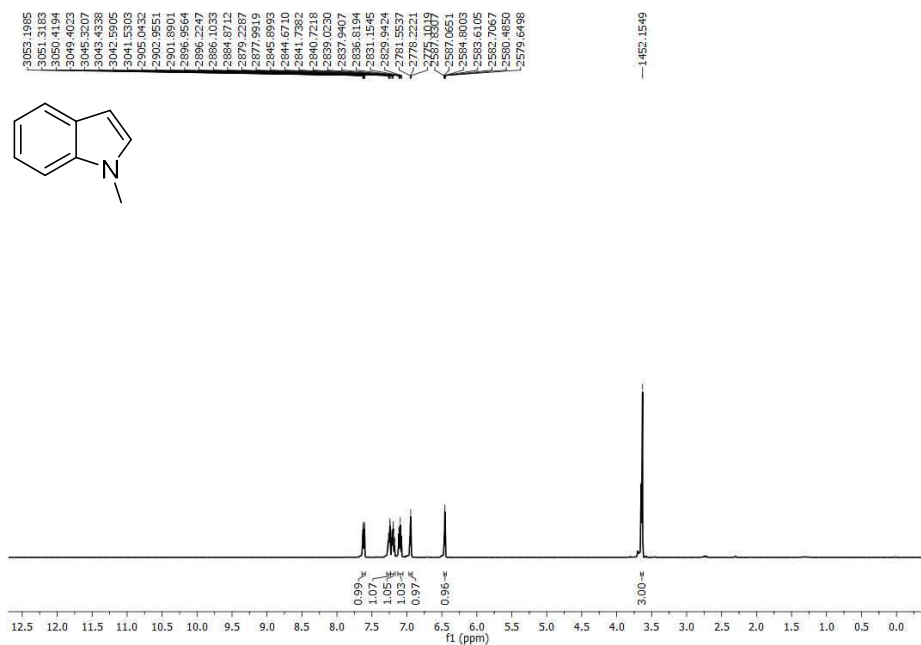


Figure 28. ¹H NMR spectrum of 96 in CDCl₃ solution (400 MHz).

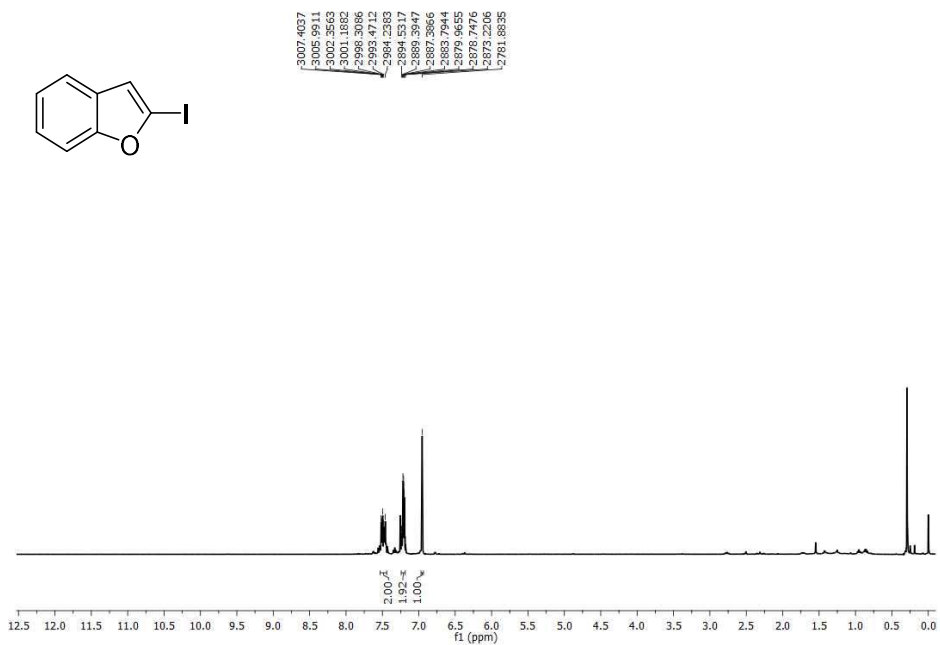


Figure 29. ¹H NMR spectrum of 99 in CDCl₃ solution (400 MHz).

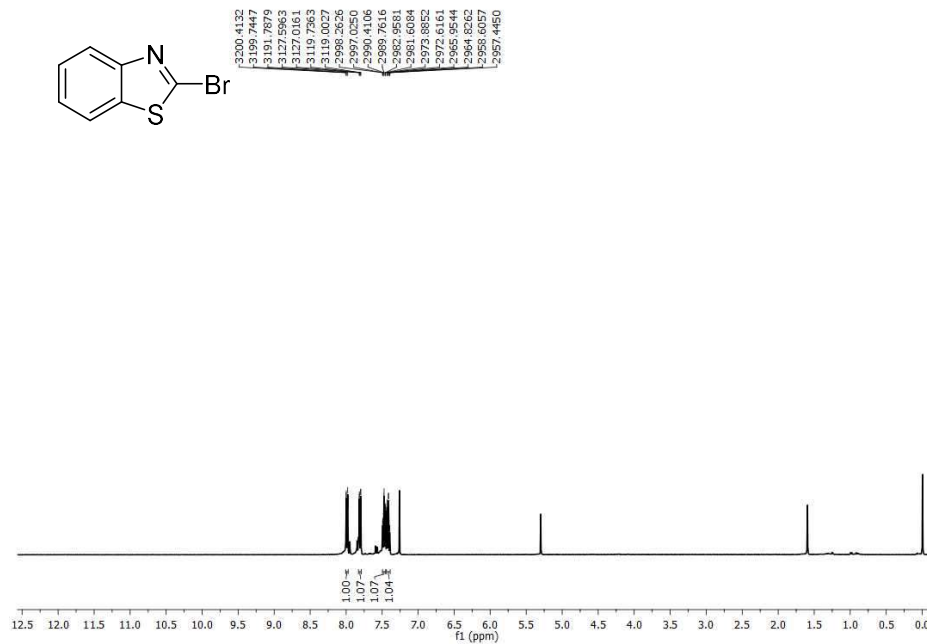


Figure 30. ¹H NMR spectrum of **101** in CDCl₃ solution (400 MHz).

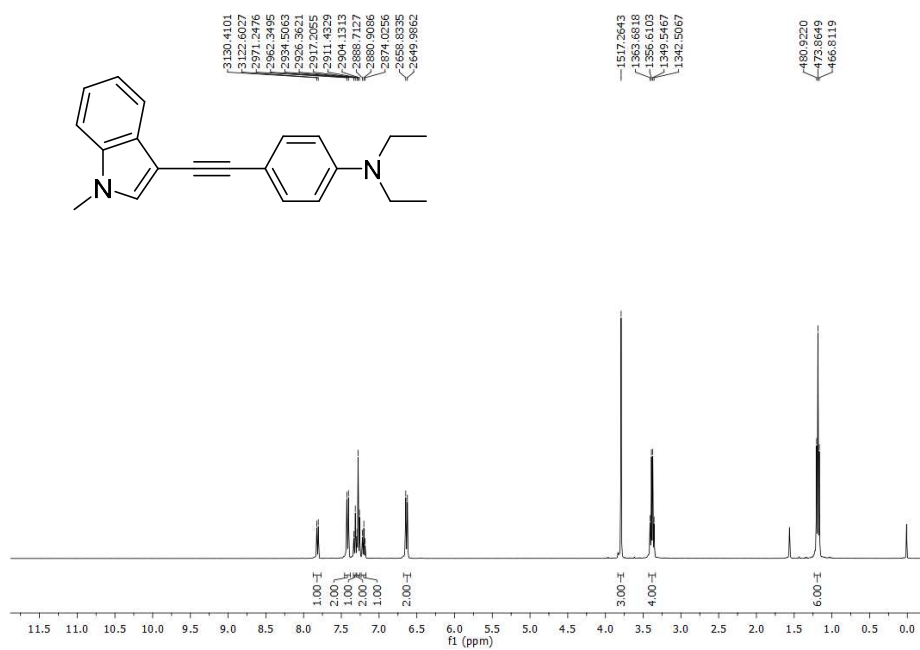


Figure 33. ¹H NMR spectrum of **106** in CDCl₃ solution (400 MHz).

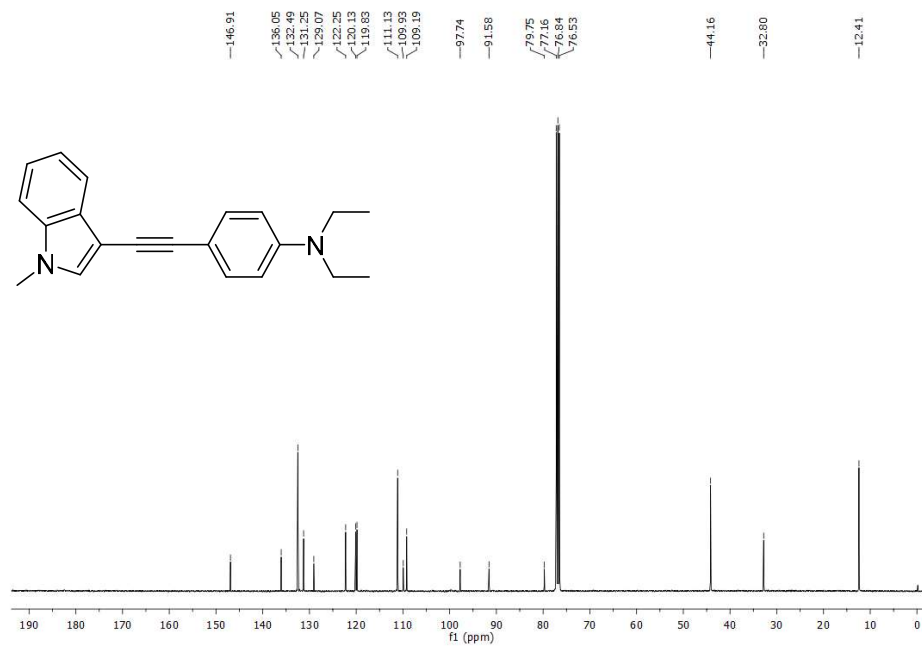


Figure 34. ¹³C NMR spectrum of **106** in CDCl₃ solution (100 MHz).

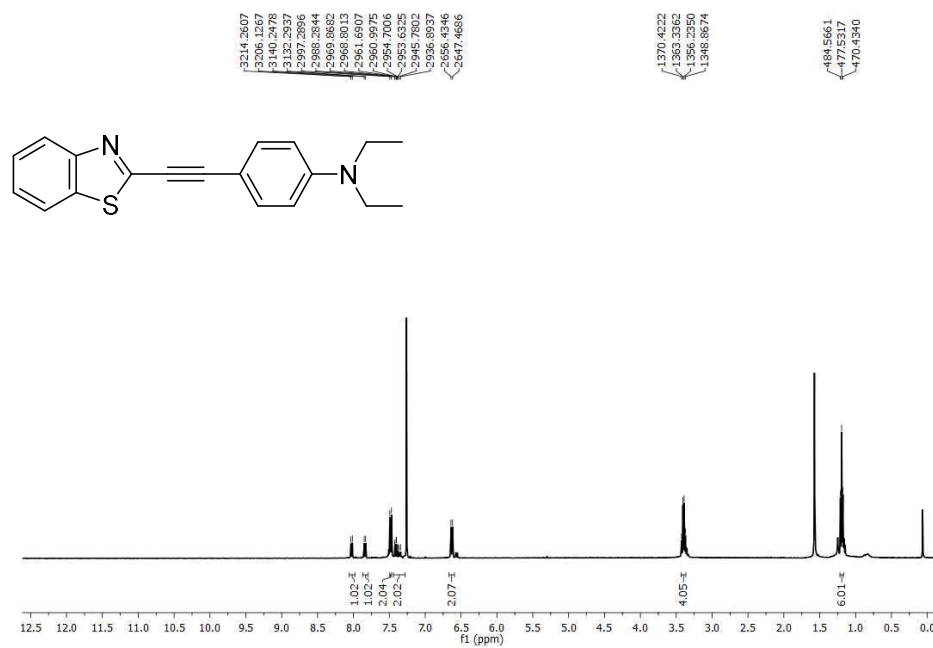


Figure 37. ¹H NMR spectrum of **108** in CDCl₃ solution (400 MHz).

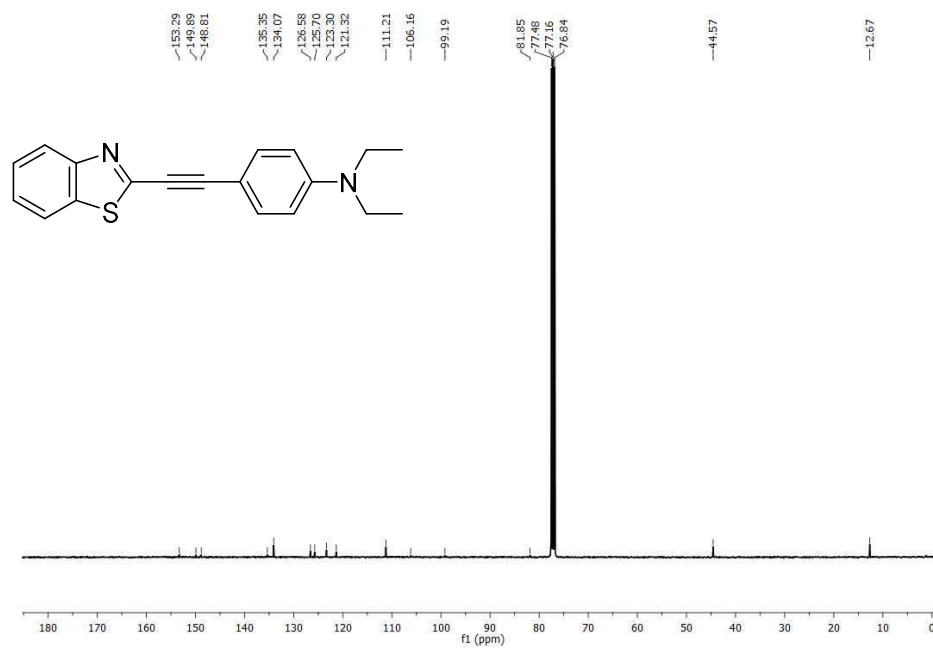


Figure 38. ¹³C NMR spectrum of **108** in CDCl₃ solution (100 MHz).

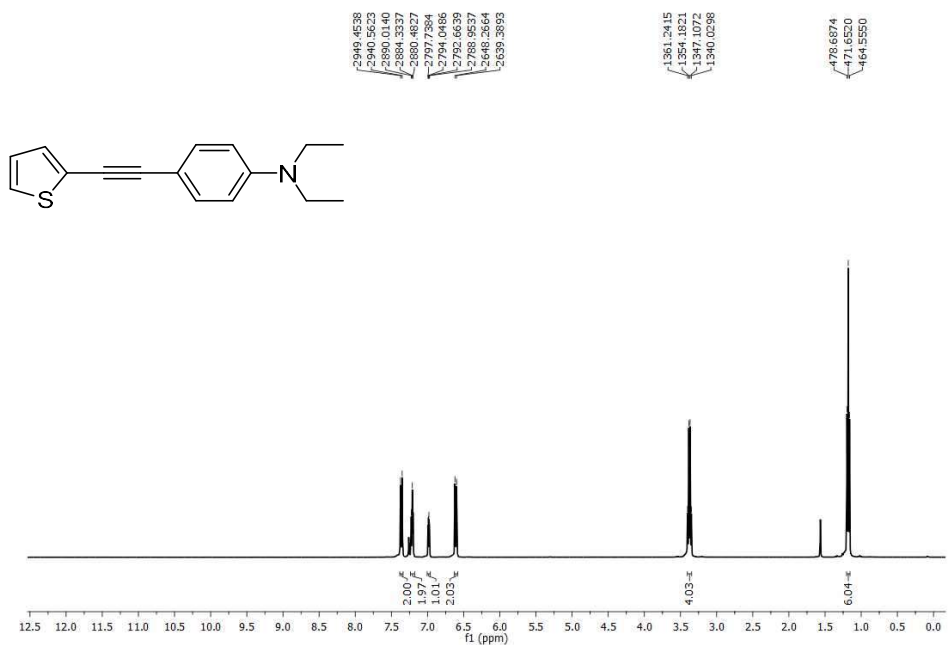


Figure 39. ¹H NMR spectrum of **109** in CDCl₃ solution (400 MHz).

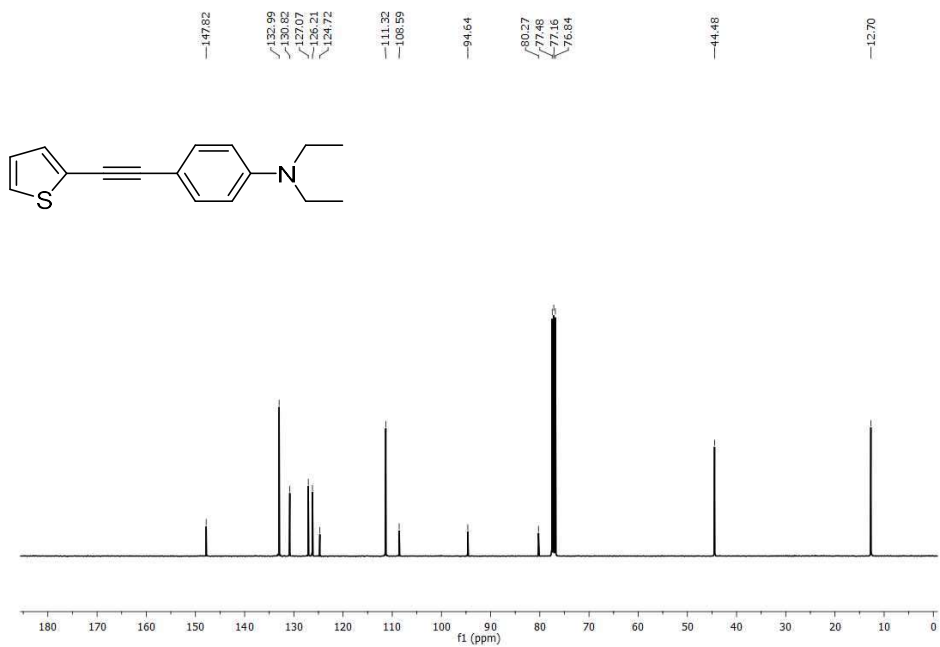


Figure 40. ¹³C NMR spectrum of **109** in CDCl₃ solution (100 MHz).

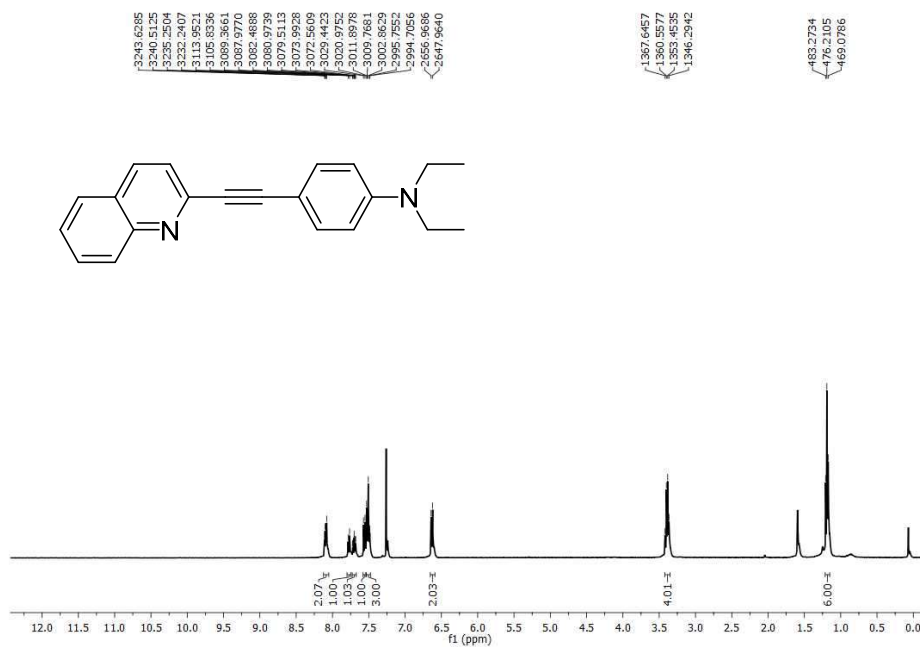


Figure 41. ¹H NMR spectrum of **110** in CDCl₃ solution (400 MHz).

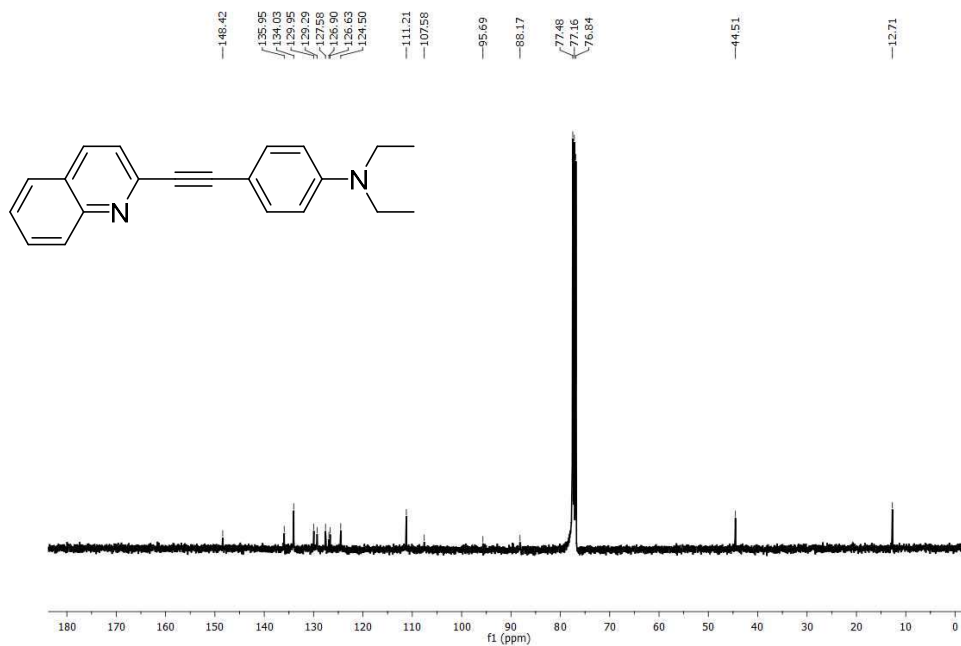


Figure 42. ¹³C NMR spectrum of **110** in CDCl₃ solution (100 MHz).

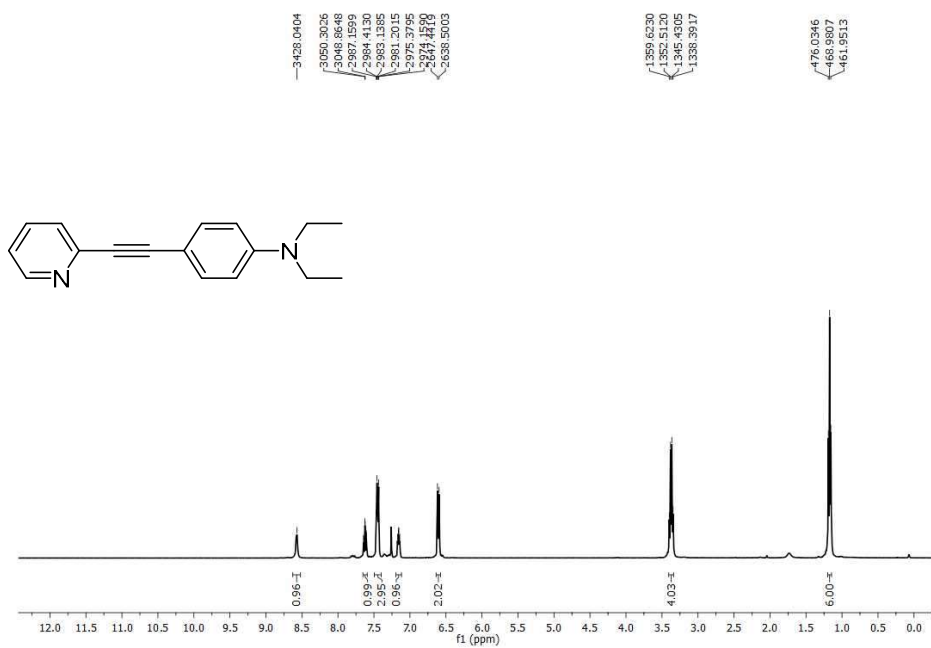


Figure 43. ¹H NMR spectrum of **111** in CDCl₃ solution (400 MHz).

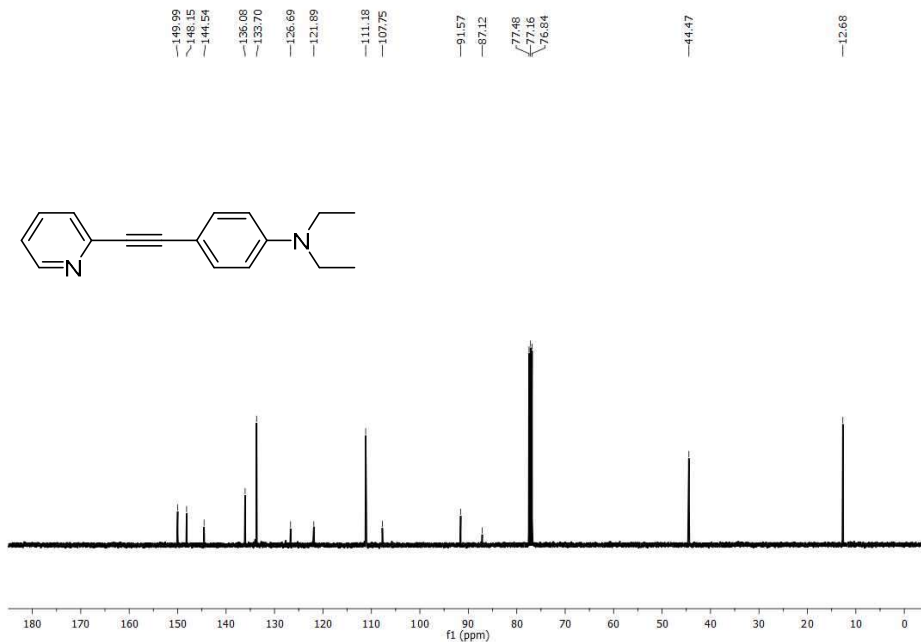


Figure 44. ¹³C NMR spectrum of **111** in CDCl₃ solution (100 MHz).

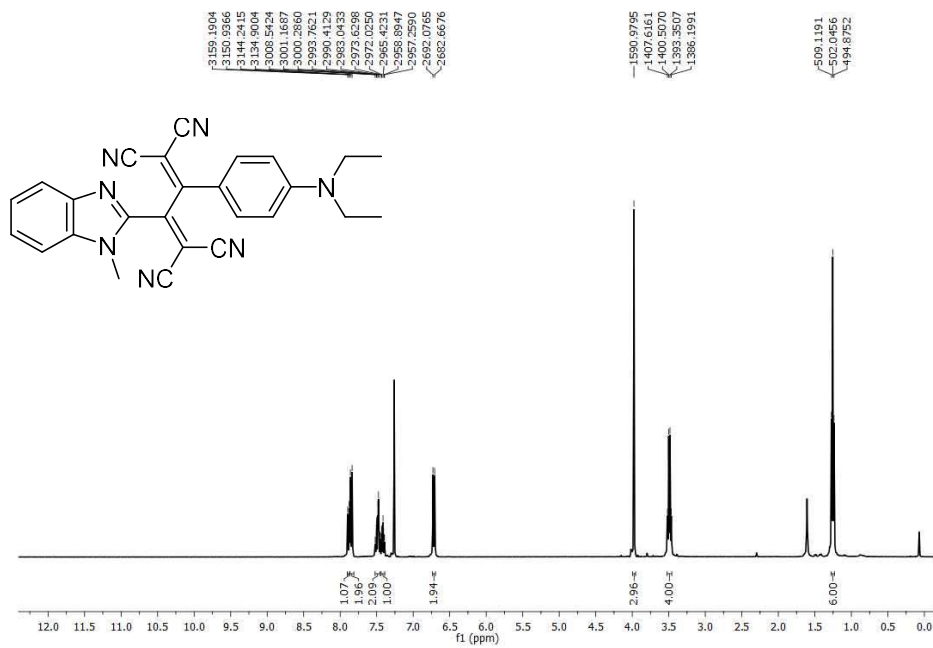


Figure 45. ¹H NMR spectrum of **112** in CDCl₃ solution (400 MHz)

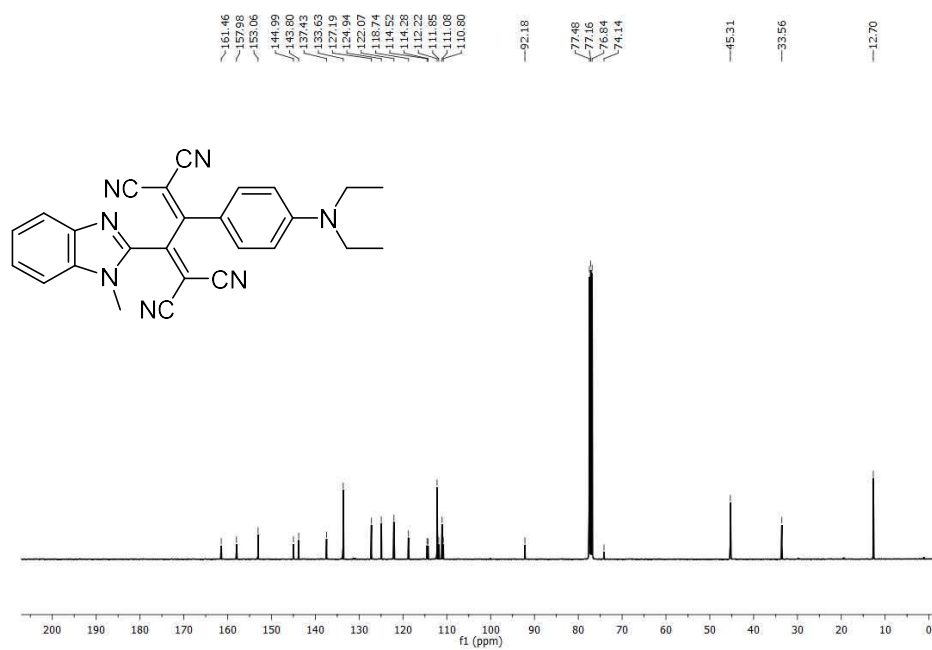


Figure 46. ¹³C NMR spectrum of **112** in CDCl₃ solution (100 MHz).

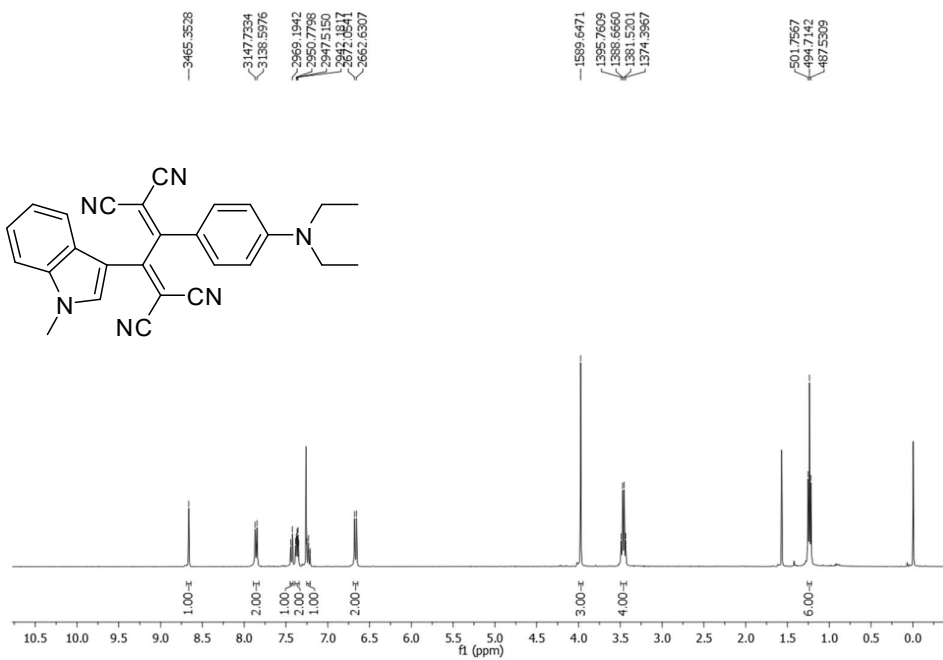


Figure 47. ¹H NMR spectrum of **113** in CDCl₃ solution (400 MHz).

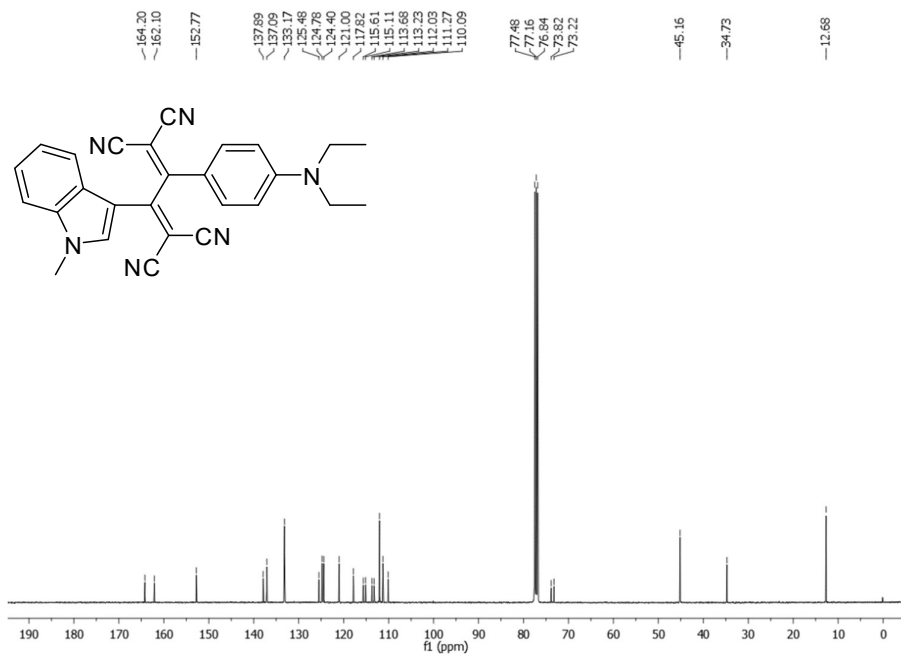


Figure 48. ¹³C NMR spectrum of **113** in CDCl₃ solution (100 MHz).

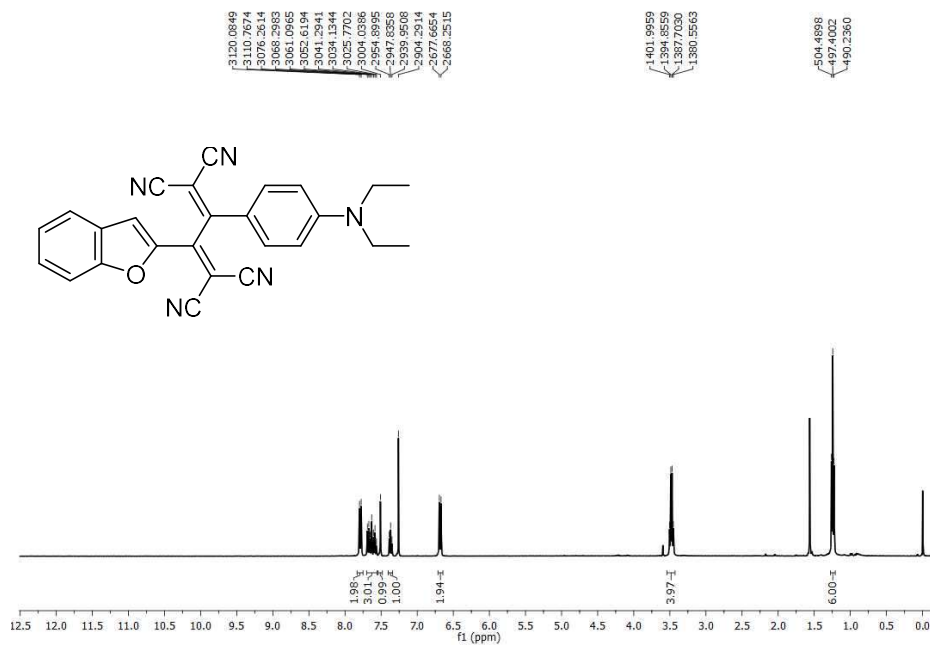


Figure 49. ¹H NMR spectrum of **114** in CDCl₃ solution (400 MHz).

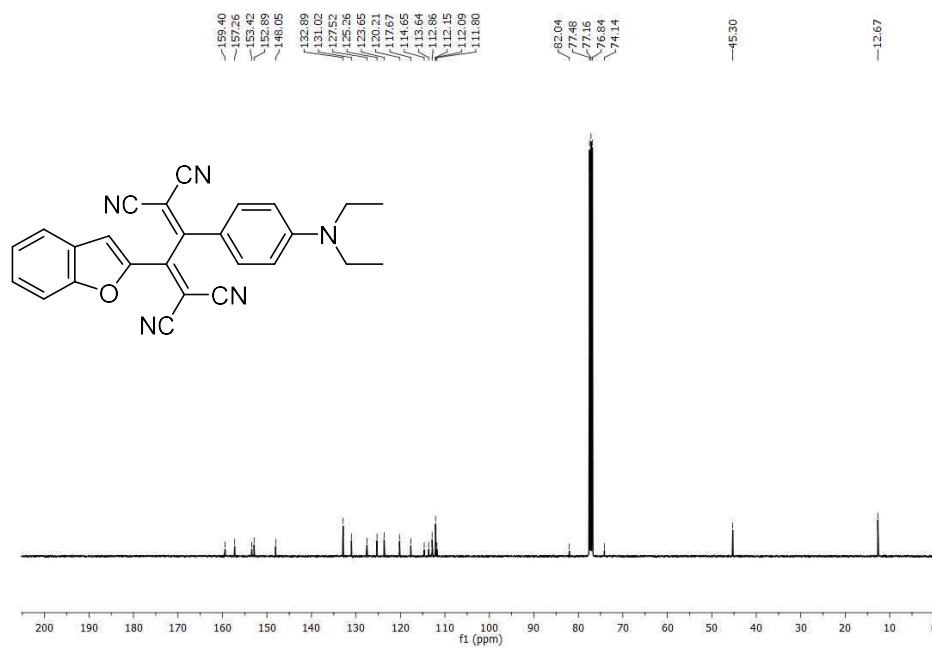


Figure 50. ¹³C NMR spectrum of **114** in CDCl₃ solution (100 MHz).

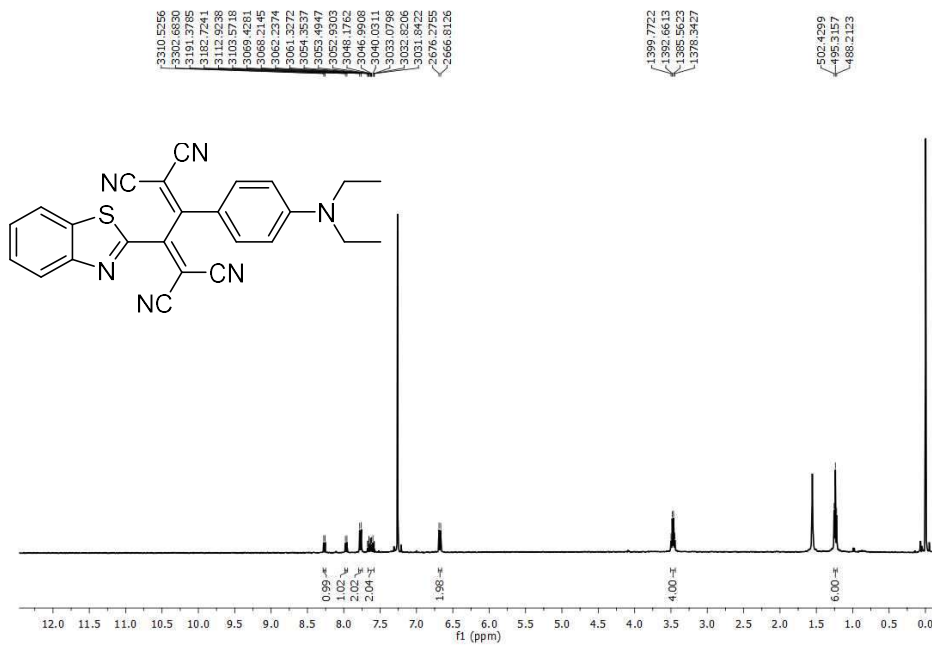


Figure 51. ¹H NMR spectrum of **115** in CDCl₃ solution (400 MHz).

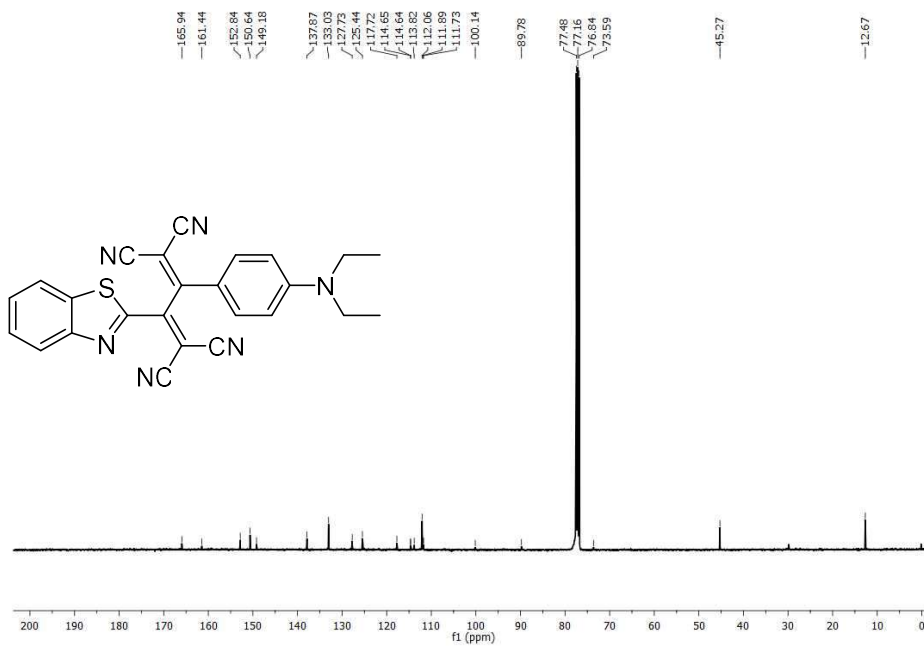


Figure 52. ¹³C NMR spectrum of **115** in CDCl₃ solution (100 MHz).

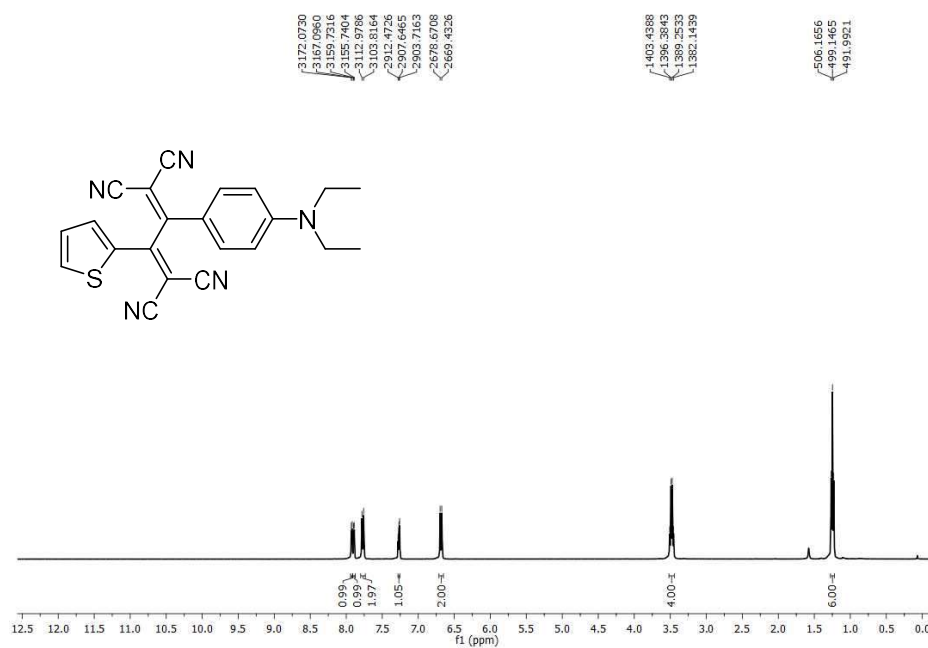


Figure 53. ¹H NMR spectrum of **116** in CDCl₃ solution (400 MHz).

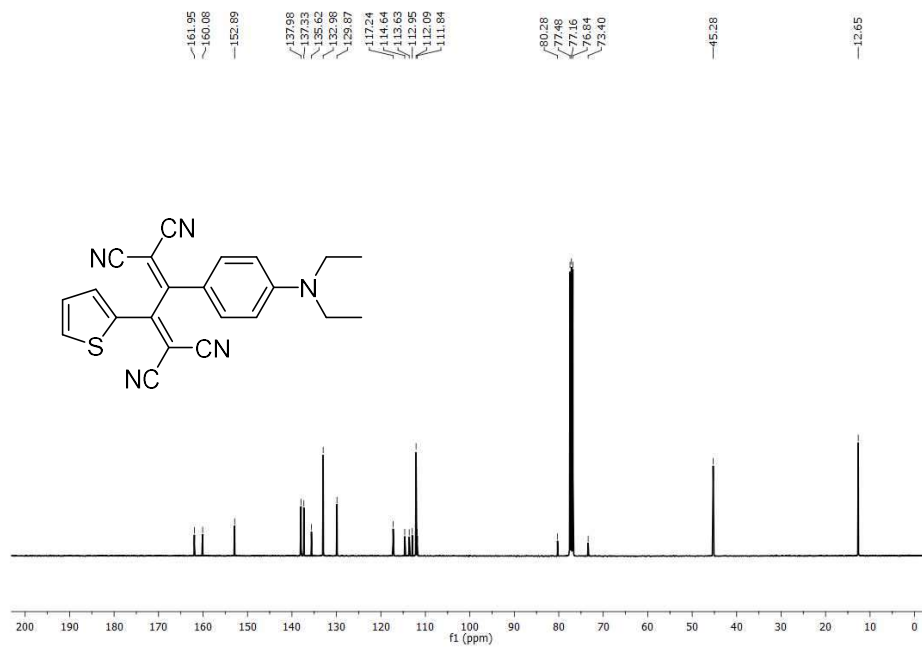


Figure 54. ¹³C NMR spectrum of **116** in CDCl₃ solution (100 MHz).

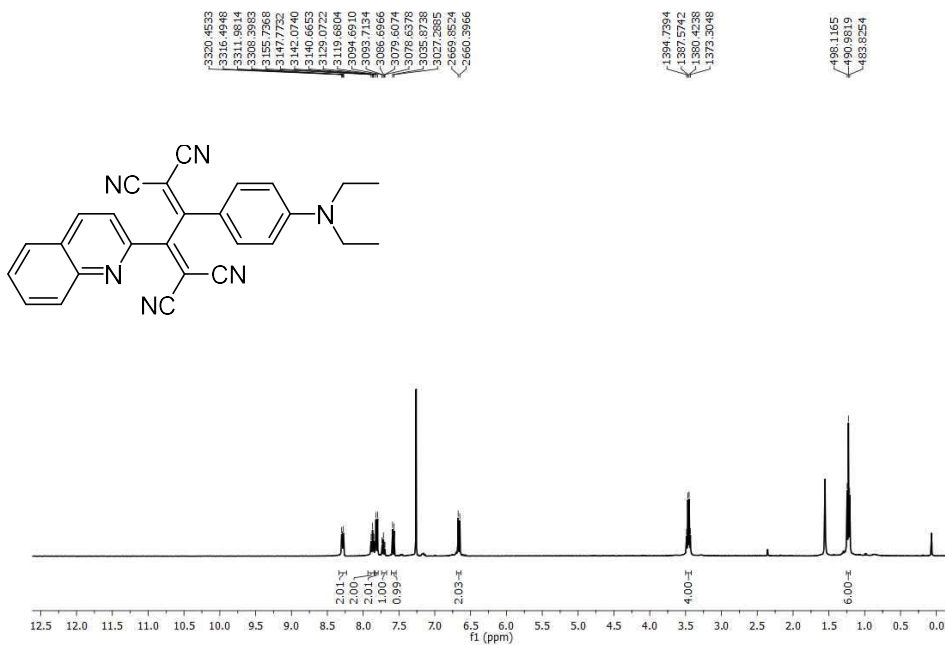


Figure 55. ¹H NMR spectrum of **117** in CDCl₃ solution (400 MHz).

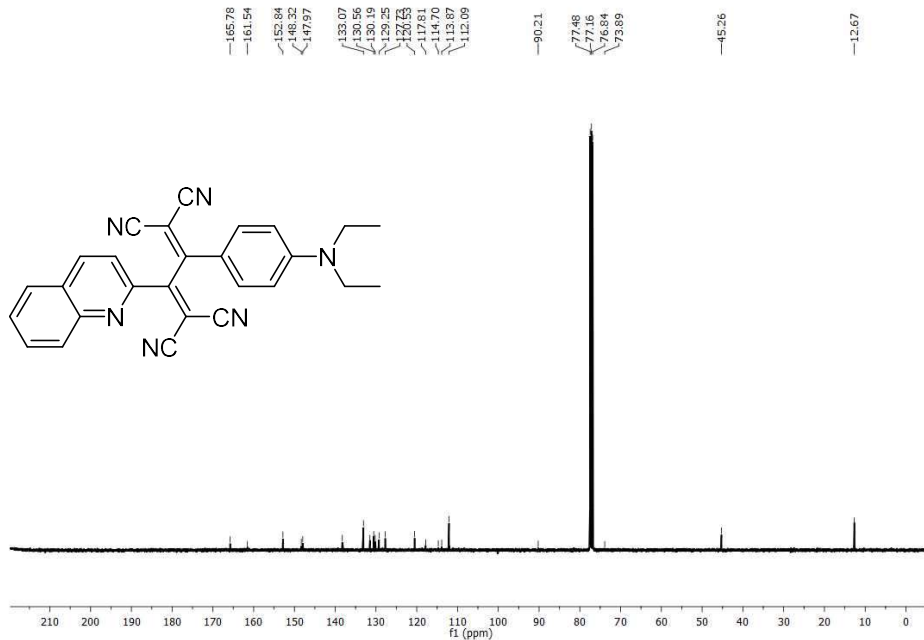


Figure 56. ¹³C NMR spectrum of **117** in CDCl₃ solution (100 MHz).

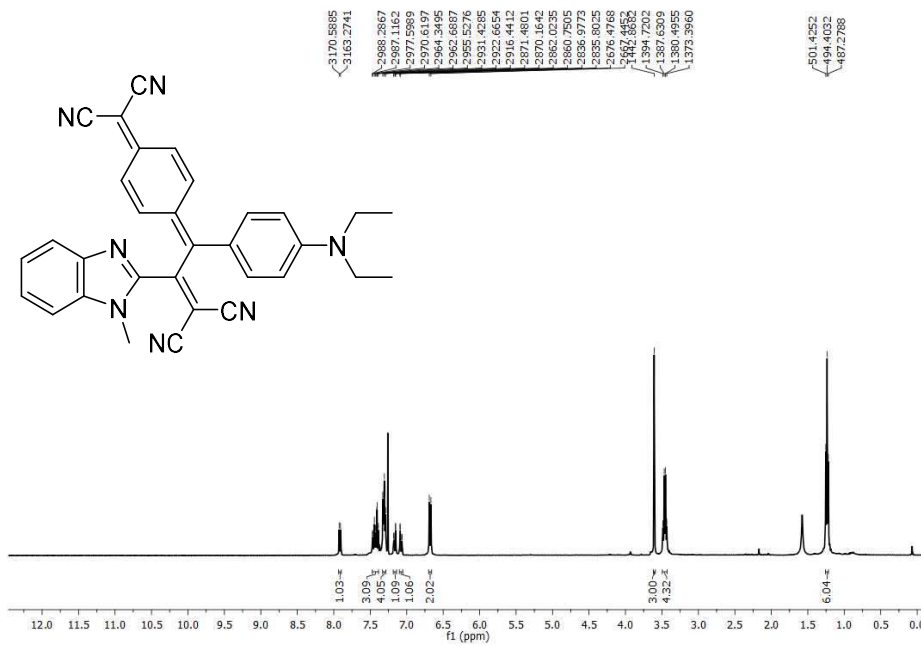


Figure 59. ¹H NMR spectrum of **119** in CDCl₃ solution (400 MHz).

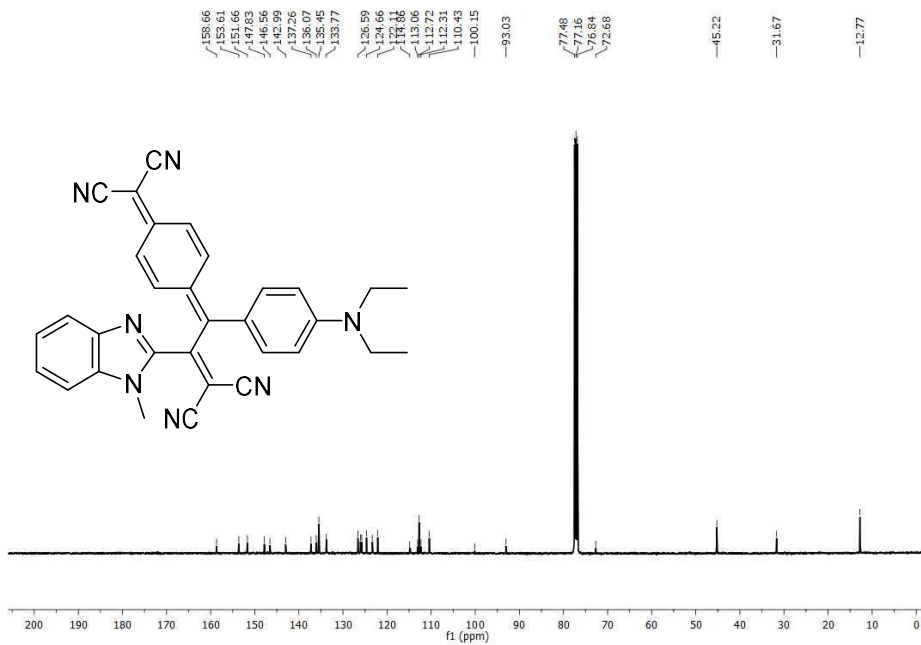


Figure 60. ¹³C NMR spectrum of **119** in CDCl₃ solution (100 MHz).

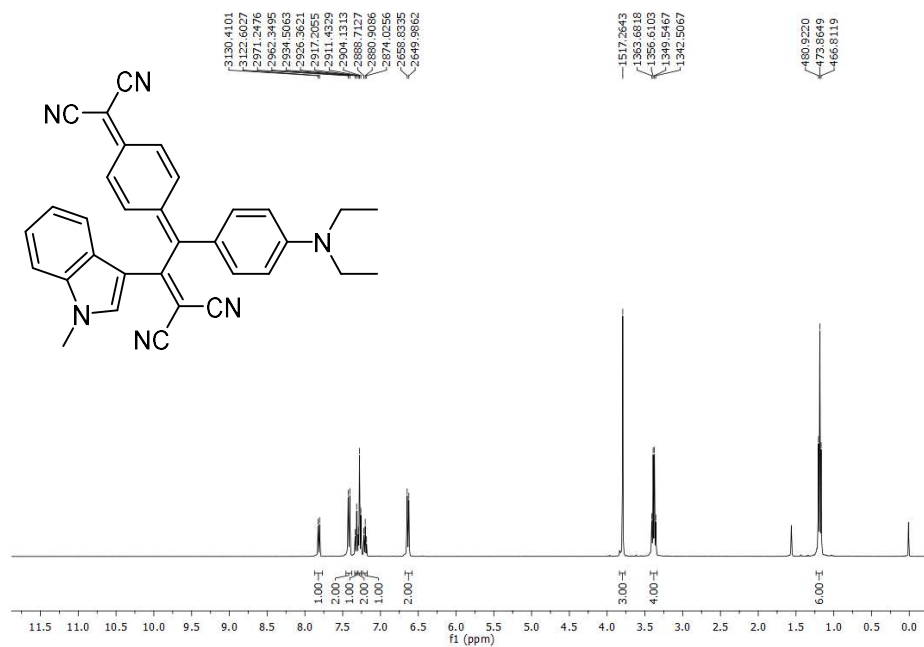


Figure 61. ¹H NMR spectrum of **120** in CDCl₃ solution (400 MHz).

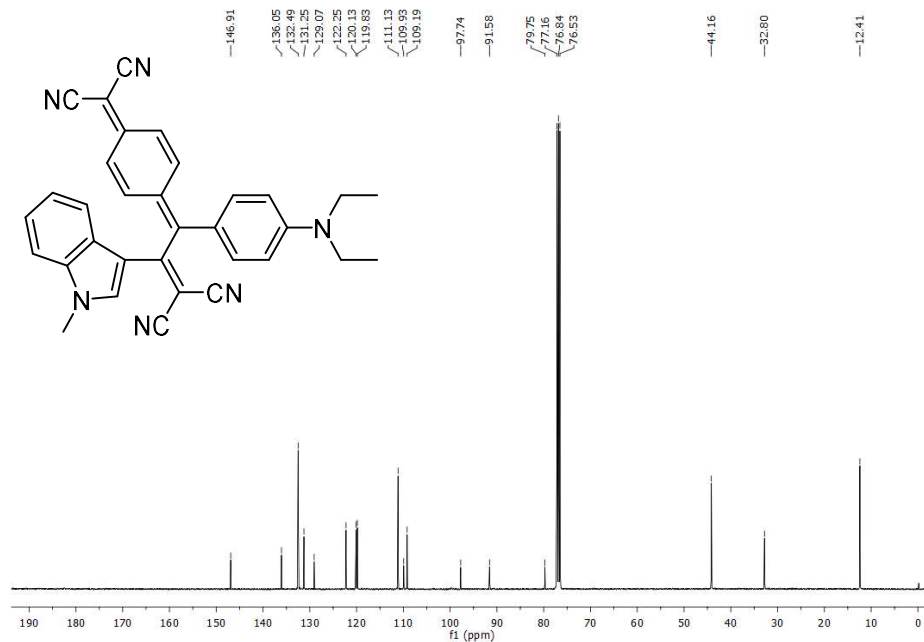


Figure 62. ¹³C NMR spectrum of **120** in CDCl₃ solution (100 MHz).

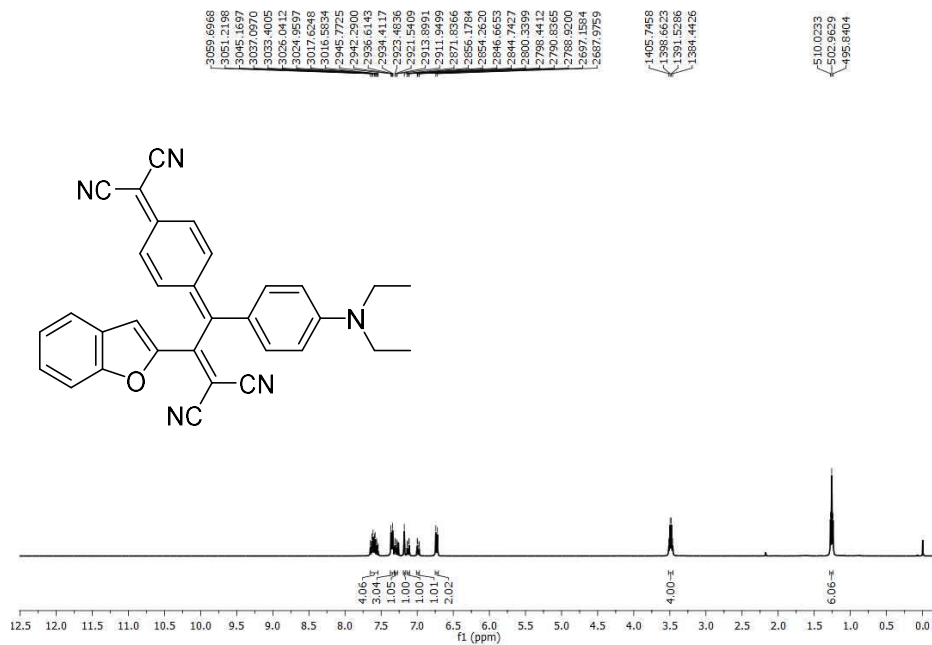


Figure 63. ¹H NMR spectrum of **121** in CDCl₃ solution (400 MHz).

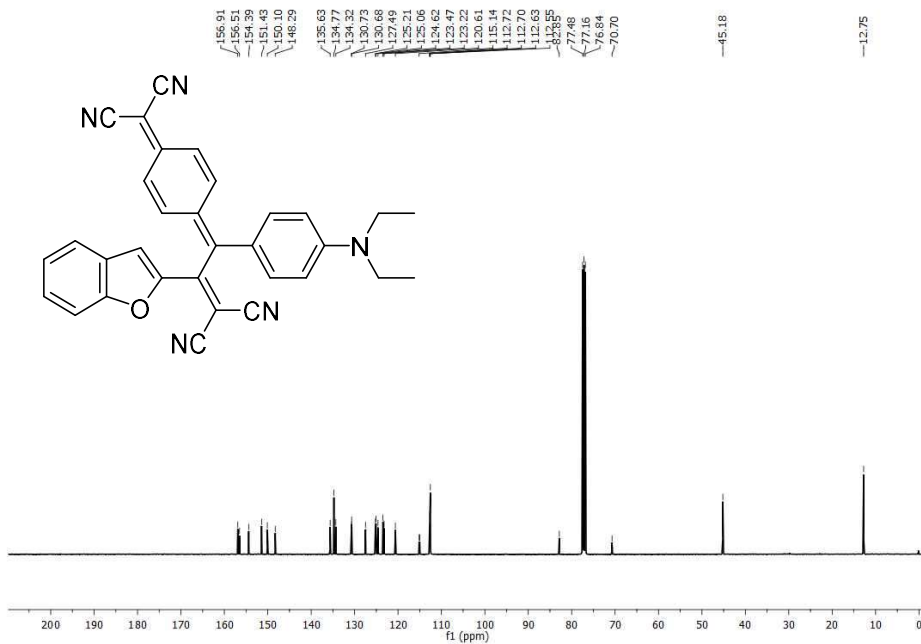


Figure 64. ¹³C NMR spectrum of **121** in CDCl₃ solution (100 MHz).

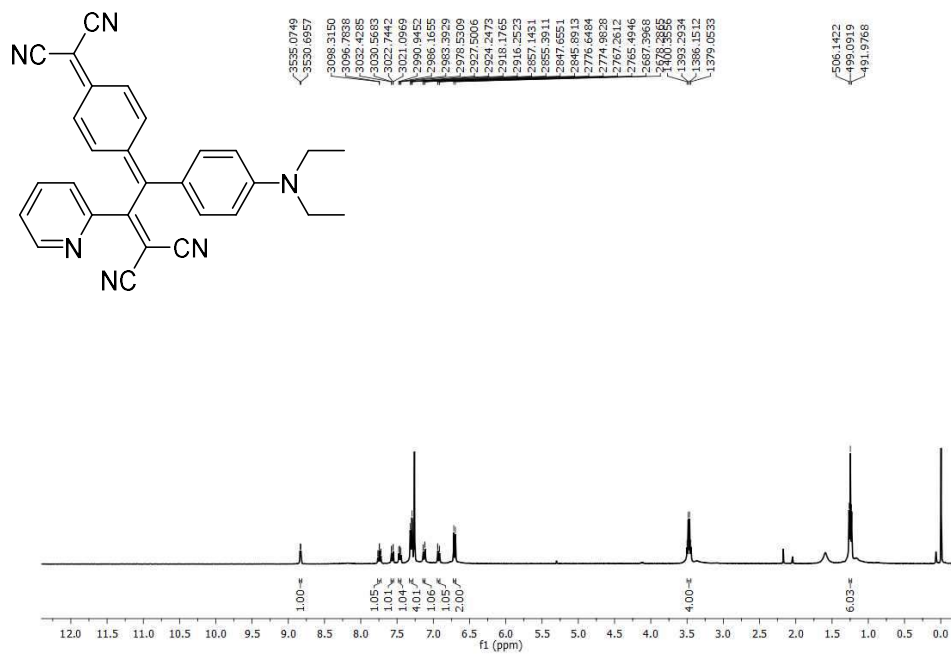


Figure 71. ¹H NMR spectrum of **124** in CDCl₃ solution (400 MHz).

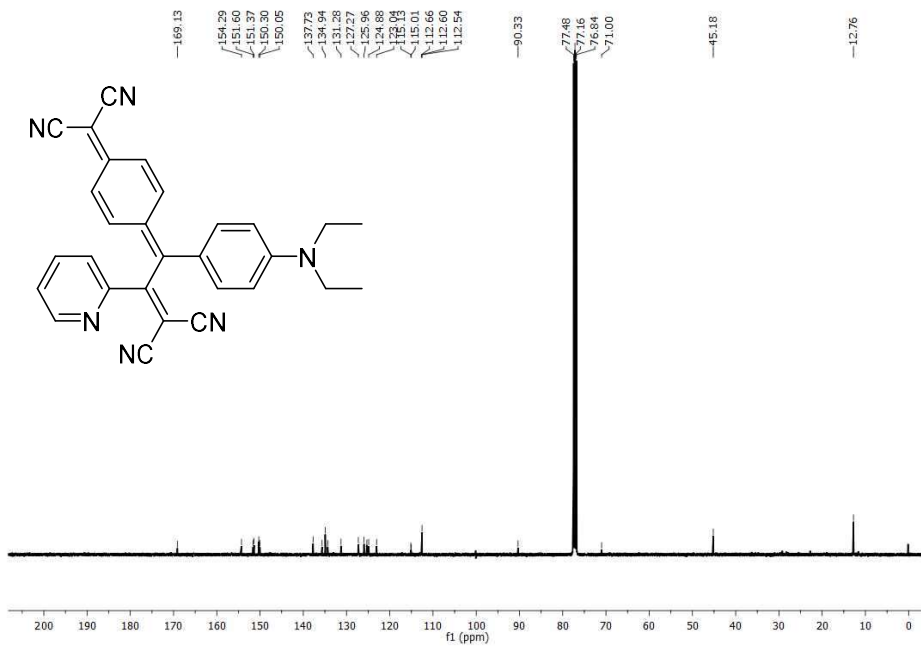


Figure 72. ¹³C NMR spectrum of **124** in CDCl₃ solution (100 MHz).

B. HR-MS

Elemental Composition Report

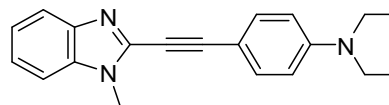
Page 1

Single Mass Analysis

Tolerance = 1000.0 PPM / DBE: min = -5.5, max = 1000.0

Element prediction: Off

Number of isotope peaks used for i-FIT = 9



Monoisotopic Mass, Even Electron Ions

1 formula(e) evaluated with 1 results within limits (all results (up to 1000) for each mass)

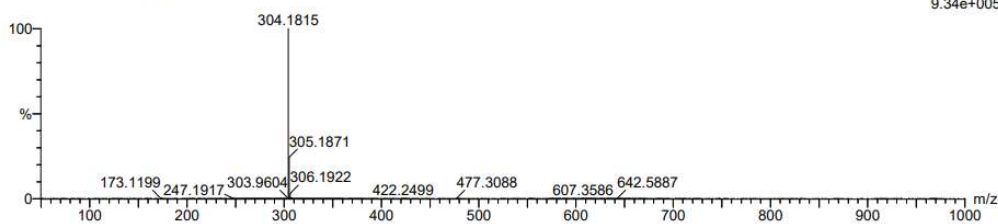
Elements Used:

C: 20-20 H: 21-22 N: 3-3

Basak Karagollu

36163_20220511_11-02 20 (0.775) Cm (14:21)

1: TOF MS ES+
9.34e+005



Minimum: -5.5
Maximum: 1000.0 1000.0 1000.0

Mass	Calc. Mass	mDa	PPM	DBE	i-FIT	i-FIT (Norm)	Formula
304.1815	304.1814	0.1	0.3	11.5	1508.2	0.0	C20 H22 N3

Elemental Composition Report

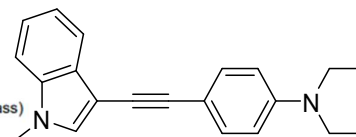
Page 1

Single Mass Analysis

Tolerance = 1000.0 PPM / DBE: min = -5.5, max = 1000.0

Element prediction: Off

Number of isotope peaks used for i-FIT = 3



Monoisotopic Mass, Even Electron Ions

1 formula(e) evaluated with 1 results within limits (all results (up to 1000) for each mass)

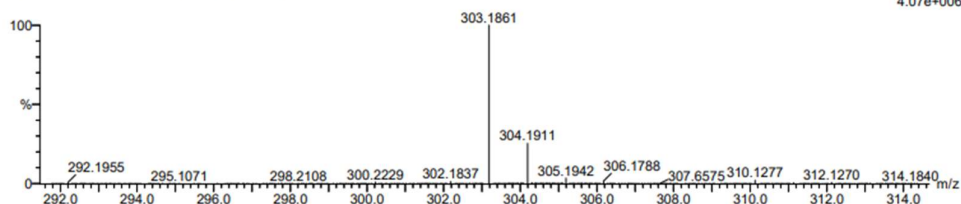
Elements Used:

C: 21-21 H: 22-23 N: 2-2

Cagatay Deniz

32149_20210326_06-01 12 (0.484) Cm (1:17)

1: TOF MS ES+
4.07e+006



Minimum: -5.5
Maximum: 1000.0 1000.0 1000.0

Mass	Calc. Mass	mDa	PPM	DBE	i-FIT	i-FIT (Norm)	Formula
303.1861	303.1861	0.0	0.0	11.5	898.5	0.0	C21 H23 N2

Elemental Composition Report

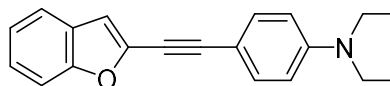
Page 1

Single Mass Analysis

Tolerance = 1000.0 PPM / DBE: min = -5.5, max = 1000.0

Element prediction: Off

Number of isotope peaks used for i-FIT = 9



Monoisotopic Mass, Even Electron Ions

1 formula(e) evaluated with 1 results within limits (all results (up to 1000) for each mass)

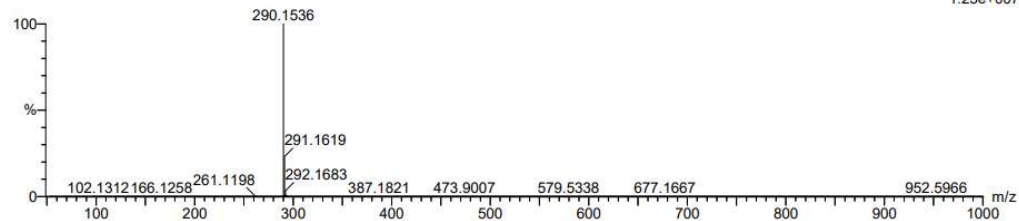
Elements Used:

C: 20-20 H: 19-20 N: 1-1 O: 1-1

Basak Karagollu

36163_20220511_08-03 9 (0.362) Cm (1:15)

1: TOF MS ES+
1.25e+007



Minimum: -5.5
Maximum: 1000.0 1000.0 1000.0

Mass	Calc. Mass	mDa	PPM	DBE	i-FIT	i-FIT (Norm)	Formula
290.1536	290.1545	-0.9	-3.1	11.5	2281.6	0.0	C20 H20 N O

Elemental Composition Report

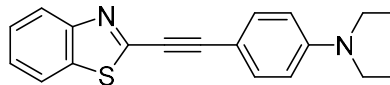
Page 1

Single Mass Analysis

Tolerance = 1000.0 PPM / DBE: min = -5.5, max = 1000.0

Element prediction: Off

Number of isotope peaks used for i-FIT = 9



Monoisotopic Mass, Even Electron Ions

1 formula(e) evaluated with 1 results within limits (all results (up to 1000) for each mass)

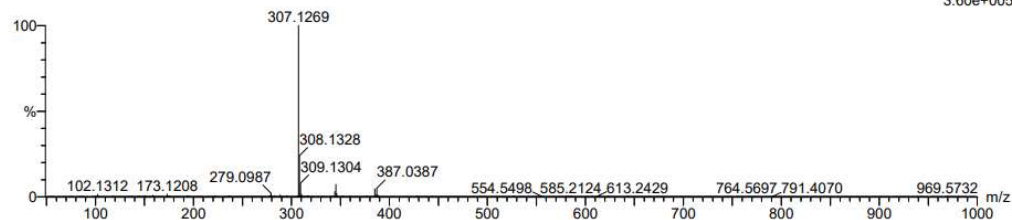
Elements Used:

C: 19-19 H: 18-19 N: 2-2 S: 1-1

Basak Karagollu

36163_20220511_09-04 24 (0.931) Cm (2:24)

1: TOF MS ES+
3.60e+005



Minimum: -5.5
Maximum: 1000.0 1000.0 1000.0

Mass	Calc. Mass	mDa	PPM	DBE	i-FIT	i-FIT (Norm)	Formula
307.1269	307.1269	0.0	0.0	11.5	1708.2	0.0	C19 H19 N2 S

Elemental Composition Report

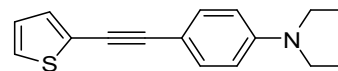
Page 1

Single Mass Analysis

Tolerance = 1000.0 PPM / DBE: min = -5.5, max = 1000.0

Element prediction: Off

Number of isotope peaks used for i-FIT = 3



Monoisotopic Mass, Even Electron Ions

1 formula(e) evaluated with 1 results within limits (all results (up to 1000) for each mass)

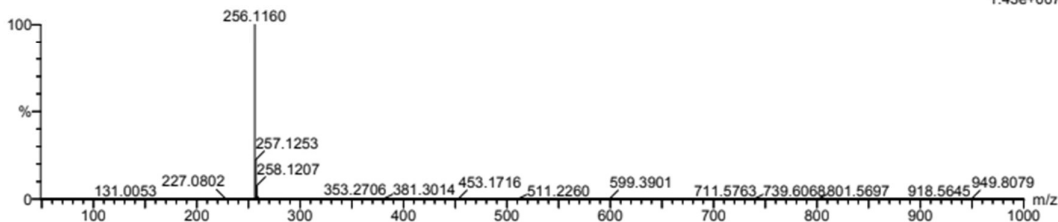
Elements Used:

C: 16-16 H: 17-18 N: 1-1 S: 1-1

Cagatay Dengiz

34144_20211104_01-06 7 (0.294) Cm (1:18)

1: TOF MS ES+
1.43e+007



Minimum: -5.5
Maximum: 1000.0 1000.0 1000.0

Mass	Calc. Mass	mDa	PPM	DBE	i-FIT	i-FIT (Norm)	Formula
256.1160	256.1160	0.0	0.0	8.5	1024.4	0.0	C16 H18 N S

Elemental Composition Report

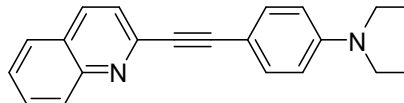
Page 1

Single Mass Analysis

Tolerance = 1000.0 PPM / DBE: min = -5.5, max = 1000.0

Element prediction: Off

Number of isotope peaks used for i-FIT = 9



Monoisotopic Mass, Even Electron Ions

1 formula(e) evaluated with 1 results within limits (all results (up to 1000) for each mass)

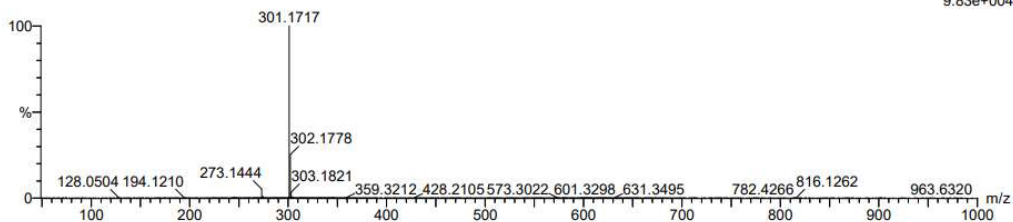
Elements Used:

C: 21-21 H: 20-21 N: 2-2

Basak Karagollu

36163_20220511_10-03 5 (0.206) Cm (1:8)

1: TOF MS ES+
9.83e+004



Minimum: -5.5
Maximum: 1000.0 1000.0 1000.0

Mass	Calc. Mass	mDa	PPM	DBE	i-FIT	i-FIT (Norm)	Formula
301.1717	301.1705	1.2	4.0	12.5	1178.5	0.0	C21 H21 N2

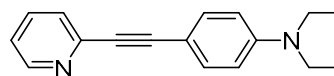
Elemental Composition Report

Single Mass Analysis

Tolerance = 1000.0 PPM / DBE: min = -5.5, max = 1000.0

Element prediction: Off

Number of isotope peaks used for i-FIT = 3



Monoisotopic Mass, Even Electron Ions

1 formula(e) evaluated with 1 results within limits (all results (up to 1000) for each mass)

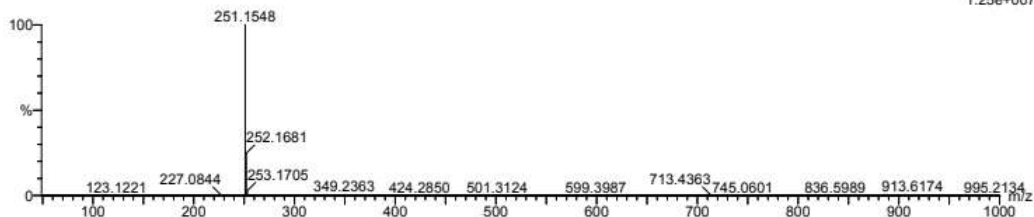
Elements Used:

C: 17-17 H: 18-19 N: 2-2

Cagatay Dengiz

34144_20211104_02-04 1 (0.070) Cm (1:9)

1: TOF MS ES+
1.25e+007



Minimum: -5.5
Maximum: 1000.0 1000.0 1000.0

Mass	Calc. Mass	mDa	PPM	DBE	i-FIT	i-FIT (Norm)	Formula
251.1548	251.1548	0.0	0.0	9.5	788.8	0.0	C17 H19 N2

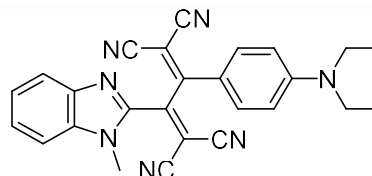
Elemental Composition Report

Single Mass Analysis

Tolerance = 1000.0 PPM / DBE: min = -5.5, max = 1000.0

Element prediction: Off

Number of isotope peaks used for i-FIT = 3



Monoisotopic Mass, Odd and Even Electron Ions

1 formula(e) evaluated with 1 results within limits (all results (up to 1000) for each mass)

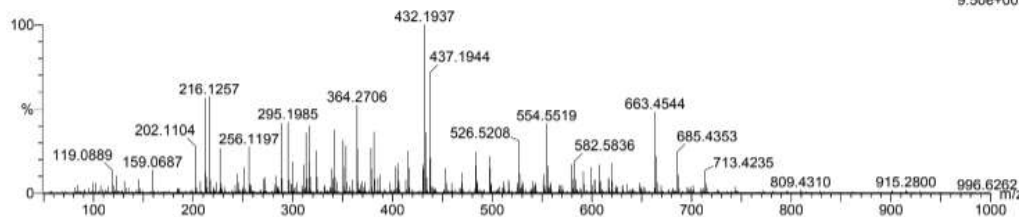
Elements Used:

C: 26-26 H: 21-22 N: 7-7

Cagatay Dengiz

34144_20211104_05-01 21 (0.829) Cm (14:24)

1: TOF MS ES+
9.50e+003



Minimum: -5.5
Maximum: 1000.0 1000.0 1000.0

Mass	Calc. Mass	mDa	PPM	DBE	i-FIT	i-FIT (Norm)	Formula
432.1937	432.1937	0.0	0.0	19.5	287.4	0.0	C26 H22 N7

Elemental Composition Report

Page 1

Single Mass Analysis

Tolerance = 1000.0 PPM / DBE: min = -5.5, max = 1000.0

Element prediction: Off

Number of isotope peaks used for i-FIT = 3

Monoisotopic Mass, Even Electron Ions

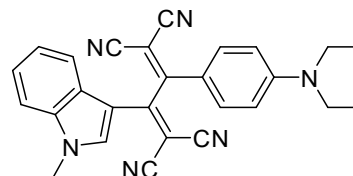
1 formula(e) evaluated with 1 results within limits (all results (up to 1000) for each mass)

Elements Used:

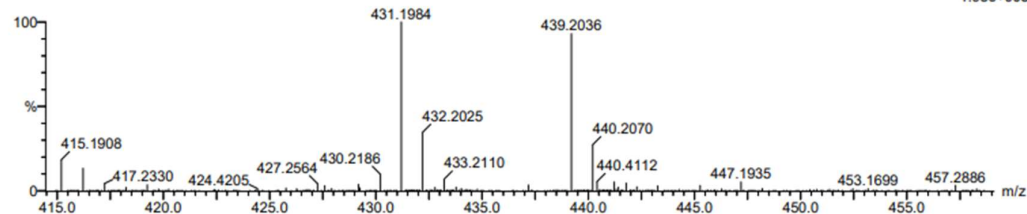
C: 27-27 H: 22-23 N: 6-6

Cagatay Dengiz

32149_20210326_07-03 6 (0.260) Cm (1:6)



1: TOF MS ES+
1.98e+005



Minimum: -5.5
Maximum: 1000.0

Mass	Calc. Mass	mDa	PPM	DBE	i-FIT	i-FIT (Norm)	Formula
431.1984	431.1984	0.0	0.0	19.5	439.7	0.0	C27 H23 N6

Elemental Composition Report

Page 1

Single Mass Analysis

Tolerance = 1000.0 PPM / DBE: min = -5.5, max = 1000.0

Element prediction: Off

Number of isotope peaks used for i-FIT = 9

Monoisotopic Mass, Even Electron Ions

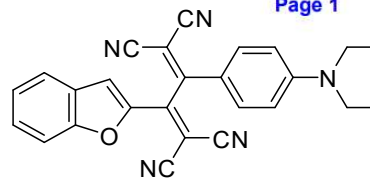
1 formula(e) evaluated with 1 results within limits (all results (up to 1000) for each mass)

Elements Used:

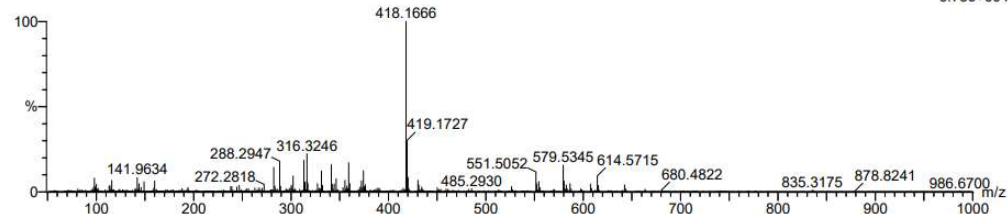
C: 26-26 H: 19-20 N: 5-5 O: 1-1

Basak Karagollu

36163_20220511_04-02 10 (0.396) Cm (9:17)



1: TOF MS ES+
6.73e+004



Minimum: -5.5
Maximum: 1000.0

Mass	Calc. Mass	mDa	PPM	DBE	i-FIT	i-FIT (Norm)	Formula
418.1666	418.1668	-0.2	-0.5	19.5	988.0	0.0	C26 H20 N5 O

Elemental Composition Report

Single Mass Analysis

Tolerance = 1000.0 PPM / DBE: min = -5.5, max = 1000.0

Element prediction: Off

Number of isotope peaks used for i-FIT = 9

Monoisotopic Mass, Even Electron Ions

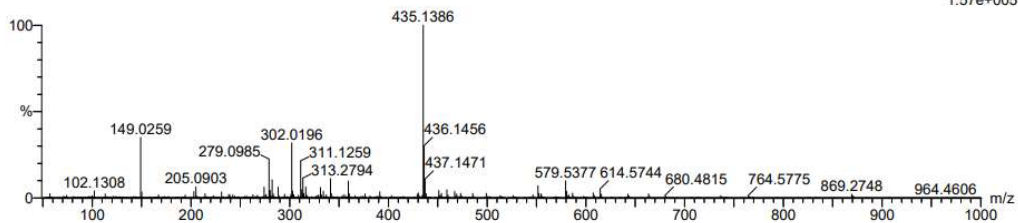
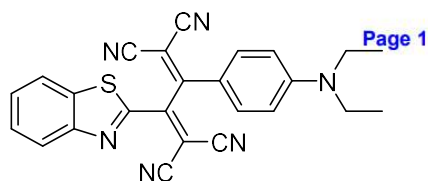
1 formula(e) evaluated with 1 results within limits (all results (up to 1000) for each mass)

Elements Used:

C: 25-25 H: 18-19 N: 6-6 S: 1-1

Basak Karagollu

36163_20220511_02-01 9 (0.362) Cm (1:9)



Minimum: -5.5
Maximum: 1000.0 1000.0 1000.0

Mass	Calc. Mass	mDa	PPM	DBE	i-FIT	i-FIT (Norm)	Formula
435.1386	435.1392	-0.6	-1.4	19.5	1194.3	0.0	C25 H19 N6 S

1: TOF MS ES+
1.57e+005

Elemental Composition Report

Single Mass Analysis

Tolerance = 1000.0 PPM / DBE: min = -5.5, max = 1000.0

Element prediction: Off

Number of isotope peaks used for i-FIT = 3

Monoisotopic Mass, Even Electron Ions

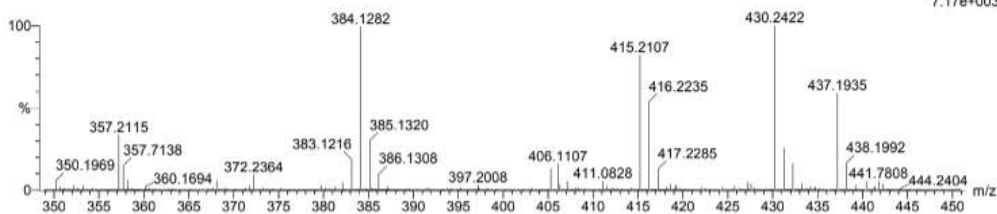
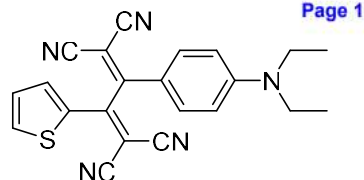
1 formula(e) evaluated with 1 results within limits (all results (up to 1000) for each mass)

Elements Used:

C: 22-22 H: 17-18 N: 5-5 S: 1-1

Çağatay Dengiz

34144_20211104_03-06 11 (0.450) Cm (8:18)



Minimum: -5.5
Maximum: 1000.0 1000.0 1000.0

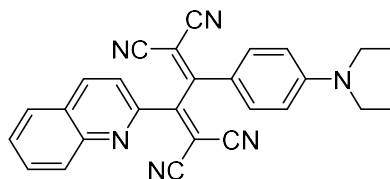
Mass	Calc. Mass	mDa	PPM	DBE	i-FIT	i-FIT (Norm)	Formula
384.1282	384.1283	-0.1	-0.3	16.5	283.3	0.0	C22 H18 N5 S

1: TOF MS ES+
7.17e+003

Elemental Composition Report

Single Mass Analysis

Tolerance = 1000.0 PPM / DBE: min = -5.5, max = 1000.0
Element prediction: Off
Number of isotope peaks used for i-FIT = 9



Page 1

Monoisotopic Mass, Even Electron Ions

1 formula(e) evaluated with 1 results within limits (all results (up to 1000) for each mass)

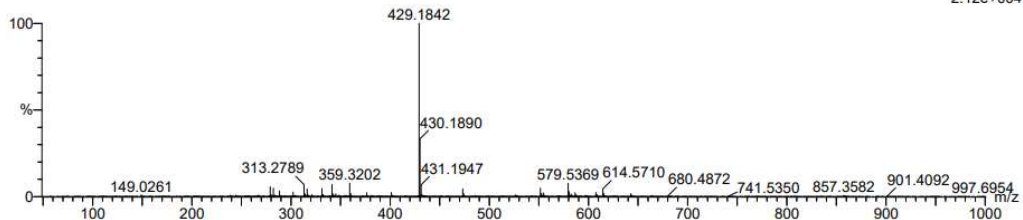
Elements Used:

C: 27-27 H: 20-21 N: 6-6

Basak Karagollu

36163_20220511_01-03 10 (0.396) Cm (3:11)

1: TOF MS ES+
2.12e+004



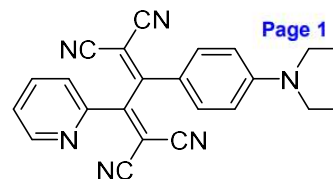
Minimum: 1000.0 1000.0 -5.5
Maximum: 1000.0 1000.0 1000.0

Mass	Calc. Mass	mDa	PPM	DBE	i-FIT	i-FIT (Norm)	Formula
429.1842	429.1828	1.4	3.3	20.5	736.1	0.0	C27 H21 N6

Elemental Composition Report

Single Mass Analysis

Tolerance = 1000.0 PPM / DBE: min = -5.5, max = 1000.0
Element prediction: Off
Number of isotope peaks used for i-FIT = 9



Page 1

Monoisotopic Mass, Even Electron Ions

1 formula(e) evaluated with 1 results within limits (all results (up to 1000) for each mass)

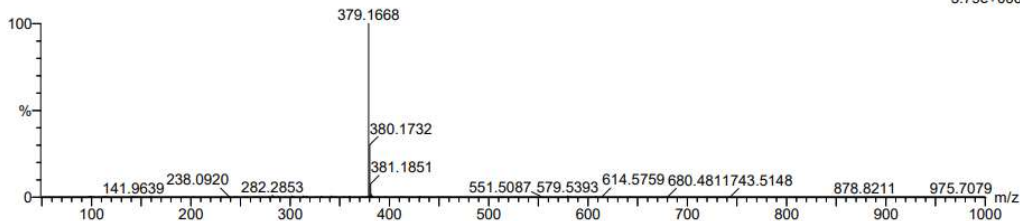
Elements Used:

C: 23-23 H: 18-19 N: 6-6

Basak Karagollu

36163_20220511_03-01 6 (0.260) Cm (1:17)

1: TOF MS ES+
3.79e+006



Minimum: 1000.0 1000.0 -5.5
Maximum: 1000.0 1000.0 1000.0

Mass	Calc. Mass	mDa	PPM	DBE	i-FIT	i-FIT (Norm)	Formula
379.1668	379.1671	-0.3	-0.8	17.5	1892.7	0.0	C23 H19 N6

Elemental Composition Report

Page 1

Single Mass Analysis

Tolerance = 1000.0 PPM / DBE: min = -5.5, max = 1000.0
 Element prediction: Off
 Number of isotope peaks used for i-FIT = 3

Monoisotopic Mass, Even Electron Ions

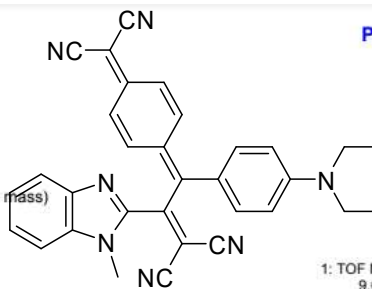
1 formula(e) evaluated with 1 results within limits (all results (up to 1000) for each mass)

Elements Used:

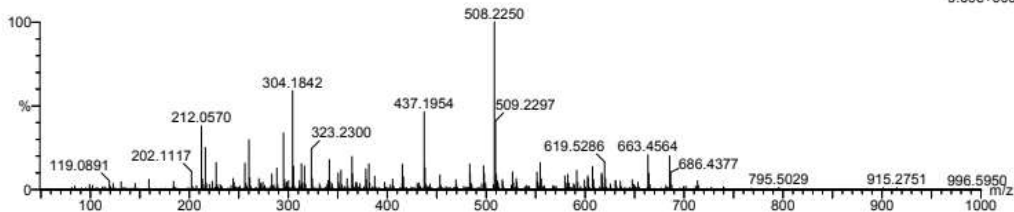
C: 32-32 H: 25-26 N: 7-7

Cagatay Dengiz

34144_20211104_06-04 21 (0.829) Cm (12:25)



1: TOF MS ES+
9.69e+003



Minimum:

Maximum: 1000.0 1000.0 -5.5 1000.0

Mass	Calc. Mass	mDa	PPM	DBE	i-FIT	i-FIT (Norm)	Formula
508.2250	508.2250	0.0	0.0	23.5	250.6	0.0	C32 H26 N7

Elemental Composition Report

Page 1

Single Mass Analysis

Tolerance = 1000.0 PPM / DBE: min = -5.5, max = 1000.0
 Element prediction: Off
 Number of isotope peaks used for i-FIT = 3

Monoisotopic Mass, Even Electron Ions

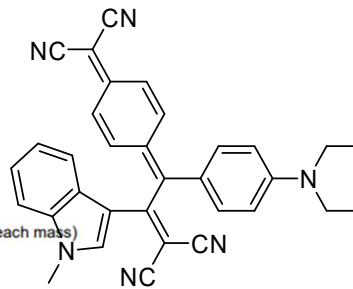
1 formula(e) evaluated with 1 results within limits (all results (up to 1000) for each mass)

Elements Used:

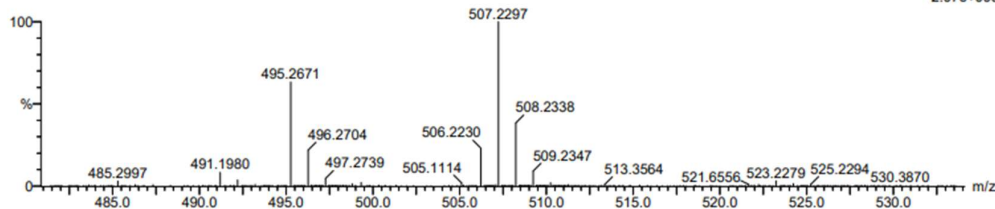
C: 33-33 H: 26-27 N: 6-6

Cagatay Dengiz

32149_20210326_08-01 8 (0.328) Cm (8:24)



1: TOF MS ES+
2.07e+006



Minimum:

Maximum: 1000.0 1000.0 -5.5 1000.0

Mass	Calc. Mass	mDa	PPM	DBE	i-FIT	i-FIT (Norm)	Formula
507.2297	507.2297	0.0	0.0	23.5	610.1	0.0	C33 H27 N6

Elemental Composition Report

Page 1

Single Mass Analysis

Tolerance = 1000.0 PPM / DBE: min = -5.5, max = 1000.0
Element prediction: Off
Number of isotope peaks used for i-FIT = 9

Monoisotopic Mass, Even Electron Ions

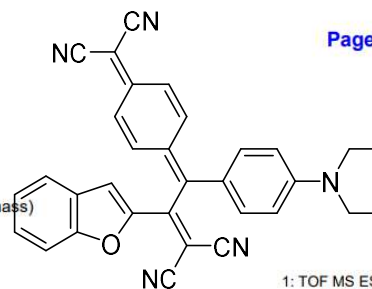
1 formula(e) evaluated with 1 results within limits (all results (up to 1000) for each mass)

Elements Used:

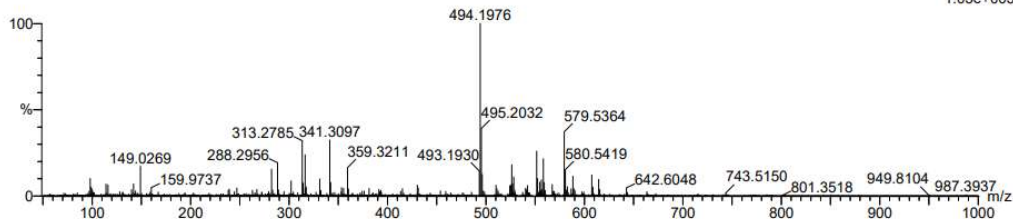
C: 32-32 H: 23-24 N: 5-5 O: 1-1

Basak Karagollu

36163_20220511_07-01 16 (0.639) Cm (7:16)



1: TOF MS ES+
1.05e+005



Minimum: -5.5
Maximum: 1000.0 1000.0 1000.0

Mass	Calc. Mass	mDa	PPM	DBE	i-FIT	i-FIT (Norm)	Formula
494.1976	494.1981	-0.5	-1.0	23.5	1057.3	0.0	C32 H24 N5 O

Elemental Composition Report

Page 1

Single Mass Analysis

Tolerance = 1000.0 PPM / DBE: min = -5.5, max = 1000.0
Element prediction: Off
Number of isotope peaks used for i-FIT = 9

Monoisotopic Mass, Even Electron Ions

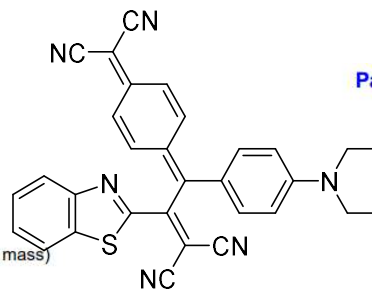
1 formula(e) evaluated with 1 results within limits (all results (up to 1000) for each mass)

Elements Used:

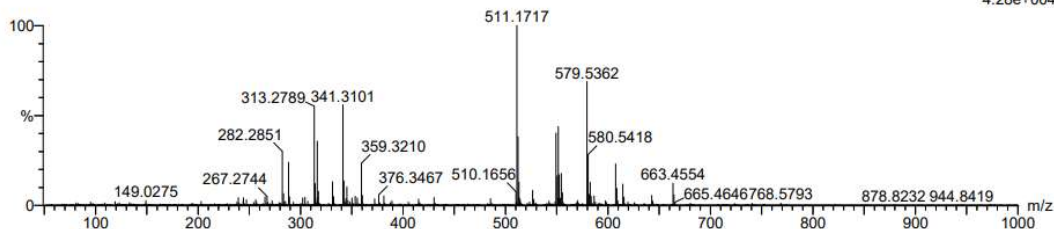
C: 31-31 H: 22-23 N: 6-6 S: 1-1

Basak Karagollu

36163_20220511_06-03 13 (0.518) Cm (4:13)



1: TOF MS ES+
4.28e+004



Minimum: -5.5
Maximum: 1000.0 1000.0 1000.0

Mass	Calc. Mass	mDa	PPM	DBE	i-FIT	i-FIT (Norm)	Formula
511.1717	511.1705	1.2	2.3	23.5	887.7	0.0	C31 H23 N6 S

Elemental Composition Report

Page 1

Single Mass Analysis

Tolerance = 1000.0 PPM / DBE: min = -5.5, max = 1000.0

Element prediction: Off

Number of isotope peaks used for i-FIT = 3

Monoisotopic Mass, Even Electron Ions

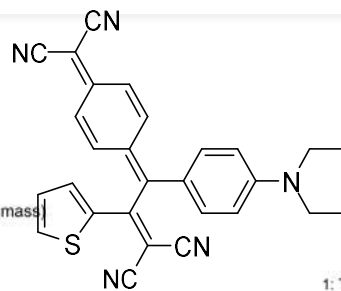
1 formula(e) evaluated with 1 results within limits (all results (up to 1000) for each mass)

Elements Used:

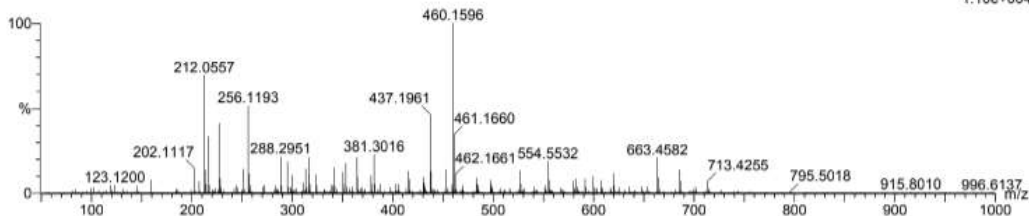
C: 28-28 H: 21-22 N: 5-5 S: 1-1

Cagatay Dengiz

34144_20211104_04-02 25 (0.965) Cm (12:25)



1: TOF MS ES+
1.10e+004



Minimum: -5.5
Maximum: 1000.0 1000.0 1000.0

Mass	Calc. Mass	mDa	PPM	DBE	i-FIT	i-FIT (Norm)	Formula
460.1596	460.1596	0.0	0.0	20.5	279.3	0.0	C28 H22 N5 S

Elemental Composition Report

Page 1

Single Mass Analysis

Tolerance = 1000.0 PPM / DBE: min = -5.5, max = 1000.0

Element prediction: Off

Number of isotope peaks used for i-FIT = 9

Monoisotopic Mass, Even Electron Ions

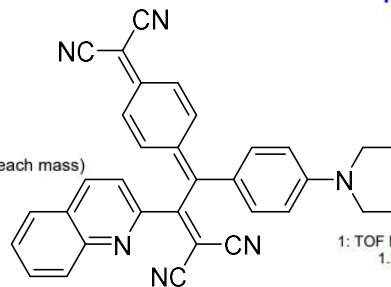
1 formula(e) evaluated with 1 results within limits (all results (up to 1000) for each mass)

Elements Used:

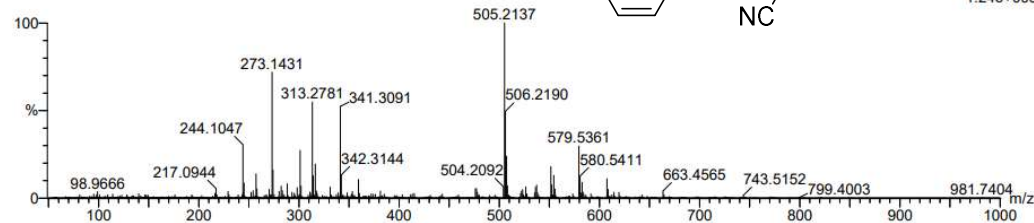
C: 33-33 H: 24-25 N: 6-6

Basak Karagollu

36163_20220511_05-03 10 (0.396) Cm (10:24)



1: TOF MS ES+
1.24e+005



Minimum: -5.5
Maximum: 1000.0 1000.0 1000.0

Mass	Calc. Mass	mDa	PPM	DBE	i-FIT	i-FIT (Norm)	Formula
505.2137	505.2141	-0.4	-0.8	24.5	1258.9	0.0	C33 H25 N6